APPENDIX 1

T. Krchová, J. Kotek, D. Jirák, J. Havlíčková, I. Císařová and P. Hermann: "Lanthanide complexes of aminoethyl-DO3A as PARACEST contrast agents based on decoordination of weakly bound amino group", *Dalton Trans.*, 2013, **42**, 15735–15747

Dalton Transactions

RSC Publishing

PAPER

View Article Online
View Journal | View Issue

Lanthanide(III) complexes of aminoethyl-DO3A as PARACEST contrast agents based on decoordination of the weakly bound amino group†

Cite this: *Dalton Trans.*, 2013, **42**, 15735

Tereza Krchová,[a] Jan Kotek,*[a] Daniel Jirák,[b] Jana Havlíčková,[a] Ivana Císařová[a] and Petr Hermann[a]

2-Aminoethyl DOTA analogues with unsubstituted ($H_3\mathbf{L^1}$), monomethylated ($H_3\mathbf{L^2}$) and dimethylated ($H_3\mathbf{L^3}$) amino groups were prepared by improved synthetic procedures. Their solid-state structures exhibit an extensive system of intramolecular hydrogen bonds, which is probably present in solution and leads to the rather high value of the last dissociation constant. The protonation sequence of $H_3\mathbf{L^1}$ in solution corresponds to that found in the solid state. The stability constants of the $H_3\mathbf{L^1}$ complexes with La^{3+} and Gd^{3+} (20.02 and 22.23, respectively) are similar to those of DO3A and the reduction of the pK_A value of the pendant amino group from 10.51 in the free ligand to 6.06 and 5.83 in the La^{3+} and Gd^{3+} complexes, respectively, points to coordination of the amino group. It was confirmed in the solid state structure of the [Yb($\mathbf{L^1}$)] complex, where disorder between the SA′ and TSA′ isomers was found. A similar situation is expected in solution, where a fast equilibration among the isomers hampers the unambiguous determination of the isomer ratio in solution. The PARACEST effect was observed in Eu(III)–$H_3\mathbf{L^1}$/$H_3\mathbf{L^2}$ and Yb(III)–$H_3\mathbf{L^1}$/$H_3\mathbf{L^2}$ complexes, being dependent on pH in the region of 4.5–7.5 and pH-independent in more alkaline solutions. The decrease of the PARACEST effect parallels with the increasing abundance of the complex protonated species, where the pendant amino group is not coordinating. Surprisingly, a small PARACEST effect was also observed in solutions of Eu(III)/Yb(III)–$H_3\mathbf{L^3}$ complexes, where the pendant amino group is dimethylated. The effect is detectable in a narrow pH region, where both protonated and deprotonated complex species are present in equilibrium. The data points to the new mechanism of the PARACEST effect, where the slow coordination–decoordination of the pendant amine is coupled with the fast proton exchange between the free amino group and bulk water mediates the magnetization transfer. The pH-dependence of the effect was proved to be measurable by MRI and, thus, the complexes extend the family of pH-sensitive probes.

Received 26th July 2013,
Accepted 27th August 2013

DOI: 10.1039/c3dt52031e

www.rsc.org/dalton

Introduction

Contrast agents (CAs) that alternate the properties of bulk water have been used for a long time to improve the resolution and utilization of magnetic resonance imaging (MRI) in medicine and molecular biology. The classical molecular CAs are based on complexes of highly paramagnetic metal ions, mainly on trivalent gadolinium.[1] The complexes change the relaxation times of the bulk water protons most frequently through the exchange of the whole coordinated water molecule. Another class of CAs is based on a completely different principle, a chemical exchange saturation transfer (CEST), was introduced some time ago.[2] The method is based on irradiation (saturation) of protons exchangeable with bulk water protons leading, after the chemical exchange, to a decrease of the bulk water proton signal. As signals of the bulk water protons and the protons to be irradiated should be

[a]*Department of Inorganic Chemistry, Universita Karlova (Charles University), Hlavova 2030, 128 40 Prague 2, Czech Republic. E-mail: modrej@natur.cuni.cz; Fax: +420-22195-1253; Tel: +420-22195-1261*

[b]*Department of Radiodiagnostic and Interventional Radiology, Magnetic Resonance Unit, Institute of Clinical and Experimental Medicine, Vídeňská 1958/9, 140 21 Prague 4, Czech Republic*

†Electronic supplementary information (ESI) available: Crystal structures of $H_3\mathbf{L^2}\cdot 6H_2O$ and $H_3\mathbf{L^3}\cdot 3.5H_2O$, and selected geometric parameters. The distribution diagram of $H_3\mathbf{L^1}$. Chemical shift dependence of $H_3\mathbf{L^1}$ on pH, and its protonation scheme. Distribution diagrams of the Ln^{3+}:$H_3\mathbf{L^1}$ systems. Temperature dependence of the ^{1}H NMR spectra of [Eu(H_2O)($\mathbf{L^1}$)] and [Yb($\mathbf{L^1}$)]. Disorder of the [Yb($\mathbf{L^1}$)] molecule found in the solid-state structure of [Yb($\mathbf{L^1}$)]·$5H_2O$, and its selected geometric parameters. Set of Z-spectra of the [Eu(H_2O)($\mathbf{L^{1,2,3}}$)] and [Yb($\mathbf{L^{1,2,3}}$)] complexes at different temperatures and pH. MRI-CEST images of phantoms of [Eu(H_2O)($\mathbf{L^1}$)] and [Yb($\mathbf{L^1}$)], and the normalized intensity of the CEST effect. ^{1}H and $^{13}C\{^1H\}$NMR spectra of $H_3\mathbf{L^1}$, $H_3\mathbf{L^2}$ and $H_3\mathbf{L^3}$. CCDC 933967, 952384–952386. For ESI and crystallographic data in CIF or other electronic format see DOI: 10.1039/c3dt52031e

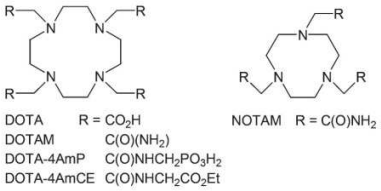

Scheme 1 Ligands discussed in the paper.

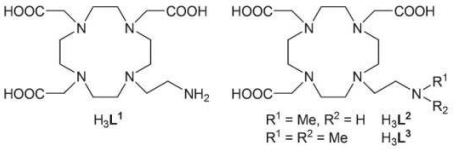

Scheme 2 Studied ligands.

separated from each other as much as possible to reduce non-specific proton irradiation, paramagnetic complexes causing the extension of the NMR chemical shift scale were suggested (PARACEST).[2,3] Most of these CAs are based on lanthanide(III) ions having suitable magnetic properties which are bound in macrocyclic ligands derived from DOTA (*e.g.*, DOTA-tetraamides, Scheme 1), ensuring the high thermodynamic stability and kinetic inertness of the complexes. The exchangeable protons in the complexes should be endowed with suitable properties and the most important one is the rate of their exchange with bulk water. There are two proton pools exhibiting PARACEST effects in Ln(III)–DOTA-tetraamide complexes: (i) protons of a coordinated water molecule if it is in a slow-exchange region, typically in the microsecond range (*e.g.* [Yb(H_2O)(DOTA-4AmCE)] complex (τ_M = 3 μs)[4] or [Eu(H_2O)(DOTAM)],[5] [Eu(H_2O)(DOTA-4AmCE)],[6] and [Eu(H_2O)(DOTA-4AmP)][4] complexes (τ_M = 55, 382 and 67 μs, respectively; for ligand structures see Scheme 1). The water molecule is bound directly to the metal ion and is close to the magnetic axis of the complexes and, thus, its protons exhibit a maximized difference in their chemical shift from the bulk water protons. (ii) Protons of *O*-coordinated amide group(s); however, these protons have their chemical shift much closer to the bulk water resonance. Nevertheless, their exchange depends on a number of external factors (*e.g.*, τ_M for [Yb(DOTAM)]$^{3+}$ lays, with a dependence on the pH, in the 400–5000 μs range[7]) and, therefore, the Ln(III) complexes of DOTA amide derivatives can be used as probes for various physiological parameters, such as pH, temperature, metabolite or metal ion concentrations, *etc.*[2c,3]

More recently, other PARACEST CAs based on different ligands (and, thus, on different pools of exchangeable protons) and/or metal ions have been suggested. Protons of the hydroxyl group are also labile and lanthanide(III) complexes of cyclen derivatives with alcohol pendant arms have been shown to exhibit a PARACEST effect.[8] Some transition metal ions can also present suitable magnetic properties and complexes of high-spin iron(II) or nickel(II) with derivatives of cyclam, cyclen or 1,4,7-triazacyclononane having 2-hydroxypropyl, acetamide (*e.g.*, DOTAM and NOTAM, see Scheme 1) or (5-aminopyridine-2-yl)methyl pendant arms have been shown to have a pronounced PARACEST effect.[9–11] Another pool of exchangeable protons, a distant non-coordinated amino group, has also been explored in some complexes of lanthanide(III)[12] as well as transition metal[9] ions.

In this work, we decided to investigate the PARACEST-related properties of complexes, where the CEST-causing amino group is directly coordinated to the central lanthanide(III) ions. To ensure complex stability, the ligands are based on a macrocyclic cyclen skeleton having three acetate and one 2-aminoethyl pendant arms, which contain primary ($H_3\mathbf{L^1}$), partially methylated secondary ($H_3\mathbf{L^2}$) and dimethylated tertiary ($H_3\mathbf{L^3}$) amino groups, see Scheme 2. Some of these ligands have already been investigated as bifunctional ligands for gadolinium(III)-based targeted MRI CAs[13] or radionuclides,[14] and, during work on this project, as pH-sensitive gadolinium(III)-based positive MRI CAs.[15]

Results and discussion

Synthesis

The ligands were synthesized (Schemes 3 and 4) by reaction of *t*-Bu_3DO3A with the appropriate amine-containing precursor. Alkylation of *t*-Bu_3DO3A with *N*-(2-bromoethyl)-phthalimide followed by sequential deprotection by trifluoroacetic acid and hydrazine led, after chromatography on anion exchanger, to zwitterionic $H_3\mathbf{L^1}$ in 59% overall yield (Scheme 3). The synthesis is more simple compared to the previously published procedure,[14] and is easily scalable and avoids HPLC purification.

To obtain ligand $H_3\mathbf{L^2}$, 2-[*N*-(ethyloxycarbonyl)-*N*-methylamino]bromoethane was used as the alkylation agent reacting with *t*-Bu_3DO3A and, after deprotection using trifluoroacetic acid and 10% aq. NaOH and chromatography on ion exchange resins, the ligand was isolated as a zwitterion in 30% overall yield (Scheme 4). Direct methylation of $H_3\mathbf{L^1}$ with a formaldehyde–formic acid mixture easily produced $H_3\mathbf{L^3}$ in high yield (Scheme 3); it is a significant improvement compared with the previous synthesis.[15]

All three studied ligands were structurally characterized in their zwitterionic forms by single-crystal X-ray diffraction analysis. Single-crystals of sufficient quality were obtained from solutions in water or aqueous ethanol. Title ligands were isolated in the form of hydrates ($H_3\mathbf{L^1}\cdot5H_2O$, $H_3\mathbf{L^2}\cdot6H_2O$ and $H_3\mathbf{L^3}\cdot3.5H_2O$, respectively). All three molecular structures are very similar, and therefore, only the molecular structure of $H_3\mathbf{L^1}$ is shown here in Fig. 1; other structures are shown in the ESI (Fig. S1 and S2†). In all three cases, the protonation scheme is the same – two protons are bound to the macrocycle amino groups bearing acetate moieties and are located mutually *trans*, and the third one is bound to the pendant

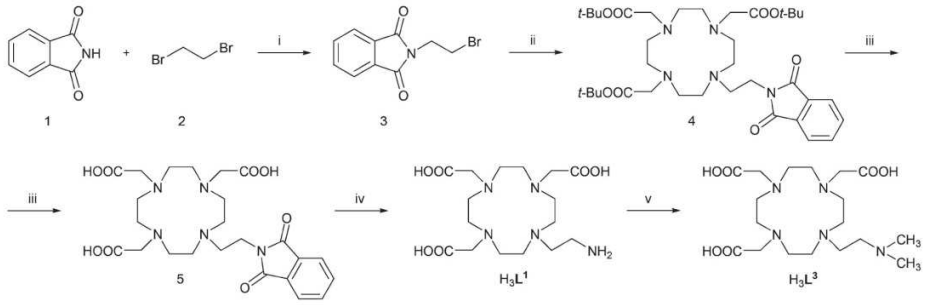

Scheme 3 Synthesis of studied ligands $H_3\mathbf{L}^1$ and $H_3\mathbf{L}^3$: (i) DMF, K_2CO_3, TBAB, 40 °C; (ii) *t*-Bu_3DO3A·HBr, MeCN, K_2CO_3, 60 °C; (iii) CF_3COOH–$CHCl_3$ (1 : 1), reflux 24 h; (iv) aq. NH_2NH_2, 90 °C, 18 h; (v) $(CH_2O)_n$, HCOOH, reflux 24 h.

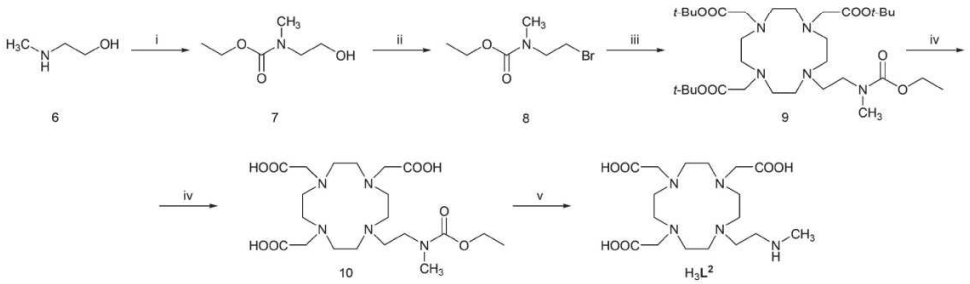

Scheme 4 Synthesis of studied ligand $H_3\mathbf{L}^2$: (i) $CH_3CH_2OC(O)Cl$, dioxan–H_2O (1 : 1), RT, 2 h; (ii) CBr_4, PPh_3, THF, RT, 1 h; (iii) *t*-Bu_3DO3A·HBr, K_2CO_3, MeCN, 60 °C; (iv) CF_3COOH–$CHCl_3$ (1 : 1), reflux 24 h; (v) 10% aq. NaOH, 90 °C, 24 h.

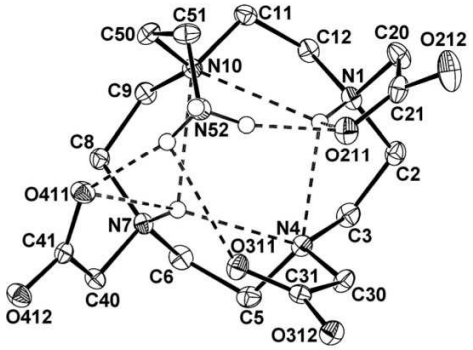

Fig. 1 Molecular structure of $H_3\mathbf{L}^1$ found in the crystal structure of $H_3\mathbf{L}^1 \cdot 5H_2O$ showing an intramolecular hydrogen bond network. The carbon-bound hydrogen atoms were omitted for clarity.

aminoethyl group. Such a protonation scheme is consistent with the form suggested on the basis of ^{1}H NMR titration (see below, Scheme S1†). The conformation of the macrocyclic unit is (3,3,3,3)-B, as usually observed for double-protonated cyclen rings (Table S1†).[16] Such a conformation is stabilized by intramolecular hydrogen bonds between the protonated and non-protonated macrocycle amino groups. Beside these interactions, the molecular structure is stabilized by further intramolecular hydrogen bonds, including protonated amines and deprotonated oxygen atoms of the carboxylate pendant arms, and the whole crystal structure is stabilized by extended hydrogen bond networks with water solvate molecules.

Stability of the complexes

The complexing properties of the most important ligand, $H_3\mathbf{L}^1$, having a primary amino group, were investigated in detail. First, the conditions for the pendant amino group deprotonation and coordination were investigated by potentiometry. The ligand's overall protonation constants β_{h10} were determined by potentiometry and are compiled together with corresponding pK_A values in Table 1; the ligand distribution diagram is shown in Fig. S3.† As the highest protonation constant β_{110} is slightly behind the $-\log[H^+]$ range suitable for potentiometric titrations, we also performed a ^{1}H NMR titration in the pH range 1.2–13.5 to confirm such a high value of the first protonation constant and to assign the individual protonation sites. The values of the dissociation constants

Table 1 Overall protonation constants (log β_{h10}) of $H_3\mathbf{L^1}$ and overall stability constants (log β_{h11}) of its lanthanide(III) complexes, and corresponding pK_A values (I = 0.1 m (Me_4N)Cl, 25 °C)

Stoichiometric coefficients			Constant	
h	l	M	log β_{hlm} [a]	pK_A
1	1	0	13.19(2)	13.19
2	1	0	23.70(2)	10.51
3	1	0	32.60(2)	8.90
4	1	0	36.47(2)	3.87
5	1	0	37.75(2)	1.27
La				
0	1	1	20.02(3)	—
1	1	1	26.08(2)	6.06
Gd				
0	1	1	22.23(4)	—
1	1	1	28.06(1)	5.83

[a] $\beta_{hlm} = [H_hL_lM_m]/\{[H]^h \cdot [L]^l \cdot [M]^m\}$.

obtained by NMR (pK_A = 13.3(3), 11.0(3), 9.3(2), 3.8(1) and 1.3(3)) are in a good agreement with those obtained by potentiometry (Table 1); the differences can be attributed to the different and non-controlled ionic strength during the NMR experiment and inaccurate (non-linear) potential–pH relationship in highly acidic/alkaline regions. However, the high value of the first protonation constant is confirmed and is clearly seen from the chemical shift dependence in the pH region 12.0–13.5 (Fig. S4†). In addition, it is possible, from pH-dependent changes of individual ^{1}H NMR signals, to determine also the sites of consecutive protonations (Scheme S1†): the first proton is distributed over all ring nitrogen atoms; the rather high value of the corresponding protonation constant is a consequence of intramolecular hydrogen bonds involving the ring nitrogen atoms as well as the pendant arms. Two pK_A values can be assigned to the partly simultaneous protonation of the pendant amino group and the second nitrogen atom of the macrocyclic ring, associated with re-location of the protons bound to the ring nitrogen atoms. The same proton distribution was also found in the zwitterionic forms of all studied ligands in the solid state (see above). The last two measured constants correspond to the protonation of the pendant carboxylate groups. Further protonations of the ring nitrogen atoms take place below pH 1. Such a protonation sequence is consistent with those commonly found for all DOTA-like ligands.

The stability constants, log β_{011}, determined for La(III) and Gd(III) ions were found to be 20.02 and 22.23, respectively (Table 1). Corresponding distribution diagrams are shown in Fig. S5 and S6.† The stability constants are lower than those reported for Ln(III)–DOTA (La(III) 22.9, Gd(III) 24.6) complexes and similar to those of Ln(III)–DO3A (Gd(III) 21.0) complexes.[17] In both studied systems, protonated species with pK_A 6.06 and 5.83 for the La(III) and Gd(III) complexes, respectively, are formed. The value for the protonation of the Gd(III)–$H_3\mathbf{L^1}$ complex is in good agreement with the reported value (5.95) determined by relaxometric measurements.[15] The distribution diagrams show that free lanthanide(III) ions are not present above pH 5.5. The protonation takes place on the pendant amino group as it is the most basic site of the in-cage complex molecule and a difference of ~4–5 orders of magnitude between the constants, corresponding to its protonation in the complexes and analogous protonation in the free ligand, points to an easier deprotonation induced by coordination of the group to the metal ion. Thus, one can conclude, that studied ligands are coordinated in an octadentate fashion involving the pendant amino group in the [Ln($\mathbf{L^1}$)] species, and that the amino group is decoordinated upon protonation in the weakly acidic region. The maximum abundance of the $[Gd(H\mathbf{L^1})]^+$ complex species in solution is observed at pH ~5.

Structure of the complexes

To study the structure and properties of the lanthanide(III) complexes of $H_3\mathbf{L^1}$, sample solutions were prepared by dissolving $LnCl_3$ and the ligand in a Ln : L = 1 : 1.1 molar ratio, adjusting the pH with aq. LiOH to 6.0, heating the solution at 60 °C overnight, re-adjusting pH to 6.5 and heating at 60 °C overnight again.

The complexes of the DOTA-like ligands are usually nona-coordinated (eight donor atoms coming from macrocyclic ligands and one site is occupied by a water molecule) and form two possible diastereomers – square-antiprismatic (SA) and twisted-square-antiprismatic (TSA) ones.[1] These diastereoisomers differ in the relative screwing of the macrocyclic (δ/λ) and pendant (Δ/Λ) chelate rings, giving rise to ΔλλλλΛ/ΛδδδδΔ (SA) and ΔδδδδΛ/ΛλλλλΔ (TSA) combinations. In the ^{1}H NMR spectra, the signals showing best the isomer ratio belongs to those of the "axial" protons of the macrocyclic chelate rings, which are the closest ones to the lanthanide(III) ion and to the magnetic axis of the complexes.[18] In the Ln(III)–DOTA-like complexes, the TSA isomer with a larger coordination cage is strongly preferred at the beginning of the lanthanide series, with the SA one becoming dominant for heavier lanthanides.[18] Although the situation is sometimes complicated by the possible presence of an octa-coordinated species (*i.e.*, without a coordinated water molecule, usually denoted as SA′/TSA′), which have a similar chemical shift range in the ^{1}H NMR spectra to the nona-coordinated SA/TSA species. Due to this fact, the abundance of twisted-square-antiprismatic isomers can slightly increase towards the end of the lanthanide series.[18,19]

The solution structures of the studied complexes were investigated by variable-temperature ^{1}H NMR. To assure the coordination of the pendant amino group, the pH of the samples was adjusted to the weakly alkaline region. However, the spectrum of the Eu(III) complex at pH 9 (Fig. S7†) acquired at 25 °C was not resolved enough to observe the required signals and to determine the isomer ratio; only very broad signals in the 17–27 ppm region (after correction for bulk magnetic susceptibility shift) were observed. Such chemical shifts are just between the regions typical for SA and TSA species, although slightly closer to the TSA one.[18] Both heating up to 90 °C or cooling to 0 °C led to a significant broadening and visual disappearance of these signals. It points to the fact that two relatively independent fluxional processes occur, affecting

the position of the axial hydrogen atoms with respect to the lanthanide(III) ion. Therefore, we can only speculate that a mixture of the isomers is present, as it is common for most of Eu(III) complexes with DOTA-like ligands.[18,19] A similar situation occurs for the Yb(III) complex. The ^{1}H NMR spectrum acquired at 25 °C and pH 8.5 (Fig. S8†) shows signals of "axial" protons as broad peaks in the 86–112 ppm region. The chemical shifts,[18,19] signal broadening and their virtual disappearance, observed either at lower and higher temperatures, point to the presence of a SA(′)/TSA(′) exchange process.

The hypothesis of ongoing SA(′)/TSA(′) isomerism is supported by the solid-state structure of the [Yb($\mathbf{L}^1$)]·5H_2O complex (Fig. 2). The central ion is octacoordinated between mutually parallel macrocycle N_4- and pendant-arm O_3N-planes, but closer to the pendant-arm one. As a result of smaller values of the trans ("opening") angles in the O_3N-plane (120° and 125° for O311–Yb1–N52 and O211–Yb1–O411 angles, respectively), comparing to the limiting value (~135°) for water coordination,[20] no water molecule is directly bound to the metal centre. During the refining of the crystal structure, the set of difference maxima in the electron density map were located close to the nitrogen and carbon atoms of the macrocycle, and pointed to some disorder in the macrocyclic unit. It was successfully modelled, leading to a calculated ratio of the SA′ : TSA′ isomers of 15 : 85% (Fig. 2 and S9†). The structural parameters of both coordination spheres fall into regions typical for the given isomers,[20] with mean torsion angles between N_4- and O_3N-planes of 37.5 and 22.5°, and separation of the N_4- and O_3N-planes of 2.50 and 2.59 Å for the SA′ and TSA′ species, respectively. Further selected geometric parameters are compiled in Table S2.†

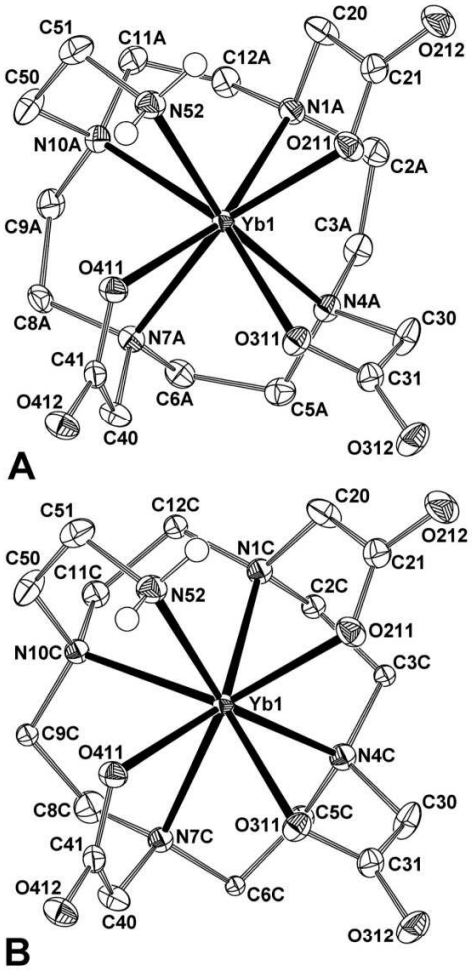

Fig. 2 Molecular structure of [Yb($\mathbf{L}^1$)] found in the crystal structure of [Yb($\mathbf{L}^1$)]·5H_2O; TSA′ (λλλλλ, 85%) species (A) and SA′ (Λδδδδ, 15%) species (B). Carbon-bound H-atoms are omitted for clarity.

Chemical exchange saturation transfer

PARACEST experiments (measurements of so-called Z-spectra) produced the clean saturation of bulk water after irradiation of the broad regions with maxima at +19.5 and +34 ppm for the Eu(III)–$H_3\mathbf{L}^1$ complex (pH = 7.67, t = 25 °C), and +42 ppm and +89 ppm for the Yb(III)–$H_3\mathbf{L}^1$ complex (pH = 7.40, t = 25 °C); chemical shifts are given with respect to the signal of the bulk water protons. In the ^{1}H NMR spectra of the Eu(III) complex acquired in aqueous solution, a broad signal at 34 ppm is observable, and disappears on selective water pre-saturation or when acquiring the spectra in D_2O (Fig. S10†). The other signal is overlapped with C–H proton signals and, therefore, cannot be distinguished in the ^{1}H NMR spectra. Also in the case of the Yb(III) complex, there are C–H proton signals in the regions corresponding to the CEST effect and, thus, it prevents the direct observation of the signals.

For both complexes, the two observed CEST signals have equal intensities. With respect to the chemical structure of the complexes, the observed effect can be theoretically caused by two exchangeable pools of protons, *i.e.*, by protons of the amino group of the pendant arm and/or by protons of the coordinated water molecule. From relaxometric data, it is known that one water molecule is coordinated in the Gd(III) complex,[15] and this fact is also undoubtedly valid for the complex of the slightly larger Eu(III) ion (but it cannot be easily confirmed by the normally used luminescence measurements due to the presence of two types of quenchers, O–H and N–H, which complicates the data evaluation). However, in the case of the complex with the significantly smaller Yb(III), an anhydrous species might be expected on the basis of the solid-state structure (see above). In such cases, three possible elucidations can be considered: (i) both signals come from the amino group, (ii) one signal belongs to the coordinated water molecule and other to the amine, and (iii) both signals belong to

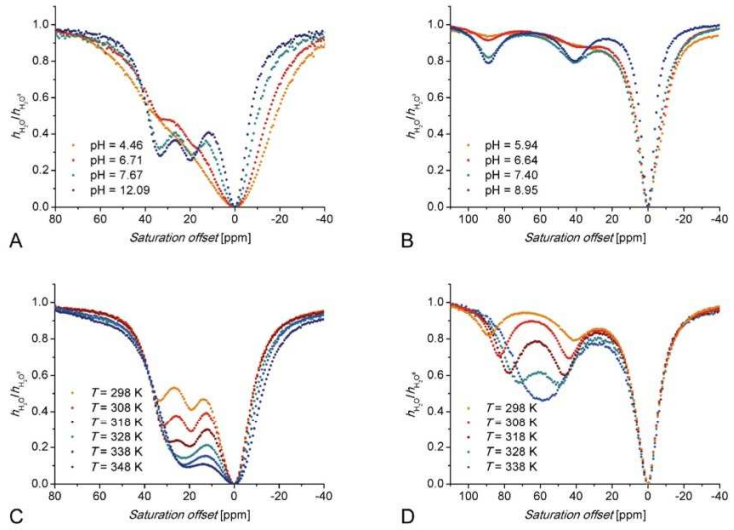

Fig. 3 Z-spectra of a 80 mM aqueous solution (H_2O–D_2O 1 : 10) of Eu(III)–$H_3\mathbf{L^1}$ complex (B_0 = 7.05 T, satpwr = 29 dB ~1000 Hz, satdly = 2 s) at T = 298 K (A) and pH = 7.40 (C). Z-spectra of a 100 mM aqueous solution (H_2O–D_2O 1 : 10) of Yb(III)–$H_3\mathbf{L^1}$ complex (B_0 = 7.05 T, satpwr = 29 dB ~1000 Hz, satdly = 2 s) at T = 298 K (B) and pH = 7.40 (D).

the water molecule. To distinguish between these possibilities, more detailed studies were carried out. The most interesting CEST behaviour was observed while changing the solution pH. The CEST effect started to be observable at pH ~6 for both of the Eu(III) and Yb(III)–$H_3\mathbf{L^1}$ complexes and reached a maximum at pH ~8, and the saturation transfer efficiency was not changed with further pH increases up to ~12; the mutual intensity ratio of the CEST peaks is not changed with pH. The results are shown in Fig. 3A and 3B and strongly support the first possibility, as when the CEST effect is caused by the coordinated water molecule (or by exchangeable protons of the amide[7] or hydroxy[8] moieties), the effect drops with increasing pH due to the faster prototropic (base-catalyzed) exchange of the corresponding protons (of the coordinated water molecule or the other mentioned pools). The behaviour reported in this work has not yet been reported in the literature. The magnitude of the CEST effect at different pH values follows an abundance of the fully deprotonated species – the CEST effect consistently disappears at lower pH with protonation and, thus, decoordination of the amino group (see potentiometric results, Table 1 and Fig. S5 and S6†). The observations mentioned above are fully consistent with the low "acidity" of the N–H bond in the studied amino derivative if compared to the generally higher acidity of the N–H proton in carboxylic amides; therefore, in the case of DOTAM complexes, base-catalysed proton exchange significantly decreases the CEST effect in alkaline solutions but, in the case of our complexes, the CEST effect remains unchanged even at very high pH.

Thus, the observed CEST signals are assigned to hydrogen atoms of the coordinated pendant amino group. Two observed signals rise from the fact that two amine hydrogen atoms become magnetically non-equivalent after the group coordination. A similar situation has been observed for the amide hydrogen atoms of DOTAM (Scheme 1).[7] The lanthanide-induced shift of the amine hydrogen atoms is higher than that of the amide hydrogen atoms in analogous complexes, as the coordinated amine group is much closer to the metal ion and to the magnetic axis of the complexes. The possibility that two signals arise from the presence of two (SA and TSA) isomers could be excluded as both signals have an equal intensity and it would imply that the SA and TSA isomers have the same abundance for both complexes, which is very improbable due to the general trends along the lanthanide series. In addition, as both isomers should have a very similar geometry of the N_3O-plane, the NMR signals associated with the protons of the amino pendant arm should have similar chemical shifts in both the SA and TSA species; however, there is a significant difference in the chemical shifts between the signals ($\Delta\delta$ ~15 and 50 ppm for Eu(III) and Yb(III) complexes, respectively). With increasing temperature, the saturation transfer becomes more effective and two amine hydrogen signals converge and, finally, coalescence around 55 °C and 65 °C for the Eu(III) and Yb(III) complexes, respectively (Fig. 3C and 3D). On further heating (up to 95 °C, Fig. S11†), the coalesced CEST signals approach slightly closer to signal of the bulk water but are still observable. Such a behaviour points to the dynamic averaging

of the non-equivalent amine hydrogen signals; it can originate from a faster coordination–decoordination equilibrium or from a faster geometry change.

Due to the insensitivity of the CEST effect to pH changes in the alkaline region, the process described above cannot be caused by neither hydroxide nor proton attack on the coordinated amino group. Therefore, the mechanism of the observed CEST effect is very probably associated with the (semi)labile coordination of the 2-aminoethyl pendant arm. Its coordination–decoordination is the rate-limiting step – when the pendant arm is coordinated, no exchange occurs but in the moment of the pendant arm decoordination, the exchange of protons of the free amino group with those of bulk water proceeds very quickly.

To support the hypothesis presented above, we prepared and studied complexes of mono- and dimethylated analogues, *i.e.*, with ligands $H_3\mathbf{L}^2$ and $H_3\mathbf{L}^3$. The complexes of $H_3\mathbf{L}^2$ showed significant CEST effects, observed as two close peaks with unequal intensity at 43 and 49.5 ppm for Eu(III) and one peak at 57 ppm for Yb(III), respectively (Fig. S12†). The two signals in the Z-spectra, observed in the case of the Eu(III) complex, can be attributed to two modes of coordination of the methylamino group, in which the methyl and hydrogen occupy equatorial/axial or reverse positions. In the case of the complex with the smaller Yb(III) ion, one of these possibilities is probably strongly preferred due to the larger steric strain around the methyl group, leading to only one observable signal in the Z-spectra. However, to our surprise, the Yb(III)–$H_3\mathbf{L}^3$ complex also exhibits a CEST effect at 26 ppm, although the CEST peak has a small intensity and is observable only in a narrow pH range 6–8.5 (Fig. 4 and S13†). In this pH region, the protonation–deprotonation of the $-NMe_2$ group is supposed (accordingly to the corresponding log K_A ~7.8 reported previously for its Gd(III) complex[15]). Thus, an equilibrium between the deprotonated (and mostly coordinated) and protonated (and uncoordinated) amino group in the complex is present. Therefore, the observation of the CEST effect can be explained by the protonation–deprotonation of the uncoordinated dimethylamino group, which is still located sufficiently close to the highly paramagnetic centre to mediate the saturation transfer to the bulk water through this process. Such an explanation is consistent with the fact that the observed CEST effect disappears at a relatively low temperature ~65 °C, which is probably due to the much faster chemical exchange process (Fig. S13†), contrary to the complexes of $H_3\mathbf{L}^1$ where the analogous signal disappearance cannot be reached even at 95 °C (see above). In the case of the Eu(III)–$H_3\mathbf{L}^3$ complex, a slight CEST effect was also observed, causing some asymmetric broadening of the water signal in the Z-spectra (Fig. S13†). This feature can be explained in a similar way to the above.

To test the applicability of the complexes as MRI pH probes, the CEST effect was measured in phantoms containing Eu(III)–$H_3\mathbf{L}^1$ and Yb(III)–$H_3\mathbf{L}^1$ complex solutions having different pH and concentrations. The final CEST images were obtained after irradiation at the CEST and symmetrical negative frequencies and subtracting the images (Fig. 5 and S14†). Normalized signal intensities are shown in Fig. S15 and S16.† The results clearly show that the prepared complexes can be successfully employed as CEST probes in the pH region relevant to living systems.

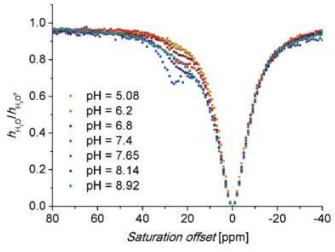

Fig. 4 Z-spectra of a 50 mM aqueous solution (H_2O–D_2O 1 : 10) of the Yb(III)–$H_3\mathbf{L}^3$ complex (B_0 = 7.05 T, T = 298 K, satpwr = 29 dB ~1000 Hz, satdly = 2 s).

Experimental

Materials and methods

Commercially available chemicals had synthetic purity and were used as received. Deionized water, used for the synthesis of the ligands and their complexes, was prepared using a deionization water system ROWAPUR 200/100. Water used for potentiometric titrations was prepared by a Milli-Q (Millipore).

t-Bu_3DO3A·HBr [1,4,7-tris(*t*-butylcarboxymethyl)-1,4,7,10-tetraazacyclododecane hydrobromide] was prepared according to the published procedure.[21] Dry solvents were prepared by the standard purification procedures[22] and stored over molecular sieves under an argon atmosphere: dry MeCN was obtained by distillation from P_2O_5, THF was dried by refluxing with potassium and distilled under an argon atmosphere.

The ESI-MS spectra were acquired on a Bruker ESQUIRE 3000 spectrometer equipped with an electrospray ion source and ion-trap detection. Measurements were carried out in the positive and negative modes. NMR characterization data (1D: ^{1}H, ^{13}C; 2D: HSQC, HMBC, ^{1}H–^{1}H COSY) were recorded on VNMRS300, Varian^{UNITY} *INOVA* 400 or Bruker Avance III 600, using 5-mm sample tubes. Chemical shifts δ are given in ppm and coupling constants J are reported in Hz. For the ^{1}H and ^{13}C measurements in D_2O, *t*-BuOH was used as the internal standard (δ_H = 1.25, δ_C = 30.29). For the measurements in $CDCl_3$, TMS was used as the internal standard (δ_H = 0.00, δ_C = 0.00). Abbreviations s (singlet), t (triplet), q (quartet), m (multiplet) and br (broad) are used in order to express the signal multiplicities. Elemental analysis was performed at the Institute of Macromolecular Chemistry of the Academy of Science of the Czech Republic (Prague).

Synthesis

***N*-(2-Bromoethyl)phthalimide (3).** Compound **3** was prepared according to a modified published procedure.[23] To a

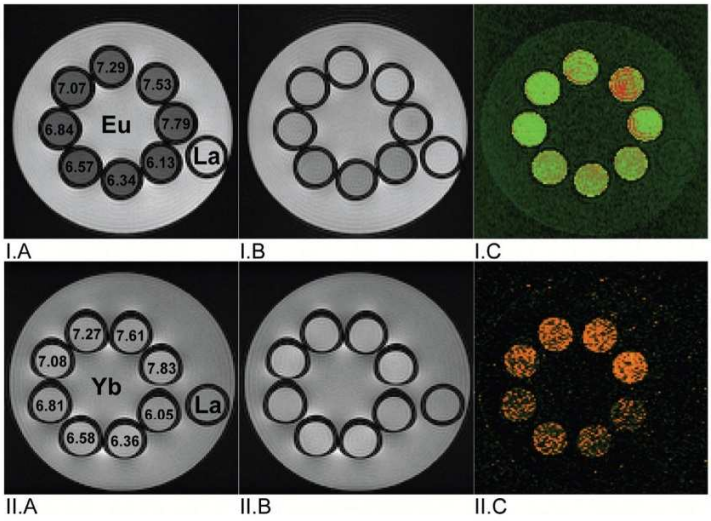

Fig. 5 MRI-CEST images of phantoms consisting of one vial containing 80 mM aq. solution of [La(H_2O)(**L^1**)] as a diamagnetic standard and eight vials containing 80 mM aq. solutions of [Eu(H_2O)(**L^1**)] and [Yb(**L^1**)] with different pH values; pH is shown in figures A. Experimental conditions: MSME pulse sequence, B_0 = 4.7 T, B_1 = 20 μT, T = 293 K, satdly = 2 s, TR = 5 s, TE = 8.9 ms, scan time = 8 min. I.A: T_1-weighted image, satfrq = 34 ppm from the bulk water signal. I.B: T_1-weighted image, satfrq = −34 ppm from the bulk water signal. I.C: The difference between images I.A and I.B in false colours. II.A: T_1-weighted image, satfrq = 89 ppm from the bulk water signal. II.B: T_1-weighted image, satfrq = −89 ppm from the bulk water signal. II.C: The difference between images II.A and II.B in false colours.

well-stirred suspension of K_2CO_3 (9.40 g, 68 mmol), 1,2-dibromoethane **2** (11.7 ml, 136 mmol) and tetrabutylammonium bromide (TBAB, 0.70 g) in DMF (20 ml), was added phthalimide **1** (5.00 g, 34 mmol) and the reaction mixture was stirred for 18 h at 40 °C. Next, the mixture was poured into water (150 ml) and the product **3** was extracted with ethylacetate (4 × 25 ml). The organic portion was concentrated *in vacuo*. The product was purified by crystallization from hot EtOH to give **3** (7.61 g, 88%).

^{1}H NMR (299.9 MHz, $CDCl_3$): δ 3.59 (2H, t, $^3J_{HH}$ = 6.6, NCH_2CH_2Br); 4.09 (2H, t, $^3J_{HH}$ = 6.6, NCH_2CH_2Br); 7.70–7.73 (2H, m, arom.); 7.84–7.86 (2H, m, arom.).

$^{13}C\{^1H\}$ NMR (75.4 MHz, $CDCl_3$): δ 28.55 (1C, NCH_2CH_2Br); 39.70 (1C, NCH_2CH_2Br); 123.93 (2C, arom.); 132.23 (2C, arom. quaternary); 134.63 (2C, arom.); 168.22 (2C, *C*O).

Elemental analysis: found (calcd for $C_{10}H_8BrNO_2$, M_r = 254.1) C: 47.68 (47.27), H: 3.07 (3.17), N: 5.32 (5.51), Br: 31.15 (31.45).

1,4,7-Tris(carboxymethyl)-10-(2-aminoethyl)-1,4,7,10-tetraazacyclododecane ($H_3L^1 \cdot 3H_2O$). Compound **4** was prepared *in situ* according to a modified published procedure.[14] To a well-stirred suspension of K_2CO_3 (2.40 g, 17.4 mmol) and *t*-Bu_3DO3A·HBr (2.59 g, 4.37 mmol) in dry MeCN (40 ml), alkylating reagent **3** (1.22 g, 4.80 mmol) was gradually added over 30 min and the reaction mixture was stirred for 24 h at 60 °C. The solids were filtered off and the filtrate was evaporated on a rotary evaporator. The oily residue was dissolved in $CHCl_3$ (20 ml) and extracted with distilled water (4 × 10 ml). The organic portion was dried over anhydrous Na_2SO_4 and concentrated *in vacuo* to give 3.40 g of yellow oil containing compound **4** contaminated with phthalhydrazide and an excess of alkylating reagent **3**. The by-product and alkylating reagent were not removed, and the crude product **4** was used in the next step without purification (only a small amount of the crude product **4** was purified for characterization purposes using HPLC).

A portion (3.35 g) of this mixture containing compound **4** was dissolved in CF_3COOH and $CHCl_3$ (30 ml, 1 : 1); the resulting solution was refluxed for 24 h. After evaporation to dryness the oily residue was dissolved in a small amount of distilled water and then loaded onto a strong cation exchange column (Dowex 50, 50–100 mesh, H^+-form, 2 × 9 cm). Acidic impurities were removed by elution with water and the product **5** was eluted with 5% aq. NH_3. Fractions containing the product (TLC check) were combined and evaporated to give 2.82 g of yellow oil containing compound **5**. The crude product **5** was used in the next step without purification.

The portion (2.80 g) of the crude product **5** was dissolved in 80% aq. $NH_2NH_2 \cdot H_2O$ (15 ml); the resulting mixture was then heated for 18 h at 90 °C and concentrated *in vacuo*. The residue was dissolved in a small amount of distilled water. Then the solution was filtered and loaded onto a strong anion exchange column (Dowex 1, OH^--form, 1.25 × 8 cm). Impurities were removed by elution with water and the product H_3L^1 was eluted with 5% aq. CH_3COOH. Fractions containing the pure product (TLC and ^{1}H NMR check) were combined and

evaporated to give $H_3\mathbf{L^1}$ (1.90 g) as an yellow oil. The crude product was purified by crystallization from hot EtOH to give $H_3\mathbf{L^1}\cdot 3H_2O$ (1.15 g, 59%) as a white powder.

Compound ***4***. HPLC: Solvent: A = CH_3CN, B = 0.1% of CF_3COOH in H_2O, C = H_2O. Gradient: A: 20–50%, 0–24 min; 50%, 24–40 min; 50–20%, 40–41 min; 20%, 41–61 min. B: 20%, 0–61 min. t_R = 17.0 min.

^{1}H NMR (299.9 MHz, $CDCl_3$): δ 1.45–1.48 (27H, m, $C(CH_3)_3$); 3.15–3.43 (18H, m, CH_2); 3.53 (4H, s, CH_2CO_2); 3.86 (2H, s, CH_2CO_2); 4.02 (2H, br, CH_2); 7.73–7.76 (2H, m, arom.); 7.84–7.87 (2H, m, arom.).

$^{13}C\{^1H\}$ NMR (150.9 MHz, $CDCl_3$): δ 27.92 (9C, $C(CH_3)_3$); 32.58, 48.97, 49.92, 50.13, 51.17, 51.86, 54.77 (13C, CH_2); 82.96 (2C, $C(CH_3)_3$); 84.28 (1C, $C(CH_3)_3$); 123.58 (2C, arom.); 131.65 (2C, arom. quaternary); 134.37 (2C, arom.); 167.85 (3C, CH_2CO_2); 169.22 (2C, NCO).

MS-ESI: (+): 688.5 ($[M + H]^+$, calcd 688.4); 710.4 ($[M + Na]^+$; calcd 710.4).

Compound ***5***. MS-ESI: (−): 518.0 ($[M - H]^-$, calcd 518.2).

$H_3\boldsymbol{L^1}\cdot 3H_2O$. ^{1}H NMR (600.2 MHz, D_2O, pD = 5.4, Fig. S17†): 2.85–2.89 (4H, m, CH_2NCH_2CO); 2.94 (2H, br, $CH_2CH_2NH_2$); 3.02–3.04 (4H, m, $CH_2N(CH_2)_2NH_2$); 3.06 (2H, t, $^3J_{HH}$ = 5.1, CH_2NH_2); 3.13 (2H, s, CH_2CO); 3.33–3.37 (2H, m, CH_2NCH_2CO); 3.40–3.45 (2H, m, CH_2NCH_2CO); 3.54–3.58 (2H, m, CH_2NCH_2CO); 3.71–3.77 (2H, m, CH_2NCH_2CO); 3.90 (4H, AB-multiplet, CH_2CO).

$^{13}C\{^1H\}$ NMR (150.9 MHz, D_2O, pD = 5.4, Fig. S18†): δ 37.01 (1C, CH_2NH_2); 48.90 (2C, $CH_2N(CH_2)_2NH_2$); 48.99 (2C, CH_2NCH_2CO); 50.82 (1C, $CH_2CH_2NH_2$); 51.00 (2C, CH_2NCH_2CO); 53.06 (2C, CH_2NCH_2CO); 55.85 (1C, CH_2CO); 58.07 (2C, CH_2CO); 171.02 (2C, CH_2CO); 178.77 (1C, CH_2CO).

MS-ESI: (+): 412.0 ($[M + Na]^+$, calcd 412.2); 428.0 ($[M + K]^+$, calcd 428.2). (−): 425.8 ($[M + K - 2H]^-$, calcd 426.2).

Elemental analysis: found (calcd for $C_{16}H_{37}N_5O_9$, M_r = 443.5) C: 43.17 (43.33), H: 8.40 (8.41), N: 15.39 (15.79).

2-[*N*-(Ethyloxycarbonyl)-*N*-methylamino]ethanol (7). To a solution of **6** (2.64 g, 35.2 mmol) in a mixture of dioxane and H_2O (30 ml, 1 : 1), ethyloxycarbonylchloride (0.96 g, 8.85 mmol) was added dropwise. The solution was stirred at room temperature for 2 h and concentrated *in vacuo*. The oily residue was dissolved in CH_2Cl_2 (30 ml) and extracted with H_2O (3 × 15 ml) and 3% aq. HCl (1 × 15 ml). The organic portion was dried over Na_2SO_4 and concentrated *in vacuo* to give 1.10 g of **7** as a colourless oil.

^{1}H NMR (299.9 MHz, $CDCl_3$): δ 1.24 (3H, t, $^3J_{HH}$ = 7.2, CH_2CH_3); 2.94 (3H, s, NCH_3); 3.41 (2H, br, NCH_2); 3.73 (2H, br, CH_2OH); 4.11 (2H, q, $^3J_{HH}$ = 7.2, CH_2CH_3).

$^{13}C\{^1H\}$ NMR (75.4 MHz, $CDCl_3$): δ 14.85 (1C, CH_2CH_3); 35.42 (1C, NCH_3); 51.92 (1C, CH_2CH_2OH); 61.40 (1C, CH_2OH); 61.74 (1C, CH_2CH_3); 158.17 (1C, CO).

MS-ESI: (+): 148.5 ($[M + H]^+$, calcd 148.1); 170.4 ($[M + Na]^+$, calcd 170.1).

2-[*N*-(Ethyloxycarbonyl)-*N*-methylamino]bromoethane (8). To a well-stirred solution of **7** (1.09 g, 7.41 mmol) in dry THF (40 ml), in a flask equipped with a drying tube, CBr_4 (3.68 g, 11.1 mmol) and PPh_3 (2.92 g, 11.1 mmol) were added. The reaction mixture was stirred for 1 h at room temperature, filtered and then evaporated on a rotary evaporator. The oily residue was dissolved in small amount of CH_2Cl_2 and purified by chromatography (SiO_2, 18 × 3.5 cm). Impurities were removed by elution with CH_2Cl_2, the pure product was eluted using a mixture of acetone and CH_2Cl_2 (1 : 9). Fractions containing the product **8** (TLC check) were combined and evaporated to give **8** (1.32 g) as a colourless oil.

^{1}H NMR (299.9 MHz, $CDCl_3$): δ 1.26 (3H, t, $^3J_{HH}$ = 6.9, CH_2CH_3); 2.97 (3H, s, NCH_3); 3.45 (2H, br, NCH_2); 3.62 (2H, br, CH_2Br); 4.14 (2H, q, $^3J_{HH}$ = 6.9, CH_2CH_3).

$^{13}C\{^1H\}$ NMR (75.4 MHz, $CDCl_3$): δ 14.89 (1C, CH_2CH_3); 29.50 (1C, CH_2Br); 35.60 (1C, NCH_3); 51.30 (1C, CH_2CH_2Br); 61.76 (1C, CH_2CH_3); 156.31 (1C, CO).

1,4,7-Tris(carboxymethyl)-10-[2-(*N*-methylamino)ethyl)]-1,4,7,10-tetraazacyclododecane ($H_3\mathbf{L^2}\cdot 5.5H_2O$). To a well-stirred suspension of K_2CO_3 (3.30 g, 23.9 mmol) and *t*-Bu_3DO3A·HBr (2.89 g, 4.85 mmol) in dry MeCN (30 ml), a solution of alkylating reagent **8** (1.32 g, 6.28 mmol) in dry MeCN (10 ml) was added dropwise. The reaction mixture was stirred for 24 h at 60 °C, filtered, and the filtrate was evaporated on a rotary evaporator. The oily residue was dissolved in $CHCl_3$ (20 ml) and extracted with distilled water (4 × 10 ml). The organic portion was dried over Na_2SO_4 and concentrated *in vacuo* to give 3.82 g of yellow oil containing compound **9** contaminated with an excess of alkylating reagent **8**. The alkylating reagent was not removed, and the crude product **9** was used in the next step without purification.

A portion (3.80 g) of the mixture containing compound **9** was dissolved in a mixture of CF_3COOH and $CHCl_3$ (30 ml, 1 : 1); the resulting solution was refluxed for 24 h and evaporated on a rotary evaporator. The oily residue was dissolved in a small amount of distilled water and evaporated (this procedure was then repeated three more times) to give 5.00 g of yellow oil containing compound **10** (it was used in the next step without purification).

The crude product **10** (5.00 g) was dissolved in 10% aq. NaOH (50 ml) and stirred for 24 h at 90 °C. Then the solution was loaded onto a strong anion exchange column (Dowex 1, OH^--form, 1.25 × 20 cm). Impurities were removed by elution with water and the product $H_3\mathbf{L^2}$ was eluted with 5% aq. CH_3COOH. Fractions containing the product (TLC and ^{1}H NMR check) were combined and evaporated to give $H_3\mathbf{L^2}$ (1.97 g) as a brownish oil. The crude product was dissolved in small amount of distilled water and anhydrous EtOH was added dropwise. Crystallization started after a few minutes, and the suspension was left overnight. The white crystalline solid was filtered off and dried under a vacuum to give $H_3\mathbf{L^2}\cdot 5.5H_2O$ (0.66 g, 30%) as a white powder.

Compound ***9***. MS-ESI: (+): 644.5 ($[M + H]^+$, calcd 644.5); 666.4 ($[M + Na]^+$; calcd 666.5).

Compound ***10***. MS-ESI: (−): 474.1 ($[M - H]^-$, calcd 474.3); 512.0 ($[M + K - 2H]^-$, calcd 512.0).

$H_3\boldsymbol{L^2}\cdot 5.5H_2O$. ^{1}H NMR (299.9 MHz, D_2O, pD = 1.15): δ 2.63 (3H, s, NCH_3); 2.80–3.15 (12H, m, CH_2); 3.20–3.63 (10H, m, CH_2); 3.97 (4H, br, CH_2CO_2).

^{1}H NMR (299.9 MHz, D_2O, pD = 5.3, Fig. S19†): δ 2.77 (3H, s, NCH_3); 2.80–2.91 (4H, m, CH_2); 2.94–3.08 (8H, m, CH_2); 3.13 (2H, s, CH_2CO$_2$); 3.31–3.46 (4H, m, CH_2); 3.52–3.60 (2H, m, CH_2); 3.70–3.76 (2H, m, CH_2); 3.89 (4H, AB-multiplet, CH_2CO$_2$).

^{13}C{^{1}H} NMR (150.9 MHz, D_2O, pD = 5.6, Fig. S20†): δ 34.93 (1C, NCH_3); 46.89 (1C, CH_2NCH_3); 48.89 (2C, CH_2); 49.03 (2C, CH_2); 50.42 (1C, CH_2CH_2NCH_3); 51.04 (2C, CH_2); 53.10 (2C, CH_2); 55.68 (1C, CH_2CO_2); 58.16 (2C, CH_2CO_2); 171.08 (2C, CH_2CO_2); 178.63 (1C, CH_2CO_2).

MS-ESI: (+): 404.3 ([M + H]$^+$, calcd 404.2); 426.9 ([M + Na]$^+$, calcd 426.2); 442.8 ([M + K]$^+$, calcd 442.2).

Elemental analysis: found (calcd for $C_{17}H_{44}N_5O_{11.5}$, M_r = 502.6) C: 40.84 (40.63), H: 9.27 (9.22), N: 13.80 (13.84).

1,4,7-Tris(carboxymethyl)-10-[2-(*N*,*N*-dimethylamino)ethyl)]-1,4,7,10-tetraazacyclododecane (H_3L^3·4H_2O). To a well-stirred solution of H_3L^1·3H_2O (100 mg, 0.225 mmol) in 10% aq. HCOOH (10 ml), paraformaldehyde (26.5 mg, 0.88 mmol) was added; the reaction mixture was refluxed for 5 h and analysed by ^{1}H NMR. To the reaction mixture, more paraformaldehyde (26.5 mg, 0.88 mmol) was added and the reaction mixture was refluxed for 5 h (this procedure was then repeated once more). After the reaction was completed, the solution was filtered and the filtrate was concentrated *in vacuo*. The residue was dissolved in a small amount of distilled water and evaporated under reduced pressure (this procedure was then repeated three more times) to give H_3L^3 (95 mg) as a yellow oil. The crude product was purified by crystallization from hot EtOH to give H_3L^3·4H_2O (78 mg, 71%) as a white powder.

^{1}H NMR (600.2 MHz, D_2O, pD = 4.8, Fig. S21†): δ 2.87–2.90 (2H, m, CH_2); 2.93 (6H, s, N(CH_3)$_2$); 2.96 (2H, t, $^3J_{HH}$ = 6.0 Hz, NCH_2CH_2N(CH$_3$)$_2$); 3.05–3.08 (4H, m, CH_2); 3.13–3.17 (2H, m, CH_2); 3.27 (2H, t, $^3J_{HH}$ = 6.0 Hz, CH_2N(CH$_3$)$_2$); 3.36 (2H, s, CH_2CO$_2$); 3.38–3.40 (2H, m, CH_2); 3.47–3.56 (6H, m, CH_2); 3.88 (4H, AB-multiplet, CH_2CO$_2$).

^{13}C{^{1}H} NMR (150.9 MHz, D_2O, pD = 4.8, Fig. S22†): δ 44.32 (2C, N(CH_3)$_2$); 48.08 (1C, CH_2, NCH_2CH_2N(CH_3)$_2$); 48.70 (2C, CH_2); 49.14 (2C, CH_2); 51.32 (2C, CH_2); 52.68 (2C, CH_2); 55.63 (1C, CH_2CO_2); 56.08 (1C, CH_2N(CH$_3$)$_2$); 57.49 (2C, CH_2CO_2); 170.51 (2C, CH_2CO_2); 177.96 (1C, CH_2CO_2).

MS-ESI: (+): 456.9 ([M + K]$^+$, calcd 456.2).

Elemental analysis: found (calcd for $C_{18}H_{43}N_5O_{10}$, M_r = 489.6) C: 44.29 (44.16), H: 8.86 (8.85), N: 14.14 (14.31).

Syntheses of Ln(III) complexes. The Ln(III) complexes of H_3L^1, H_3L^2 and H_3L^3 for NMR, NMR CEST and MRI CEST experiments were prepared by mixing the lanthanide(III) chloride (Eu^{3+}, Yb^{3+}, La^{3+}) with 1.1 equiv. of the ligand in a small amount of distilled water, adjusting to pH 6 with 1 M aq. LiOH, and stirring overnight at 60 °C. Then the pH was re-adjusted to 6.5 with 1 M aq. LiOH and the solution was stirred overnight at 60 °C.

Eu^{3+}–H_3L^1. MS-ESI: (+): 540.1 ([M + H]$^+$, calcd 540.2); 562.1 ([M + Na]$^+$; calcd 562.1). (−): 573.9 ([M + Cl]$^-$, calcd 574.1).

Yb^{3+}–H_3L^1. MS-ESI: (+): 561.1 ([M + H]$^+$, calcd 561.2); 683.1 ([M + Na]$^+$; calcd 683.2). (−): 594.9 ([M + Cl]$^-$, calcd 595.1).

Eu^{3+}–H_3L^2. MS-ESI: (+): 553.6 ([M + H]$^+$, calcd 554.2). (−): 587.7 ([M + Cl]$^-$, calcd 588.1).

Yb^{3+}–H_3L^2. MS-ESI: (+): 581.8 ([M + Li]$^+$, calcd 581.2). (−): 609.6 ([M + Cl]$^-$, calcd 609.1).

Eu^{3+}–H_3L^3. MS-ESI: (+): 574.7 ([M + Li]$^+$, calcd 574.2). (−): 602.6 ([M + Cl]$^-$, calcd 602.1).

Yb^{3+}–H_3L^3. MS-ESI: (+): 595.8 ([M + Li]$^+$, calcd 595.2). (−): 623.6 ([M + Cl]$^-$, calcd 623.1).

X-Ray diffraction

Single-crystals of H_3L^1·5H_2O were prepared by slow evaporation of the aqueous solution. The crystals of H_3L^2·6H_2O were prepared by evaporation of the ethanolic solution, and the crystals of H_3L^3·3.5H_2O were prepared by the slow cooling of a saturated hot ethanolic solution. The Yb^{3+}–H_3L^1 complex for crystallization was prepared by mixing the ligand with 1.1 equiv. of the $YbCl_3$ in a small amount of distilled water. The pH was adjusted to ~6 with 1 M NaOH, and the mixture was stirred overnight at 60 °C. Then the pH was re-adjusted to 6.5 and the solution was stirred overnight at 60 °C. The complex was purified on a Al_2O_3 column by chromatography. The pure product was eluted using a mixture of EtOH–H_2O–conc. aq. NH_3 (10 : 8 : 1). Single crystals of [Yb(L^1)]·5H_2O were prepared from a concentrated aqueous solution of the complex by slow diffusion of the THF vapours.

The diffraction data were collected by employing a ApexII CCD diffractometer using Mo-K$_\alpha$ radiation (λ = 0.71073 Å) at 150(1) K and analyzed using the SAINT V8.27B (Bruker AXS Inc., 2012) program package. The structures were solved by direct methods (SHELXS97[24]) and refined by full-matrix least-squares techniques (SHELXL97[25]). The relevant data for the structures have been provided.†

Crystal data

H_3L^1·5H_2O: $C_{16}H_{41}N_5O_{11}$, M = 479.54, monoclinic, a = 7.80380(10), b = 16.7236(3), c = 17.8081(3) Å, β = 92.1431(12)°, U = 2322.47(6) Å^3, space group $P2_1/c$, Z = 4, 5358 total reflections, 4408 intense reflections, $R_1[I > 2\sigma(I)]$ = 0.0344, wR_2(all data) = 0.0873. CCDC 952386.† All non-hydrogen atoms were refined anisotropically. Although all hydrogen atoms could be found in the electron difference map, those bound to carbon atom were fixed in theoretical positions using a riding model with U_{eq}(H) = 1.2U_{eq}(C) to keep the number of refined parameters low. Hydrogen atoms bound to nitrogen or oxygen atoms were fully refined.

H_3L^2·6H_2O: $C_{17}H_{45}N_5O_{12}$, M = 511.58, monoclinic, a = 9.4479(7), b = 17.7199(14), c = 15.5379(9) Å, β = 106.573(2)°, U = 2493.2(3) Å^3, space group $P2_1/n$, Z = 4, 5723 total reflections, 4765 intense reflections, $R_1[I > 2\sigma(I)]$ = 0.0415, wR_2(all data) = 0.1129. CCDC 952384.† The strategy of refinement was the same as that described in the previous case. Beside this, several solvate water molecules were refined as twisted in two positions with some disordered hydrogen atoms in two positions with half-occupancy.

H_3L^3·3.5H_2O: $C_{18}H_{42}N_5O_{9.50}$, M = 480.57, monoclinic, a = 7.4798(2), b = 15.9561(4), c = 20.0951(6) Å, β = 91.5670(10)°,

U = 2397.42(11) Å^3, space group $P2_1/n$, Z = 4, 5503 total reflections, 4686 intense reflections, $R_1[I > 2\sigma(I)]$ = 0.0370, wR_2-(all data) = 0.0952. CCDC 952385.† The refining strategy was the same as described above.

[Yb(**L**^{1})]·5H_2O: $C_{16}H_{38}N_5O_{11}Yb$, M = 649.55, monoclinic, a = 16.8708(7), b = 7.5238(4), c = 18.4880(9) Å, β = 90.4230(10)°, U = 2346.7(2) Å^3, space group $P2_1/c$, Z = 4, 5374 total reflections, 5160 intense reflections, $R_1[I > 2\sigma(I)]$ = 0.0137, wR_2(all data) = 0.0306. CCDC 933967.† Preliminary refinement revealed a number of different maxima of the electronic density, which were located close to the carbon and nitrogen atoms of the macrocyclic part of the molecule. It pointed to a disorder of the macrocycle in a similar way as already reported in the literature (see, *e.g.*, ref. 20*c*, Fig. S9†). It was successfully modelled using the anisotropic refinement of atoms occupying positions with a higher occupancy, whilst the less occupied part was refined in isotropic mode. All other non-hydrogen atoms were refined anisotropically. Although hydrogen atoms could be found in the electron difference map, they were fixed in theoretical (C–H) or original (N–H, O–H) positions using the riding model with U_{eq}(H) = 1.2U_{eq}(X) to keep the number of refined parameters low.

HPLC

The analytical HPLC system consisted of a gradient pump Beta 10 (ECOM) equipped with a mixer Knauer A0285 and dual UV-detector (ECOM). Analysis was performed on a LunaPHC8 column (150 × 4.6 mm, Phenomenex, the flow rate 1 ml min^{-1}). The mobile phase was continuously vacuum degassed in a DG 3014 degasser (ECOM) and it was mixed in the gradient pump from the stock solutions. The detector wavelengths were set to 210 and 254 nm. Injection volumes were 20 µl (concentrations of the samples were 1 mg ml^{-1}).

The preparative HPLC system was composed of a gradient pump LCD 50 K (ECOM) and UV-Vis detector LCD 2083 (ECOM). Preparation was performed on a LunaPHC8 (250 × 21.1 mm, Phenomenex, the flow rate was maintained at 20 ml min^{-1}). The detector wavelengths were set to 210 nm. The mobile phase was prepared separately and degassed using an ultrasound probe (Cole-Parmer 750-Watt Ultrasonic Homogenizer). Injection volumes were 1 ml. The collection and processing of the data was performed using Clarity (DataApex) software.

Potentiometry

Potentiometric titrations[26] were carried out in a vessel thermostatted at 25.0 ± 0.1 °C, at a constant ionic strength (I = 0.1 M (Me_4N)Cl) using a PHM 240 pH-meter, a GK 2401B combined glass electrode and a 2 ml ABU 900 automatic piston burette (all Radiometer). The initial volume was *ca.* 5 ml and the ligand concentration in the titration vessel was *ca.* 0.004 M. An inert atmosphere was provided by the constant passage of argon saturated with the vapour of the solvent [0.1 M (Me_4N)Cl]. Extra HCl was added to the starting solution to run titrations in the −log[H$^+$] range 2.0–12.0 (for protonation constants) and 1.8–6.0 for the Gd^{3+} and La^{3+} stability constants. Titrations were performed with a (Me_4N)OH solution. Titrations with metal ions were performed at metal-to-ligand molar ratios of 1 : 1. Ligand titrations consisted of about 40 points per titration and were run in triplicate. As the complexation was too slow for conventional titration, the "out-of-cell" method was used;[26] about 25 points per titration, two parallel titrations, three weeks at room temperature for equilibration. To calculate the protonation constants of the ligand and the stability constants of the complexes, the OPIUM[27] software package was used.

The overall protonation constants β_{h10} are concentration constants defined as $\beta_{h10} = [H_hL]/[H]^h\cdot[L]$ (they can be transferred into stepwise dissociation constants as $pK_A(H_hL) = \log \beta_h - \log \beta_{h-1}$). The concentration stability constants β_{hlm} are generally defined by $\beta_{hlm} = [H_hL_lM_m]/([H]^h\cdot[L]^l\cdot[M]^m)$. The value of p$K_w$ used was 13.81.

^{1}H NMR titrations

The ^{1}H NMR titration over the whole pH region (31 points), for determination of the protonation constants, was performed at 25 °C (ligand concentration: 0.05 M; no ionic strength control) in H_2O on a Brucker Avance (III) 600 (B_0 = 14.1 T), using 5 mm sample tubes. ^{1}H NMR spectra were measured without presaturation of the water signal. A coaxial capillary with D_2O (for the lock) and *t*-BuOH (as external standard; δ_H = 1.25 ppm) was used. The solution pH (0.5–13.5) was adjusted with aqueous HCl or NMe_4OH solutions and measured with a combined glass electrode (Mettler Toledo) and pH-meter (3505 pH Meter, JENWAY) calibrated with standard buffers. Protonation constants were calculated with the OPIUM software package.[27]

CEST experiments

All Z-spectra were recorded on a VNMRS300 operating at 299.9 MHz (B_0 = 7.05 T), using 5 mm sample tubes and a coaxial capillary with D_2O and *t*-BuOH as the external standard. Samples were of 25–100 mM concentration in the mixture of H_2O and D_2O (1 : 10) or in H_2O; pH was adjusted with aqueous HCl or LiOH solutions. Standard pulse sequences for presaturation experiments were used. Saturation offsets were set using the array-function (increment 200–250 Hz). Other measurement parameters are listed below each figure.

MRI CEST images were measured with phantoms consisting of one vial containing an aqueous solution of the La^{3+}-complex as a control and eight (resp. five) vials containing aqueous solution of Eu^{3+} or Yb^{3+}-complexes with different pH values or concentrations. All MRI CEST images were acquired on a 4.7 T scanner (Bruker BioSpec, Germany) using RARE (Rapid Acquisition with Refocused Echoes) or MSME (Multi Slice Multi Echo) pulse sequences with presaturation pulse. Experimental conditions: TR = 5000 ms, TE = 8.9 ms, resolution 0.35 × 0.35 × 2 mm, turbo factor = 4 (in RARE sequence). Other measurement parameters are listed below each figure. Parameters of presaturation pulse: B_1 = 20 µT, satdly = 2 s. For all MR experiments, the resonator coil was used.

All MR images were processed using an in-house program, written in Matlab (The Mathworks Inc, USA), where the signal intensity was normalized to unit slope and receiver gain. Then the difference image between the images acquired with negative and positive frequency offset of the saturation frequency was calculated. Difference images were analysed using ImageJ software (NIH, USA), regions of interest were outlined manually.

Conclusions

We prepared 2-aminoethyl derivatives of DO3A and showed that the coordinated amino group mediates NMR saturation transfer to the bulk water. We suggest a new mechanism for the PARACEST effect, consisting of the coordination–decoordination of the amino group having an optimal rate, combined with the very fast protonation–deprotonation of the group while the group is non-bound to the paramagnetic metal ion. The pH-dependence of the saturation transfer parallels with the abundance of the species with the coordinated amino group. This novel type of PARACEST agent broadens the arsenal of pH-sensitive probes for possible *in vivo* pH measurements by MRI.

Acknowledgements

We thank J. Plutnar and Z. Tošner for their help with the setting of the CEST pulse sequences. The financial support of the Ministry of Education of the Czech Republic (no. MSM0021620857), the Grant Agency of the Czech Republic (no. 207/11/1437) and the Grant Agency of the Charles University (no. 110213) is acknowledged.

Notes and references

1 (*a*) P. Caravan, J. J. Ellison, T. J. McMurry and R. B. Lauffer, *Chem. Rev.*, 1999, **99**, 2293–2352; (*b*) P. Hermann, J. Kotek, V. Kubíček and I. Lukeš, *Dalton Trans.*, 2008, 3027–3047; (*c*) C. F. G. C. Geraldes and S. Laurent, *Contrast Media Mol. Imaging*, 2009, **4**, 1–23.

2 (*a*) J. Zhou and P. C. M. van Zijl, *Prog. Nucl. Magn. Reson. Spectrosc.*, 2006, **48**, 109–136; (*b*) Y. Wu, M. Evbuomwan, M. Melendez, A. Opina and A. D. Sherry, *Future Med. Chem.*, 2010, **2**, 351–366; (*c*) E. Terreno, D. D. Castelli and S. Aime, *Contrast Media Mol. Imaging*, 2010, **5**, 78–98; (*d*) P. C. M. van Zijl and N. N. Yadav, *Magn. Reson. Med.*, 2011, **65**, 927–948; (*e*) G. Liu, X. Song, K. W. Y. Chan and M. T. McMahon, *NMR Biomed.*, 2013, **26**, 810–828.

3 (*a*) S. Zhang, M. Merritt, D. E. Woessner, R. E. Lenkinski and A. D. Sherry, *Acc. Chem. Res.*, 2003, **36**, 783–790; (*b*) M. Woods, D. E. Woessner and A. D. Sherry, *Chem. Soc. Rev.*, 2006, **35**, 500–511; (*c*) S. Viswanathan, Z. Kovács, K. N. Green, S. J. Ratnakar and A. D. Sherry, *Chem. Rev.*, 2010, **110**, 2960–3018; (*d*) T. C. Soesbe, Y. Wu and A. D. Sherry, *NMR Biomed.*, 2013, **26**, 829–838.

4 S. Zhang and A. D. Sherry, *J. Solid State Chem.*, 2003, **171**, 38–43.

5 M. Woods, A. Pasha, P. Zhao, G. Tireso, S. Chowdhury, G. Kiefer, D. E. Woessner and A. D. Sherry, *Dalton Trans.*, 2011, **40**, 6759–6764.

6 S. Zhang, K. Wu, M. C. Biewer and A. D. Sherry, *Inorg. Chem.*, 2001, **40**, 4284–4290.

7 S. Zhang, L. Michaudet, S. Burgess and A. D. Sherry, *Angew. Chem., Int. Ed.*, 2002, **41**, 1919–1921.

8 (*a*) C.-H. Huang and J. R. Morrow, *Inorg. Chem.*, 2009, **48**, 7237–7243; (*b*) C.-H. Huang and J. R. Morrow, *J. Am. Chem. Soc.*, 2009, **131**, 4206–4207; (*c*) C.-H. Huang, J. Hammell, S. J. Ratnakar, A. D. Sherry and J. R. Morrow, *Inorg. Chem.*, 2010, **49**, 5963–5970; (*d*) J. Hammell, L. Buttarazzi, C.-H. Huang and J. R. Morrow, *Inorg. Chem.*, 2011, **50**, 4857–4867; (*e*) D. D. Castelli, E. Terreno and S. Aime, *Angew. Chem., Int. Ed.*, 2011, **50**, 1798–1800.

9 S. J. Dorazio, P. B. Tsitovich, K. E. Siters, J. A. Spernyak and J. R. Morrow, *J. Am. Chem. Soc.*, 2011, **133**, 14154–14156.

10 (*a*) S. J. Dorazio and J. R. Morrow, *Inorg. Chem.*, 2012, **51**, 7448–7450; (*b*) S. J. Dorazio, P. B. Tsitovich, S. A. Gardina and J. R. Morrow, *J. Inorg. Biochem.*, 2012, **117**, 212–219; (*c*) P. B. Tsitovich and J. R. Morrow, *Inorg. Chim. Acta*, 2012, **393**, 3–11.

11 A. O. Olatunde, S. J. Dorazio, J. A. Spernyak and J. R. Morrow, *J. Am. Chem. Soc.*, 2012, **134**, 18503–18505.

12 (*a*) B. Yoo and M. D. Pagel, *J. Am. Chem. Soc.*, 2006, **128**, 14032–14033; (*b*) G. Liu, Y. Li and M. D. Pagel, *Magn. Reson. Med.*, 2007, **58**, 1249–1256; (*c*) T. Chauvin, P. Durand, M. Bernier, H. Meudal, B.-T. Doan, F. Noury, B. Badet, J.-C. Beloeil and É. Tóth, *Angew. Chem., Int. Ed.*, 2008, **47**, 4370–4372; (*d*) T. Chauvin, S. Torres, R. Rosseto, J. Kotek, B. Badet, P. Durand and É. Tóth, *Chem.–Eur. J.*, 2012, **18**, 1408–1418; (*e*) V. R. Sheth, G. Liu, Y. Li and M. D. Pagel, *Contrast Media Mol. Imaging*, 2012, **7**, 26–34; (*f*) V. R. Sheth, Y. Li, L. Q. Chen, C. M. Howison, C. A. Flask and M. D. Pagel, *Magn. Reson. Med.*, 2012, **67**, 760–768.

13 (*a*) J. A. Duimstra, F. J. Femia and T. J. Meade, *J. Am. Chem. Soc.*, 2005, **127**, 12847–12855; (*b*) A. Mishra, J. Pfeuffer, R. Mishra, J. Engelmann, A. K. Mishra, K. Ugurbil and N. K. Logothetis, *Bioconjugate Chem.*, 2006, **17**, 773–780.

14 A. K. Mishra and J.-F. Chatal, *New J. Chem.*, 2001, **25**, 336–339.

15 G. B. Giovenzana, R. Negri, G. A. Rolla and L. Tei, *Eur. J. Inorg. Chem.*, 2012, 2035–2039.

16 M. Meyer, V. Dahaoui-Gindrey, C. Lecomte and R. Guilard, *Coord. Chem. Rev.*, 1998, **178–180**, 1313–1405.

17 K. Kumar, C. A. Chang, L. C. Francesconi, D. D. Dischino, M. F. Malley, J. Z. Gougoutas and M. F. Tweedle, *Inorg. Chem.*, 1994, **33**, 3567–3575.

18 S. Aime, M. Botta, M. Fasano, M. P. M. Marques, C. F. G. C. Geraldes, D. Pubanz and A. E. Merbach, *Inorg. Chem.*, 1997, **36**, 2059–2068.

19 (*a*) J. Rudovský, P. Cígler, J. Kotek, P. Hermann, P. Vojtíšek, I. Lukeš, J. A. Peters, L. Vander Elst and R. N. Muller, *Chem.–Eur. J.*, 2005, **11**, 2373–2384; (*b*) P. Lebdušková,

P. Hermann, L. Helm, É. Tóth, J. Kotek, K. Binnemans, J. Rudovský, I. Lukeš and A. E. Merbach, *Dalton Trans.*, 2007, 493–501; (*c*) T. Vitha, V. Kubíček, J. Kotek, P. Hermann, L. Vander Elst, R. N. Muller, I. Lukeš and J. A. Peters, *Dalton Trans.*, 2009, 3201–3214; (*d*) D. D. Castelli, M. C. Caligara, M. Botta, E. Terreno and S. Aime, *Inorg. Chem.*, 2013, **52**, 7130–7138.

20 (*a*) I. Lukeš, J. Kotek, P. Vojtíšek and P. Hermann, *Coord. Chem. Rev.*, 2001, **216–217**, 287–312; (*b*) P. Vojtíšek, P. Cígler, J. Kotek, J. Rudovský, P. Hermann and I. Lukeš, *Inorg. Chem.*, 2005, **44**, 5591–5599; (*c*) J. Kotek, J. Rudovský, P. Hermann and I. Lukeš, *Inorg. Chem.*, 2006, **45**, 3097–3102.

21 (*a*) A. Dadabhoy, S. Faulkner and P. G. Sammes, *J. Chem. Soc., Perkin Trans. 2*, 2002, 348–357; (*b*) D. A. Moore, *Org. Synth.*, 2008, **85**, 10–14.

22 D. D. Perrin and W. L. F. Armarego, *Purification of Laboratory Chemicals*, Pergamon Press, Oxford, 3rd edn, 1988.

23 N. Cesari, C. Biancalani, C. Vergelli, V. Dal Piaz, A. Graziano, P. Biagini, C. Ghelardini, N. Galeotti and M. P. Giovannoni, *J. Med. Chem.*, 2006, **49**, 7826–7835.

24 G. M. Sheldrick, *SHELXS97, Program for Crystal Structure Solution from Diffraction Data*, University of Göottingen, Göottingen, 1997.

25 G. M. Sheldrick, *SHELXL97, Program for Crystal Structure Refinement from Diffraction Data*, University of Göottingen, Göottingen, 1997.

26 (*a*) P. Táborský, P. Lubal, J. Havel, J. Kotek, P. Hermann and I. Lukeš, *Collect. Czech. Chem. Commun.*, 2005, **70**, 1909–1942; (*b*) M. Försterová, I. Svobodová, P. Lubal, P. Táborský, J. Kotek, P. Hermann and I. Lukeš, *Dalton Trans.*, 2007, 535–549.

27 M. Kývala and I. Lukeš, International Conference Chemometrics 95, p. 63, Pardubice, Czech Republic, 1995. Full version of "*OPIUM*" available (free of charge) on: http://web.natur.cuni.cz/~kyvala/opium.html.

APPENDIX 1

Electronic supplementary information (ESI)

for

Lanthanide(III) complexes of aminoethyl-DO3A as PARACEST contrast agents based on decoordination of the weakly bound amino group

Tereza Krchová,[a] Jan Kotek,[a]* Daniel Jirák,[b] Jana Havlíčková,[a] Ivana Císařová,[a] Petr Hermann[a]

[a] *Department of Inorganic Chemistry, Universita Karlova (Charles University), Hlavova 2030, 128 40 Prague 2, Czech Republic. Tel: +420-22195-1261. Fax: +420-22195-1253. E-mail: modrej@natur.cuni.cz.*

[b] *Department of Radiodiagnostic and Interventional Radiology, Magnetic Resonance Unit, Institute of Clinical and Experimental Medicine, Vídeňská 1958/9, 140 21 Prague 4, Czech Republic.*

Content:

Electronic Supplementary Material (ESI) for Dalton Transactions
This journal is © The Royal Society of Chemistry 2013

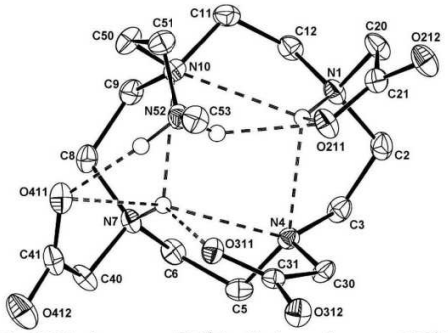

Fig. S1 Molecular structure of $H_3\mathbf{L}^2$·6H_2O found in the crystal structure of $H_3\mathbf{L}^2$·6H_2O. Dashed lines show system of intramolecular hydrogen bonds. Carbon-bound hydrogen atoms are omitted for sake of clarity.

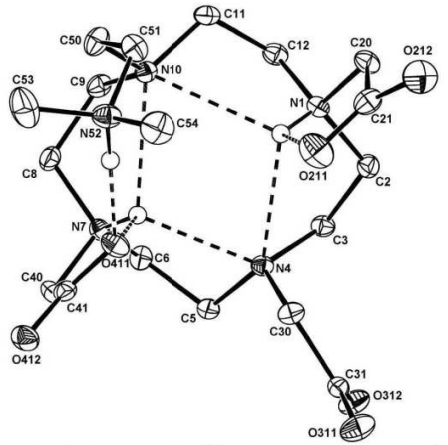

Fig. S2 Molecular structure of $H_3\mathbf{L}^3$·3.5H_2O found in the crystal structure of $H_3\mathbf{L}^3$·3.5H_2O. Dashed lines show system of intramolecular hydrogen bonds. Carbon-bound hydrogen atoms are omitted for sake of clarity.

Table S1 Torsion angles in the macrocyclic units found in the crystal structures of $H_3\mathbf{L}^1 \cdot 5H_2O$, $H_3\mathbf{L}^2 \cdot 6H_2O$ and $H_3\mathbf{L}^3 \cdot 3.5H_2O$.

Torsion angle, °	$H_3\mathbf{L}^1$	$H_3\mathbf{L}^2$	$H_3\mathbf{L}^3$
N1-C2-C3-N4	–49.71(13)	–47.30(16)	–53.54(13)
C2-C3-N4-C5	170.56(10)	168.61(12)	166.59(9)
C3-N4-C5-C6	–88.19(11)	–90.39(14)	–90.36(11)
N4-C5-C6-N7	–63.19(12)	–64.59(15)	–58.02(12)
C5-C6-N7-C8	153.42(10)	154.47(11)	159.90(9)
C6-N7-C8-C9	–73.43(12)	–73.59(14)	–76.06(12)
N7-C8-C9-N10	–58.24(13)	–55.17(16)	–58.50(13)
C8-C9-N10-C11	167.89(10)	167.82(12)	163.69(9)
C9-N10-C11-C12	–78.57(12)	–78.52(14)	–80.67(11)
N10-C11-C12-N1	–62.61(12)	–67.48(14)	–68.79(12)
C11-C12-N1-C2	159.05(9)	158.99(11)	160.83(9)
C12-N1-C2-C3	–76.48(12)	–73.82(15)	–66.10(12)

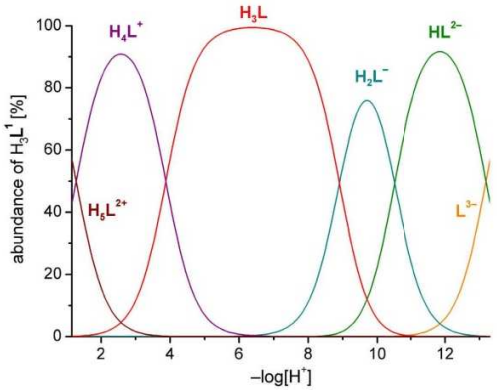

Fig. S3 The distribution diagram of $H_3\mathbf{L}^1$.

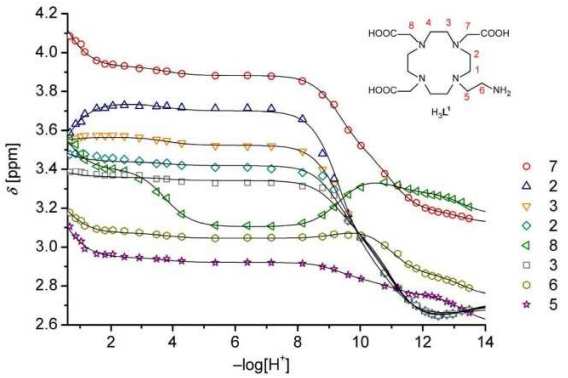

Fig. S4 pH dependence of δ_{1i} of $H_3\mathbf{L}^1$ (B_0 = 14.1 T, 25 °C). Dependence of chemical shifts of protons 1 and 4 were not included as they are overlapping with other signals. At pH below 9, individual protons of CH_2 groups 2 and 3 became nonequivalent resulting in two signals for each of groups.

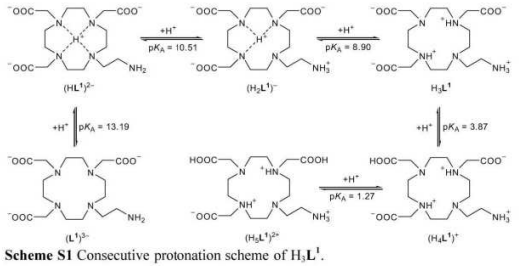

Scheme S1 Consecutive protonation scheme of $H_3\mathbf{L}^1$.

APPENDIX 1

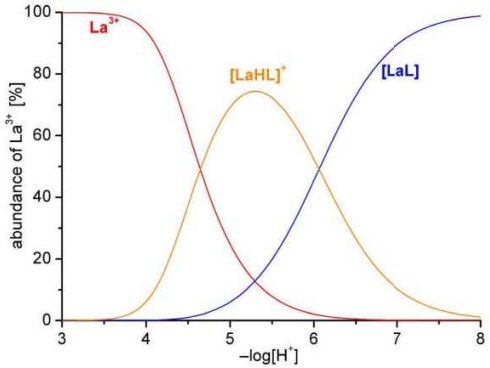

Fig. S5 Distribution diagram of the La^{3+}:$H_3\mathbf{L}^1$ ($c_M = c_L = 0.004$ M) system ($I = 0.1$ M $(NMe_4)Cl$, 25 °C); determined by potentiometry, L = $(\mathbf{L}^1)^{3-}$.

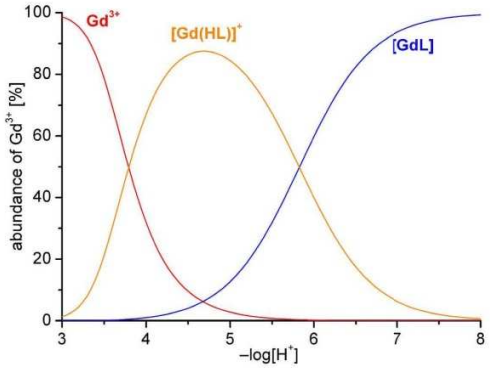

Fig. S6 Distribution diagram of the Gd^{3+}:$H_3\mathbf{L}^1$ ($c_M = c_L = 0.004$ M) system ($I = 0.1$ M $(NMe_4)Cl$, 25 °C); determined by potentiometry, L = $(\mathbf{L}^1)^{3-}$.

Electronic Supplementary Material (ESI) for Dalton Transactions
This journal is © The Royal Society of Chemistry 2013

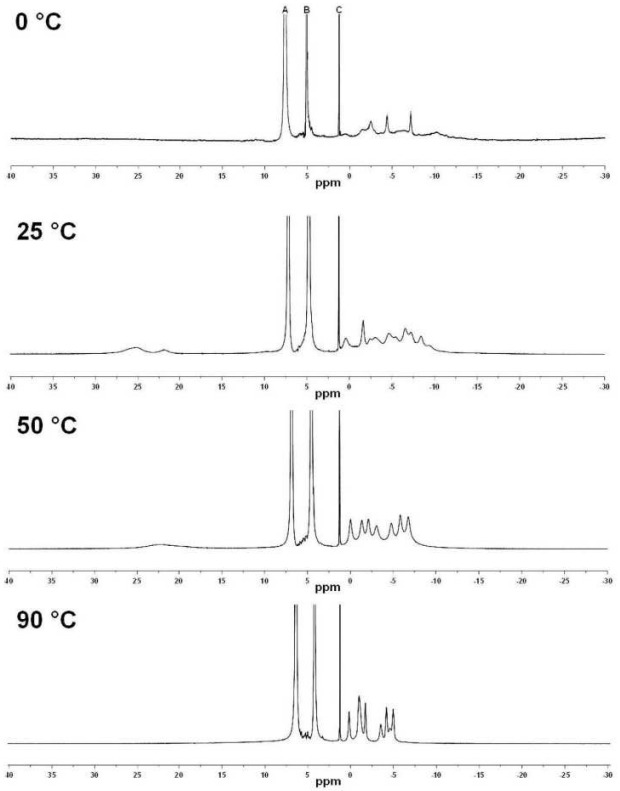

Fig. S7 ^{1}H NMR spectra of [Eu(H_2O)($\mathbf{L}^1$)] (0.1 M solution in D_2O, $B_0 = 7.05$ T for 25, 50 and 90 °C and 9.4 T for 0 °C; pD = 9.0). A coaxial capillary with D_2O and *t*-BuOH was used as external standard ($\delta_H = 1.25$ ppm). Signals assignment: A = HDO in sample solution, B = HDO in capillary, C = *t*-BuOH in capillary

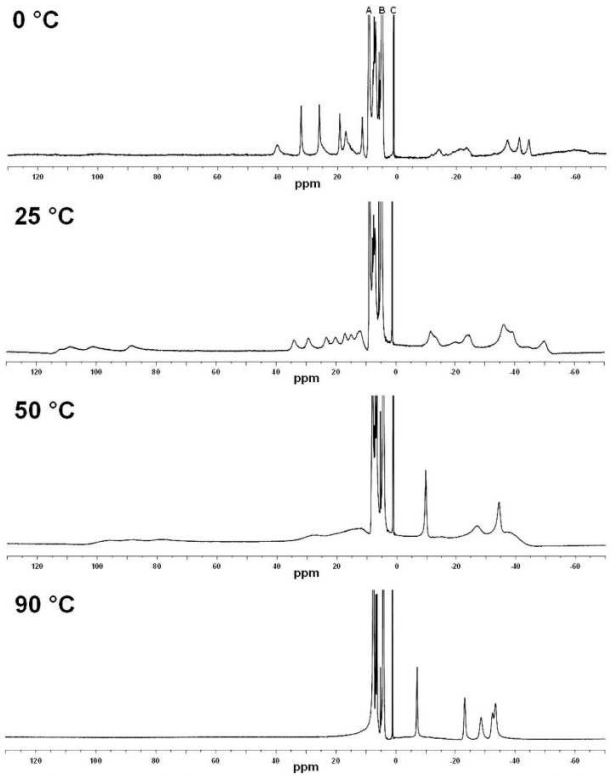

Fig. S8 ^{1}H NMR spectra of [Yb(**L^1**)] (0.1 M solution in D_2O, B_0 = 7.05 T for 25, 50 and 90 °C and 9.4 T for 0 °C; pD = 8.5). A coaxial capillary with D_2O and *t*-BuOH was used as external standard (δ_H = 1.25 ppm). Signals assignment: A = HDO in sample solution, B = HDO in capillary, C = *t*-BuOH in capillary.

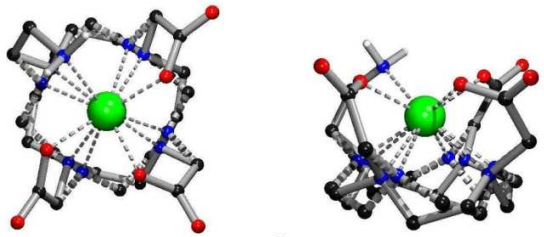

A **B**

Fig. S9 Disorder of the [Yb(L^1)] molecule found in the solid-state structure of [Yb(**L^1**)]·5H_2O. Figure shows overlay of both disordered complex species, more abundant (85 %) TSA' isomer is represented using solid bonds and less abundant (15 %) SA' isomer using dashed bonds. **A**: Top view. **B**: Side view. Carbon-bound hydrogen atoms are omitted for clarity reasons. Colour code: Yb – green; N – blue; O – red; C – black; H – grey.

Table S2 Geometric parameters of coordination sphere of Yb^{3+} ion in the crystal structure of [Yb(**L^1**)]·5H_2O.

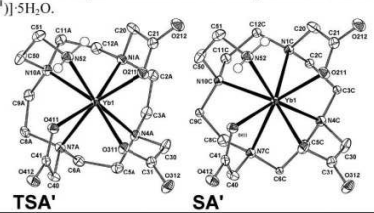

TSA' **SA'**

Coordination distances, Å		Distances from planes, Å	
N_4 plane of TSA' unit		NQA–OQ	2.5919
Yb1–N1A	2.519(2)	NQC–OQ	2.5042
Yb1–N4A	2.562(2)	Yb1–NQA	1.482(2)
Yb1–N7A	2.516(2)	Yb1–NQC	1.396(2)
Yb1–N10A	2.553(2)	Yb1–OQ	1.111(2)
N_4 plane of SA' unit		Dihedral angles of pendants in TSA' unit, °	
Yb1–N1C	2.535(12)	N1A-NQA-OQ-O211	–23.47(8)
Yb1–N4C	2.466(13)	N4A-NQA-OQ-O311	–23.90(8)
Yb1–N7C	2.498(13)	N7A-NQA-OQ-O411	–23.46(8)
Yb1–N10C	2.525(12)	N10A-NQA-OQ-N52	–19.15(8)
O_3N plane		Dihedral angles of pendants in SA' unit, °	
Yb1–O211	2.2707(12)	N1C-NQC-OQ-O211	–38.5(4)
Yb1–O311	2.2564(12)	N4C-NQC-OQ-O311	–38.8(4)
Yb1–O411	2.2764(12)	N7C-NQC-OQ-O411	–38.8(4)
Yb1–N52	2.4485(15)	N10C-NQC-OQ-N52	–34.3(4)

NQA – the centroid of the N_4-plane in TSA arrangement; NQC – the centroid of the N_4-plane in SA arrangement; OQ – the centroid of the O_3N-plane.

APPENDIX 1

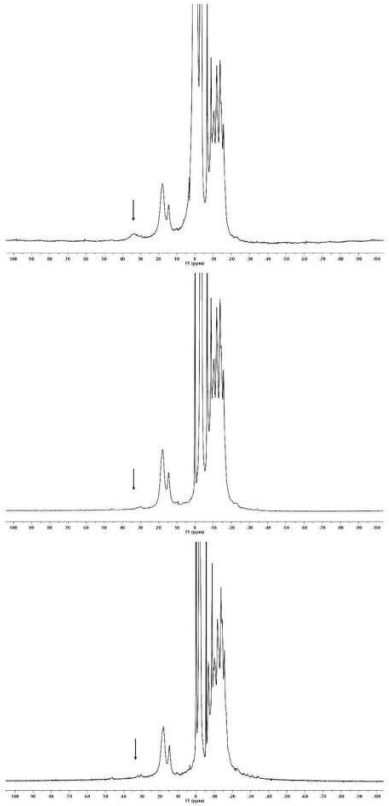

Fig. S10 A: ^{1}H NMR spectrum of [Eu(H_2O)(**L^1**)] (~1 M solution in H_2O, B_0 = 7.05 T, 25 °C, pH = 7.9). **B**: ^{1}H NMR spectrum of [Eu(H_2O)(**L^1**)] (~1 M solution in H_2O, B_0 = 7.05 T, 25 °C, pH = 7.9); water signal was saturated. **C**: ^{1}H NMR spectrum of [Eu(H_2O)(**L^1**)] (~1 M solution in D_2O, B_0 = 7.05 T, 25 °C, pD = 7.9). In all spectra, a coaxial capillary with D_2O and *t*-BuOH was used. Chemical shift of H_2O in solution was referenced to 0 ppm.

Electronic Supplementary Material (ESI) for Dalton Transactions
This journal is © The Royal Society of Chemistry 2013

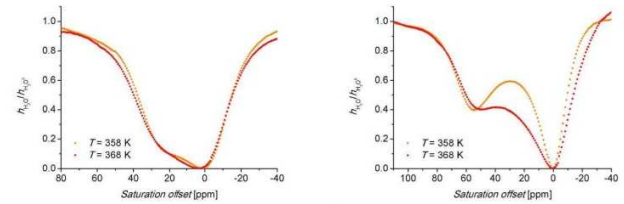

Fig. S11 Z-spectra of 70 mM aq. solution of **A**: [Eu(H_2O)(**L^1**)] and **B**: [Yb(**L^1**)] complexes (B_0 = 7.05 T, satpwr = 29 dB (~1000 Hz), satdly = 2 s) at pH = 7.40.

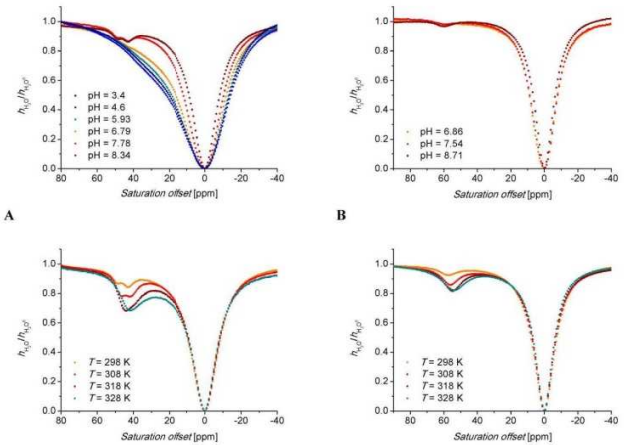

Fig. S12 A,**C**: Z-spectra of a 25 mM aq. solution (H_2O/D_2O 1:10) of [Eu(H_2O)(**L^2**)] complex (B_0 = 7.05 T, satpwr = 29 dB~1000 Hz, satdly = 2 s). **A**: T = 298 K. **C**: pH = 8.16. **B**,**D**: Z-spectra of a 25 mM (**B**) or 50 mM (**D**) aq. solution (H_2O/D_2O 1:10) of [Yb(**L^2**)] complex (B_0 = 7.05 T, satpwr = 29 dB~1000 Hz, satdly = 2 s). **B**: T = 298 K. **D**: pH = 8.35.

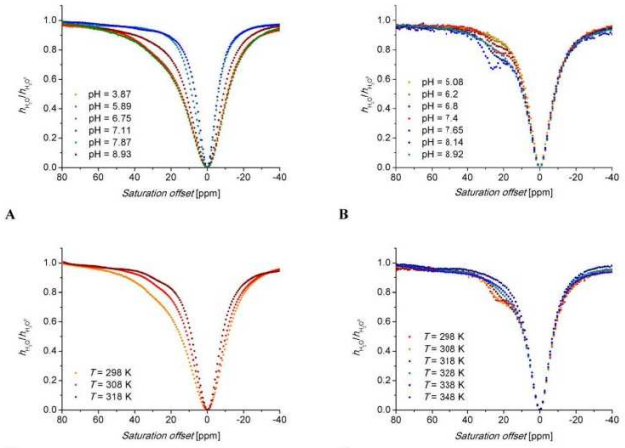

Fig. S13 A,**C**: Z-spectra of 25 mM aq. solution (H_2O/D_2O 1:10) of [Eu(H_2O)(**L**^{1})] complex (B_0 = 7.05 T, satpwr = 29 dB (~1000 Hz), satdly = 2 s); **A**: T = 298 K. **C**: pH = 5.40. **B**,**D**: Z-spectra of 50 mM aq. solutions (H_2O/D_2O 1:10) of the [Yb(**L**^{1})] complex (B_0 = 7.05 T, satpwr = 29 dB (~1000 Hz), satdly = 2 s); **B**: T = 298 K, **D**: pH = 7.72.

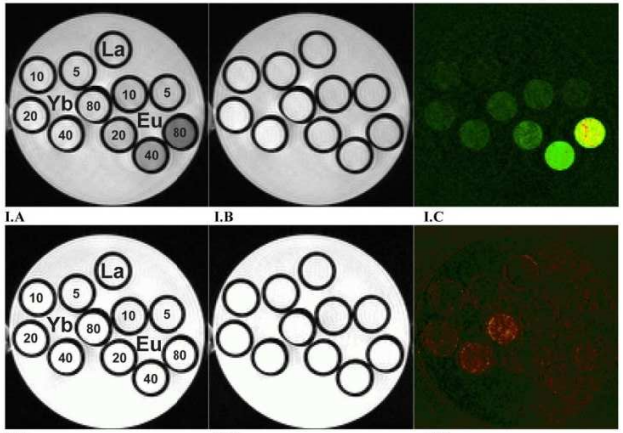

Fig. S14 MRI-CEST images of phantom consisting of one vial containing 80 mM aq. solution of [La(H_2O)(**L**^{1})] as a standard and five vials containing aqueous solution of [Eu(H_2O)(**L**^{1})] and [Yb(**L**^{1})] with different concentrations; pH = 7.4; concentrations (mM) are given as labels in figures **A**. Experimental conditions: RARE pulse sequence, B_0 = 4.7 T, B_1 = 20 μT, T = 293 K, satdly = 2 s, TR = 5 s, TE = 8.9 ms, scan time = 2 min. **I.A**: T_1-weighted image, satfrq = 34 ppm from the bulk water signal. **I.B**: T_1-weighted image, satfrq = –34 ppm from the bulk water signal. **I.C**: The difference between images **I.A** and **I.B** in false colours. **II.A**: T_1-weighted image, satfrq = 89 ppm from the bulk water signal. **II.B**: T_1-weighted image, satfrq = –89 ppm from the bulk water signal. **II.C**: The difference between images **II.A** and **II.B** in false colours.

APPENDIX 1

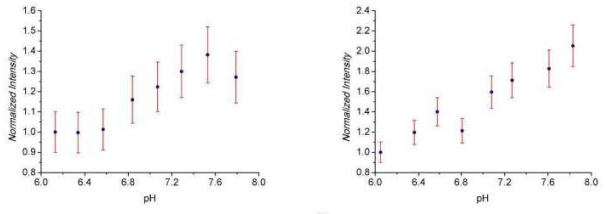

A **B**

Fig. S15 pH dependence of normalized intensity of the CEST effect (20 μT, MRI 4.7 T). **A**: [Eu(H_2O)(**L^1**)], data from Fig. 5-I.C. **B**: [Yb(**L^1**)], data from Fig. 5-II.C.

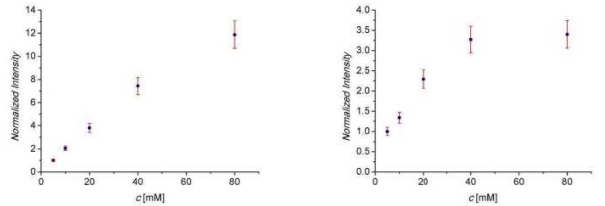

A **B**

Fig. S16 Concentration dependence of normalized intensity of the CEST effect (20 μT, MRI 4.7 T). **A**: [Eu(H_2O)(**L^1**)], data from Fig S14-I.C. **B**: [Yb(**L^1**)], data from Fig. S14-II.C.

Electronic Supplementary Material (ESI) for Dalton Transactions
This journal is © The Royal Society of Chemistry 2013

Characterization ^{1}H and ^{13}C{^{1}H} NMR spectra of the ligands

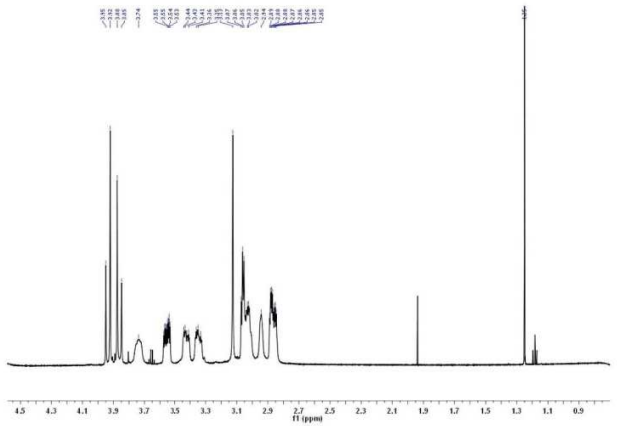

Fig. S17 ^{1}H NMR spectrum of H_3**L^1** in D_2O, pD = 5.4.

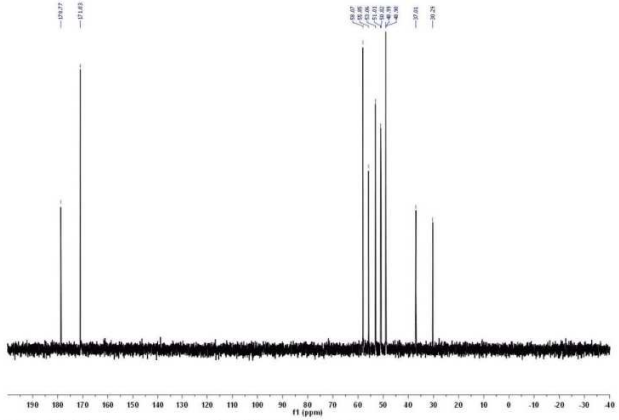

Fig. S18 ^{13}C{^{1}H} NMR spectrum of H_3**L^1** in D_2O, pD = 5.4.

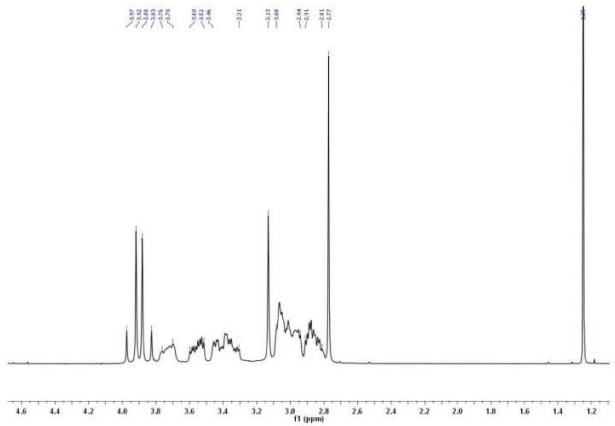

Fig. S19 ^{1}H NMR spectrum of $H_3\mathbf{L}^2$ in D_2O, pD = 5.3.

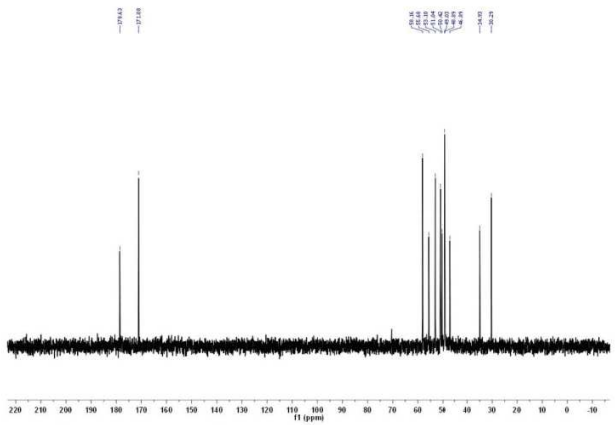

Fig. S20 ^{13}C NMR spectrum of $H_3\mathbf{L}^2$ in D_2O, pD = 5.6.

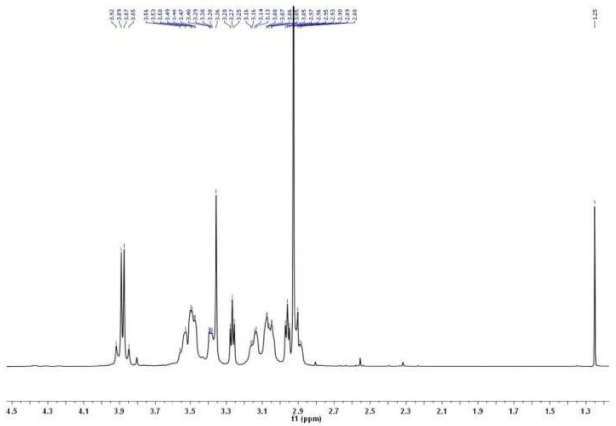

Fig. S21 ^{1}H NMR spectrum of $H_3\mathbf{L}^3$ in D_2O, pD = 4.8.

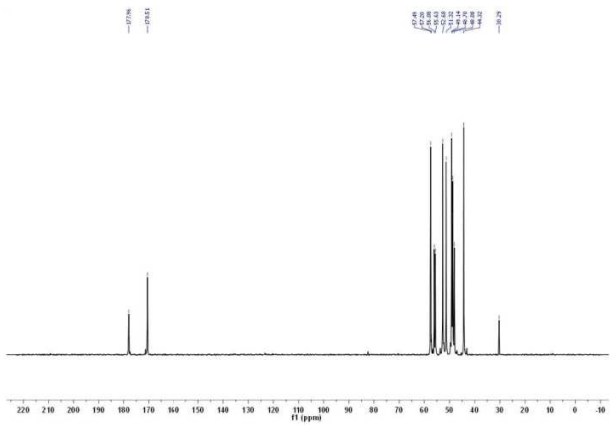

Fig. S22 ^{13}C{^{1}H} NMR spectrum of $H_3\mathbf{L}^3$ in D_2O, pD = 4.8.

APPENDIX 2

T. Krchová, A. Gálisová, D. Jirák, P. Hermann and J. Kotek: "Ln(III)-complexes of DOTA analogue with ethylenediamine pendant arm as pH-responsive PARACEST contrast agents", *Dalton Trans.*, 2016, **45**, 3486–3496

Dalton Transactions

PAPER

View Article Online
View Journal | View Issue

Cite this: *Dalton Trans.*, 2016, **45**, 3486

Ln(III)-complexes of a DOTA analogue with an ethylenediamine pendant arm as pH-responsive PARACEST contrast agents†

T. Krchová,[a] A. Gálisová,[b] D. Jirák,[b,c] P. Hermann[a] and J. Kotek*[a]

Received 11th November 2015,
Accepted 11th January 2016

DOI: 10.1039/c5dt04443j

www.rsc.org/dalton

A novel macrocyclic DO3A derivative containing a linear diamine pendant arm, H_3do3aNN, was prepared and its protonation and complexation properties were studied by means of potentiometry. It determined ligand consecutive protonation constants log K_{An} = 12.62, 10.28, 9.67, 8.30, 3.30 and 1.58 and stability constants of selected lanthanide (Eu(III), Yb(III)) complexes log K_{EuL} = 23.16 and log K_{YbL} = 22.76. The complexes could be protonated on the pendant amino group(s) with log K(HLM) ≈ 5.6 and log K(H_2LM) ≈ 4.8. Solution structures of both complexes were studied by NMR spectroscopy. The study revealed that the complex species exist exclusively in the form of twisted-square-antiprismatic (TSA) isomers. The complexes show significant pH dependence of the Chemical Exchange Saturation Transfer (CEST) between their amino groups and the bulk water molecules in the pH range of 5–8. Thus, the pH dependence of the magnetization transfer ratio of CEST signals can be used for pH determination using magnetic resonance imaging techniques in a pH range relevant for *in vivo* conditions.

Introduction

Magnetic resonance imaging (MRI), due to its non-invasive character and spatial resolution (down to a mm^3 at clinical magnetic fields), is currently one of the most important diagnostic methods used in clinical medicine.[1] Relevant diagnostic information from MRI images can be obtained even with the natural contrast between various tissues. However, for further improvement of image contrast and resolution, exogenous contrast agents (CAs) based on complexes of highly paramagnetic metal ions or superparamagnetic nanocrystalline materials altering the relaxation times of bulk water are widely used.[1,2] In addition to common MRI T_1- and T_2-contrast agents, which shorten the longitudinal (T_1) and transversal (T_2) relaxation times,[2] a new class of CAs based on a Chemical Exchange Saturation Transfer (CEST) mechanism was introduced in the past decade.[3,4]

The principle of the CEST effect is based on saturation of the proton signal of the contrast agent molecule by a selective radiofrequency pulse. This saturation is transferred to the surrounding water molecules *via* chemical exchange of the labile protons between the contrast agent and bulk water resulting in a decrease in the water signal intensity and, therefore, darkening of the corresponding area in the MR image. To reduce any nonspecific water proton irradiation and to increase the sensitivity of the CEST CAs, paramagnetic complexes (PARACEST agents) are used to shift the resonance frequency of the exchangeable protons far away from that of bulk water.[4–6] These agents contain a paramagnetic metal ion chelated by a multidentate ligand. Most often, Ln(III) complexes of ligands derived from DOTA (thus ensuring high stability and kinetic inertness of the complexes) have been used.[6,7] As alternatives, complexes of transition metal ions having suitable magnetic properties, such as Ni(II), Fe(II) or Co(II), with ligands based on cyclam, cyclen, 1,4,7-triazacyclononane or 1,4,10-trioxa-7,13-diazacyclopenta-decane, *etc.* have also been reported (Fig. 1).[8]

One of the major advantages of CEST agents is the possibility to modulate water signal intensity by a selective presaturation pulse and, therefore, image contrast produced by these CAs can be switched "on" or "off" at will by selecting the appropriate irradiation frequency. This fact makes it possible to detect several agents in the same sample.[9] Another advan-

[a]*Department of Inorganic Chemistry, Faculty of Science, Universita Karlova (Charles University), Hlavova 2030, 128 43 Prague 2, Czech Republic. E-mail: modrej@natur.cuni.cz; Fax: +420-221951253; Tel: +420-221951261*

[b]*Department of Radiodiagnostic and Interventional Radiology, Magnetic Resonance Unit, Institute for Clinical and Experimental Medicine, Vídeňská 1958/9, Prague 4, 140 21, Czech Republic*

[c]*Institute of Biophysics and Informatics, 1st Faculty of Medicine, Universita Karlova (Charles University), Salmovská 1, 120 00 Prague 2, Czech Republic*

†Electronic supplementary information (ESI) available: X-ray diffraction data, temperature- and pH-dependence of NMR spectra of studied compounds, additional *Z*-spectra and magnetization transfer ratio spectra of studied complexes, protonation and stability constants of studied ligand and its complexes, tentative structures of isomeric complex species with different protonation. CCDC 1430249. For ESI and crystallographic data in CIF or other electronic format see DOI: 10.1039/c5dt04443j

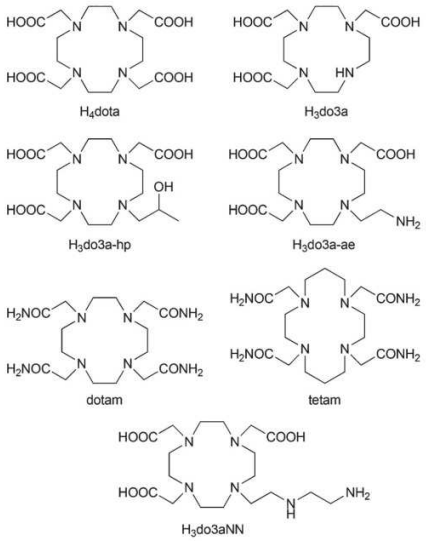

Fig. 1 Structural formulas of the ligands discussed in the text.

tage lies in the sensitivity of the proton exchange rate (k_{ex}) to a number of external factors and, thus, the CEST complexes are suitable for measuring various physiological parameters, such as temperature, pH, metabolite or metal ion concentration, *etc.*[4c,5,6]

Recently, a lot of effort has been invested into developing MRI CAs capable of reporting on *in vivo* changes of pH in a tissue as they could serve as valuable biomarkers of disease progression or indicators for the choice of treatment.[10] Several studies have demonstrated the unique ability of PARACEST CAs to act as pH sensors and nowadays ratiometric methods are being explored to make the assessments independent of the local concentration of the CAs.[11] For example, a Yb(III) analogue of the clinically approved MRI CA [Gd(do3a-hp)] (ProHance®, ligand shown in Fig. 1) shows two independent well-resolved PARACEST peaks at 71 and 99 ppm originating from the protons of the coordinated alcohol group of individual complex isomers.[11a] The ratio of these two PARACEST signals is pH-dependent, which can be used to develop a concentration-independent method of pH measurement, and the Yb(III) complex has been already tested for measuring extracellular pH in murine melanoma.[11b] Similarly, the PARACEST peaks of a Co(II) complex of tetam (Fig. 1) have distinct pH dependencies and the two most shifted signals (at 95 and 112 ppm) were shown to be suitable for pH mapping.[8e]

It was shown that Ln(III) complexes of cyclen derivatives with pendant arms containing an amido-amine pendant arm,[11g,h] or a (semi)coordinating amino group[12] produced a pH-sensitive PARACEST effect in the pH region relevant for living systems. Based on these findings, we decided to synthesize a new macrocyclic ligand H_3do3aNN (Fig. 1) containing a semi-labile coordinating pendant arm with two (primary and secondary) amino groups (as two potentially independent proton exchanging pools), and to investigate the PARACEST properties of its Ln(III) complexes.

Results and discussion

Synthesis

The synthesis of H_3do3aNN is shown in Scheme 1. The alkylation agent **3** was prepared by CBr_4/PPh_3 bromination of ethyl-carbamate-protected *N*-(2-aminoethyl)ethanolamine **2**. The alkylation of tBu$_3$do3a·HBr was performed using a slight excess of the alkylation agent as, under the reaction conditions, the alkylation agent undergoes elimination of HBr. The tBu-ester groups were removed by reflux in a CF_3CO_2H : $CHCl_3$ 1 : 1 mixture and the ethyl-carbamate protection groups were removed by hydrolysis in 10% aq. NaOH. Surprisingly, in this reaction step, preferential formation of the urea-derivative **6** was observed, with only trace amounts of the required compound H_3do3aNN. However, the intermediate **6** can be isolated by crystallization in a zwitterionic form with 42% overall yield (based on tBu$_3$do3a). The identity of the intermediate **6** was confirmed by a single-crystal X-ray diffraction study (see ESI and Fig. S1†). Hydrolysis of **6** with aq. HCl produced H_3do3aNN with a high yield. The best way to obtain the product in the solid form was trituration of the evaporated reaction mixture in dry THF or EtOH overnight. However, the resulting off-white solid is very hygroscopic and has to be

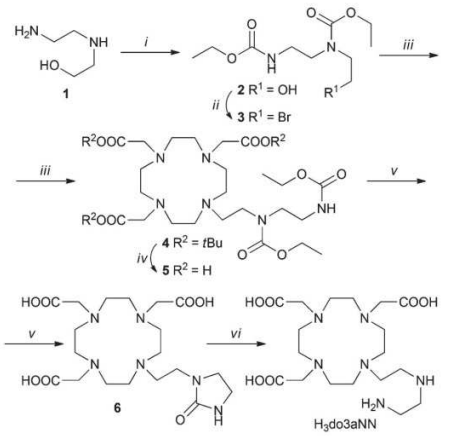

Scheme 1 Synthesis of H_3do3aNN. (i) $CH_3CH_2OC(O)Cl$, dioxane : H_2O (1 : 1), RT, 2 h; (ii) CBr_4, PPh_3, THF, RT, 1 h; (iii) tBu$_3$do3a·HBr, K_2CO_3, MeCN, 60 °C, 24 h; (iv) CF_3CO_2H : $CHCl_3$ (1 : 1), reflux 18 h; (v) 10% aq. NaOH, 90 °C, 24 h; (vi) aq. HCl (1 : 1), 95 °C, 7 d.

stored in a desiccator over P_2O_5. All other attempts (different organic solvents used for trituration or crystallization) led to the isolation of the title ligand as oil. To prevent possible esterification by EtOH, the use of THF was preferred for trituration.

Thermodynamic behaviour of H_3do3aNN and its Ln(III) complexes

Potentiometric titrations of the ligand performed in the pH range of 1.6–12.2 revealed six consecutive protonation processes in this region (Tables 1 and S1†). Based on comparison with the literature data,[12,13] the first protonation step ($\log K_P(HL) = 12.6$) can be attributed to the protonation of one of (or to sharing of a proton over several of) the macrocycle amino groups. The next three protonation steps proceed in part simultaneously due to the similarity of the constants ($\log K_P(H_2L) = 10.3$, $\log K_P(H_3L) = 9.7$ and $\log K_P(H_4L) = 8.3$) and occur on one other macrocycle amino group and two amino groups of the pendant *N*-(2-aminoethyl)-2-aminoethyl moiety (the value reported for analogous protonation of a 2-aminoethyl pendant moiety for H_3do3a-ae is $\log K_P = 8.9$).[12] Further protonations of H_3do3aNN proceed on the carboxylate groups and lie in the usual range.

Stability constants of [Ln(do3aNN)] (23.16 and 22.76 for the Eu(III) and Yb(III) complexes, respectively, Tables 1 and S2†) were obtained by the out-of-cell titration technique. The values are slightly lower compared with those reported for H_4dota itself, but lie in the expected range, as can be seen from a comparison with the values reported for the related ligand H_3do3a-ae – although, in that case, stability constants were determined for other lanthanides: La(III), $\log K_{LaL} = 20.02$, and Gd(III), $\log K_{GdL} = 22.23$.[12] However, according to the distribution diagram of the Eu(III)–H_3do3aNN system shown in Fig. 2, the metal complexation is not quantitative until pH ≈ 6 due to a combination of low affinity of the amino groups for Ln(III) ions and high donor-site basicity.

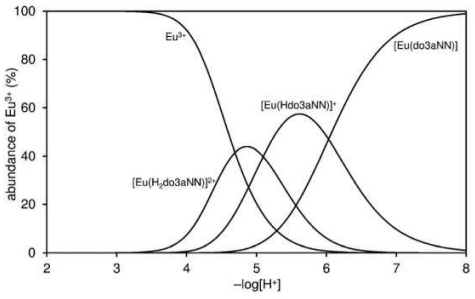

Fig. 2 Distribution diagram of metal-containing species in the Eu(III)–H_3do3aNN system ($c_M = c_L = 0.004$ M, 25 °C, $I = 0.1$ NMe_4Cl).

Equilibrated protonation steps of [Ln(do3aNN)] proceed with $\log K_P(HLM) = 6.03/6.22$ and those of the $[Ln(Hdo3aNN)]^+$ species occur with $\log K_P(H_2LM) = 5.09/5.07$ for the Eu(III)/Yb(III) complexes, respectively (Tables 1 and S2†). They are close to the values of analogous protonation constants reported for [Ln(do3a-ae)] complexes ($\log K_P(HLM) = 6.06$ and 5.83 for La(III)/Gd(III) systems).[12] The observed values are slightly higher than the protonation constants found for the pre-formed complexes under "non-equilibrium" conditions: in such experiments, complexes were pre-formed at pH ≈ 7 and were titrated employing the standard ("fast") acid–base titration method. The corresponding observed protonation constants were $\log K_P(HLM) = 5.57$ and 5.67, and $\log K_P(H_2LM) = 4.84$ and 4.85 for Eu(III)/Yb(III), respectively (Table S3†). From these slight differences between the protonation constants, one can conclude that, during out-of-cell titrations, protons in the $[Ln(Hdo3aNN)]^+$ and $[Ln(H_2do3aNN)]^{2+}$ species are probably located not only on the amine pendant arm but, at least

Table 1 Equilibrium constants ($\log K_P$ and $\log K_{ML}$)[a] of H_3do3aNN (0.1 M NMe_4Cl, 25 °C) and its complexes, and the comparison with corresponding constants reported for related ligands

Equilibrium	H_3do3aNN	H_3do3a-ae[b]	H_4dota	H_3do3a-hp[c]	H_3do3a[c]
$H^+ + L^{n-} \leftrightarrow HL^{1-n}$	12.62(2)	13.19	11.74[c]	11.17	12.46
$H^+ + L^{1-n} \leftrightarrow H_2L^{2-n}$	10.28(2)	10.51	9.76[c]	9.33	9.49
$H^+ + L^{2-n} \leftrightarrow H_3L^{2-n}$	9.67(2)	8.90	4.68[c]	4.99	4.26
$H^+ + L^{3-n} \leftrightarrow H_4L^{2-n}$	8.30(3)	3.87	4.11[c]	3.80	3.51
$H^+ + L^{4-n} \leftrightarrow H_5L^{2-n}$	3.30(3)	1.27	2.37[c]	2.84	1.97
$H^+ + L^{5-n} \leftrightarrow H_6L^{2-n}$	1.58(3)	—	—	—	—
$Eu^{3+} + L^{n-} \leftrightarrow [Eu(L)]^{3-n}$	23.16(5)	—	24.2[d]	—	—
$H^+ + [Eu(L)]^{3-n} \leftrightarrow [Eu(HL)]^{4-n}$	6.03(5)	—	—	—	—
$H^+ + [Eu(HL)]^{4-n} \leftrightarrow [Eu(H_2L)]^{5-n}$	5.09(7)	—	—	—	—
$Yb^{3+} + L^{n-} \leftrightarrow [Yb(L)]^{3-n}$	22.76(4)	—	24.0[d]	—	—
$H^+ + [Yb(L)]^{3-n} \leftrightarrow [Yb(HL)]^{4-n}$	6.22(4)	—	—	—	—
$H^+ + [Yb(HL)]^{4-n} \leftrightarrow [Yb(H_2L)]^{5-n}$	5.07(4)	—	—	—	—
$Gd^{3+} + L^{n-} \leftrightarrow [Gd(L)]^{3-n}$	—	22.23	24.67[c]	24.5	22.02

[a] $K_P = [H_hL]/\{[H]\cdot[H_{h-1}L]\}$ or $[H_hLM]/\{[H]\cdot[H_{h-1}LM]\}$; $K_{ML} = [ML]/\{[L]\cdot[M]\}$. [b] Ref. 12. [c] Ref. 13. [d] Ref. 14.

partly, also on the macrocycle amino groups. The suggested structures of individual species with tentative protonation sites are shown in Schemes S1 and S2.†

Unfortunately, the [Ln(do3aNN)] complexes are not fully kinetically inert, and slowly dissociate at pH < 6. This was confirmed by a xylenol orange test: after the addition of a solution of the pre-formed complex (at pH = 7.5) to a buffered solution of xylenol orange at pH = 5.5, the colour gradually changed on standing from orange to orange-violet as a result of free metal appearance in the solution. A quantitative measurement revealed the dissociation of about 9–10% of the complex after standing for one week at room temperature (compare Fig. S16 and S17†). From a thermodynamic point of view, the extent of complex dissociation should be less than 20% at pH = 5 (see the distribution diagram shown in Fig. 2). It was confirmed by independent experiments that neither the free metal aqua ion nor the free ligand interferes with the ^{1}H NMR or CEST measurements. Therefore, conclusions drawn from PARACEST experiments (see below) are fully valid even at pH 5–6.

Solution structure of the [Ln(H$_n$do3aNN)]‡ complexes

It is well-known that in Ln(III) complexes of DOTA-like ligands the central Ln(III) is coordinated between two planes – one formed by the macrocycle amino groups (N_4-plane), and the other by the oxygen atoms of the carboxylate pendant moieties (O_4-plane), and these species exhibit two types of isomerisms in solution.[15] The first type is connected with the conformation of the macrocycle ethylene bridges, *i.e.* with the sign of the torsion angle around the C–C bond (δ/λ), and the second one is related to the direction of rotation of the pendant arms (Δ/Λ). A combination of these isomerisms leads to the formation of two diastereomeric pairs of enantiomers (*i.e.* four isomers): ΔλλλλΛδδδδ (SA, square-antiprismatic) and ΔδδδδΛλλλλ (TSA, twisted-square-antiprismatic).[2] The isomer ratio in solution can be determined from the ^{1}H NMR spectra using the "axial" protons of the macrocyclic chelate ring, which are the ones closest to the Ln(III) ion and to the principal magnetic axis, and usually can be easily found in the ^{1}H NMR spectra.[16] Therefore, the solution structures of the [Eu(do3aNN)] and [Yb(do3aNN)] complexes were investigated by variable-temperature ^{1}H NMR spectroscopy (Fig. S2 and S3†). The pD of the samples in D_2O was adjusted to the alkaline region to ensure full deprotonation and coordination of the pendant amino group. In both complexes, only one set of signals was detected pointing to the presence of only one diastereomer. The signals of "axial" protons appear in the range typical for the TSA isomers (Eu(III): 9–13 ppm, Yb(III): 45–62 ppm; with respect to the signal of bulk water referenced to 0 ppm). No ^{1}H NMR signals of "axial" CH_2 protons attributable to an SA isomer were observed (such signals typically lie in the chemical shift regions of 25–40 ppm and 100–150 ppm for Eu(III) and Yb(III) complexes, respectively).[16,17] Thus, based on the ^{1}H NMR data, exclusive formation of the TSA isomer is expected. With increasing temperature, the ^{1}H NMR signals become broader, pointing to the occurrence of a conformational change of the complex molecules (Fig. S2 and S3†).

‡Such a formula is used when more species differing in protonation are present in a solution. For the range of *n* refer to the distribution diagram shown in Fig. 2.

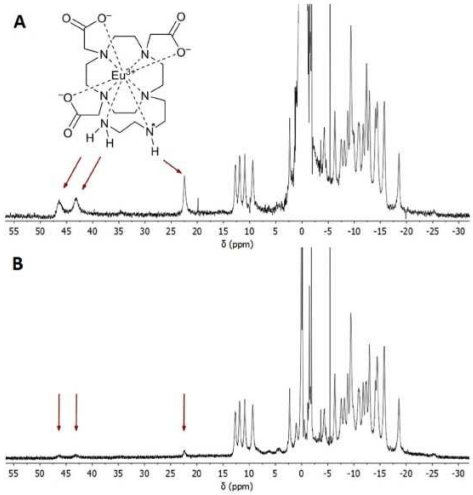

Fig. 3 (A) ^{1}H NMR spectrum of the [Eu(H$_n$do3aNN)] complex (0.09 M solution in H_2O, B_0 = 7.05 T, 25 °C, pH = 6.75). (B) The same sample, the signal of water was saturated. Arrows show the positions of exchangeable (N–H) protons. The chemical shift of H_2O in the sample solution was referenced to 0 ppm.

To identify the signals of exchangeable (N–H) protons in the ^{1}H NMR spectra, samples of the [Eu(H$_n$do3aNN)] and [Yb(H$_n$do3aNN)] complexes were investigated in H_2O at 25 and 5 °C (Fig. 3, 4, S4 and S5†). In the ^{1}H NMR spectra of the [Eu(H$_n$do3aNN)] complex recorded in H_2O at pH = 6.75 (Fig. 3A), three main signals of exchangeable protons (one narrow signal at 22.2 and two broad signals at 43.3 and 46.5 ppm; with respect to the bulk water signal) can be observed, which disappear upon bulk water presaturation (Fig. 3B). Of these, only the signals at 43.3 and 46.5 ppm are influenced by water presaturation at pH = 11.7, whilst the signal at 22.2 ppm remains unaffected (Fig. 4A and B). When recording ^{1}H NMR spectra in a D_2O solution (pD = 10.7), none of the three signals are observable (Fig. 4C and S2†). Based on this behaviour, the narrow signal at 22.2 ppm is attributed to the coordinated secondary amino group. The assignment is supported by the similarity of the chemical shift of this signal to that of one of the $-NH_2$ protons of the [Eu(do3a-ae)] complex (19.5 ppm).[12] The two broad signals are attributed to the coordinated primary amino group and this assignment is supported by their coalescence at higher temperatures (Fig. S6†).

The primary amino group is expected to be coordinated in a position capping the O_3N-plane formed by the pendant

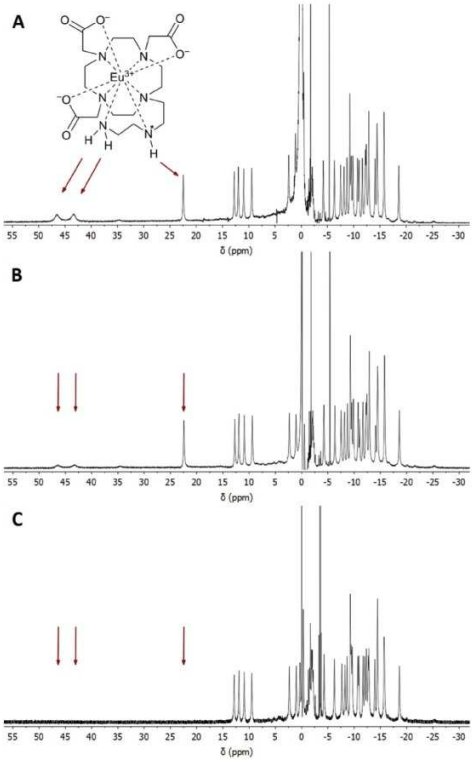

Fig. 4 (A) ^{1}H NMR spectrum of the [Eu(do3aNN)] complex in H_2O (0.09 M, B_0 = 7.05 T, 25 °C, pH = 11.70). (B) The same sample, the signal of water was saturated. (C) ^{1}H NMR spectrum of the [Eu(do3aNN)] complex in D_2O (0.04 M, B_0 = 7.05 T, 25 °C, pD = 10.73). Arrows show the positions of exchangeable (N–H) protons. The chemical shifts of H_2O/HDO in the sample solutions were referenced to 0 ppm.

donor atoms and, thus, close to the magnetic axis of the complex. Therefore, the corresponding protons are markedly influenced by the paramagnetic ion and their chemical shifts lie in the range typical for a coordinated water molecule.[5,18] However, the presence of these signals in ^{1}H NMR spectra also in an alkaline solution (and the presence of a corresponding CEST effect in *Z*-spectra at alkaline pH, see below) clearly excludes the possibility that these signals belong to a coordinated water molecule, the signal of which disappears in the alkaline region.[19] In slightly acidic solutions where protonation of the uncoordinated primary amino group (and thus, its decoordination) is expected, even a proton of the secondary amino group is exchanged with bulk water on an NMR time scale. In contrast, in an alkaline solution, only the exchange of the terminal primary amino group protons is observable.

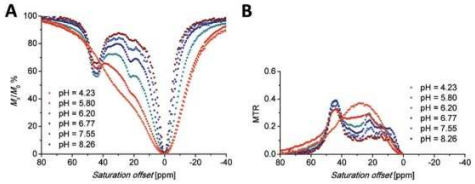

Fig. 5 (A) *Z*-Spectra of an 83 mM aqueous solution of the [Eu($H_n$do3aNN)] complex (B_0 = 7.05 T, B_1 = 21.7 μT (920 Hz), RF presaturation pulse applied for 2 s, 25 °C). (B) Corresponding MTR spectra.

Besides the three signals of exchangeable protons of the [Eu(do3aNN)] complex discussed above, a small signal at ≈35 ppm was found in the ^{1}H NMR spectra (Fig. 3 and 4), better seen at a lower temperature (37.5 ppm, Fig. S5A†).

At this chemical shift, a minor exchangeable pool of protons was found also in the CEST experiments (see discussion of *Z*-spectra below), accompanied by two other peaks in *Z*-spectra lying at 10 and 15 ppm, which are visible especially at low saturation power (Fig. 5 and S7A†). Due to the absence of any ^{1}H NMR signals of "axial" CH_2 protons attributable to the SA isomer, the presence of this isomer in the solution can be excluded. Therefore, these minor exchangeable proton pools were attributed to another TSA isomer that originates from the chirality of the nitrogen atom of the secondary amino group caused by coordination of this group. Judging by the similarity of the chemical shift of the exchangeable proton pool at 35 ppm to one of the signals attributed to the coordinated amino group in [Eu(do3a-ae)] (34 ppm),[12] one can suggest that this signal belongs to the secondary amino group of the TSA isomer with reverse orientation of H *vs.* the $CH_2CH_2NH_2$ substituents (*i.e.* with opposite chirality of the coordinated secondary amine). The results of simple molecular modelling shown in Fig. S9† suggest that apical coordination of the primary amino group is possible only in the Δδδδδ-S/Λλλλλ-R enantiomeric pair, and thus, this isomer is suggested to be the major one, leaving the Δδδδδ-R/Λλλλλ-S species as the minor isomer. In the case of this low-abundance isomer, the position of the primary amino group is not suitable for coordination close to the magnetic axis and, therefore, the signals of the primary amino group in *Z*-spectra are significantly closer (at 10 and 15 ppm, Fig. S7†) to the free water signal. As both protons of the primary amino group have individual signals, their resolution triggered by coordination or by fixing in an intramolecular hydrogen bond system is expected.

A similar behaviour was observed also for the [Yb(do3aNN)] complex. In an alkaline solution, there are two signals disappearing in D_2O, see Fig. S4† – a narrow signal of the proton of the secondary amino group at 35 ppm (this assignment is supported by the similarity of the chemical shift of the analogous ^{1}H NMR signal of [Yb(do3a-ae)], 42 ppm)[12] and a very broad signal of NH_2 protons at 82–104 ppm (the signals cannot be distinguished at 25 °C, but split at 5 °C, Fig. S5B†). As in the previous case, only the signal attributable to the primary

amino group is affected by water presaturation in an alkaline solution, Fig. S4B†. Minor signals of another TSA isomer are also observable in ^{1}H NMR spectra, and minor exchangeable pools of protons were found in CEST experiments at low saturation power (three other peaks in *Z*-spectra at 17, 26 and 57 ppm, Fig. S7B†).

CEST experiments

Saturation transfer experiments in solutions ranging from slightly acidic to slightly alkaline (pH 5.7–8.3) revealed two signals in the ^{1}H *Z*-spectra of each complex. These signals are centred at +22.2 and +44.4 ppm for the Eu(III) complex (Fig. 5A) and +35 and +95 ppm for the Yb(III) complex (Fig. 6A).

The broad signals at the higher chemical shifts (44.4 and 95 ppm for the Eu(III) and Yb(III) complex, respectively) correspond to the averaged signals of the primary amino group. This broad signal splits into two distinct signals of magnetically non-equivalent protons at a lower intensity of presaturation pulses and at low temperatures (Fig. S7A†), similar to the behaviour of this group found in ^{1}H NMR spectra (Fig. 3, 4, S5 and S6†). The *Z*-spectra signals with lower chemical shifts (22.2 and 35 ppm for the Eu(III) and Yb(III) complex, respectively) were attributed to the signal of the proton of the secondary amino group. Thus, the *Z*-spectra of both complexes clearly confirm the presence of proton-exchanging pools that belong to the protons of the primary and secondary amino groups as they were identified in the ^{1}H NMR spectra (see above).

Besides the signals attributable to the major isomer, a set of minor signals (at 10, 15 and 35 ppm, distinguishable especially when low saturation power was applied) appears in the *Z*-spectra of the [Eu(H$_n$do3aNN)] complex (Fig. S7A†). At slightly acidic to neutral pH, all three *Z*-signals are apparent. In contrast, in the alkaline region only the signals at 10 and 15 ppm remain in the *Z*-spectra, implying their assignment to the primary amino group, with the last one (at 35 ppm) belonging to the secondary amino group. These signals belong to the less abundant isomer with opposite chirality of the coordinated secondary amino group (see discussion of ^{1}H NMR spectra above). A similar set of minor signals (at 17, 26 and 57 ppm) appears also in the *Z*-spectra of the [Yb(H$_n$do3aNN)] complex (Fig. S7B†).

The shape of the *Z*-spectra of the [Ln(H$_n$do3aNN)] complexes (Ln = Eu, Yb) has significant pH dependence in slightly acidic to neutral regions (Fig. 5A and 6A). To see the differences in *Z*-spectra more clearly, the magnetization transfer ratio (MTR) spectra were constructed (Fig. 5B and 6B). At pH < 5.5, the CEST effect of the coordinated primary amino group gradually disappears as a consequence of protonation and decoordination of the group. Simultaneously, a new, very broad CEST signal appears centred at ≈25–30 ppm for both complexes. Although partial dissociation of the complexes occurs in this pH region (see above for discussion of thermodynamic properties), the free metal aqua ions as well as the free ligand are CEST-silent (as proved by an independent experiment) and, therefore, these new signals can be attributed to the chemical exchange of the protonated primary amino group of the complex. Such a group – whilst uncoordinated – is still paramagnetically shifted, but not as much as when the group is coordinated. On the other hand, an effective CEST of the secondary amino group was detected for the Eu(III) and Yb(III) complexes in the pH region of ≈5.5–8.5. At higher pH values, the chemical exchange of the NH proton becomes too slow to transfer saturation to bulk water and, thus, the CEST effect of the secondary amino group is not observable (Fig. 5A, 6A and S8†). It is consistent with the ^{1}H NMR spectra of the studied complexes (Fig. 4 and S4†), where the signals of secondary amino groups are observable even in alkaline solutions

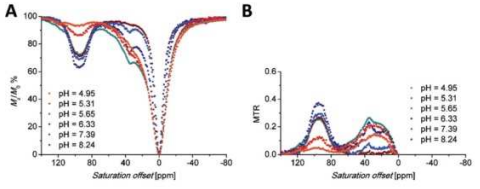

Fig. 6 (A) *Z*-Spectra of an 87 mM aqueous solution of the [Yb(H$_n$do3aNN)] complex (B_0 = 7.05 T, B_1 = 21.7 μT (920 Hz), RF presaturation pulse applied for 2 s, 25 °C). (B) Corresponding MTR spectra.

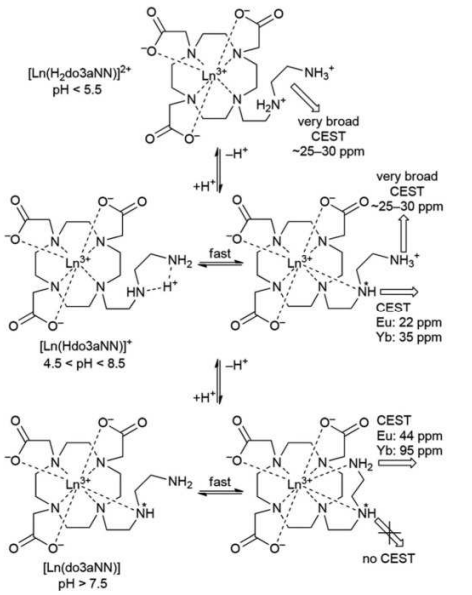

Scheme 2 A suggested mechanism of origin of pH-dependent CEST effects on [Ln(H$_n$do3aNN)] complexes. In hepta/octa-coordinated species, binding of a water molecule(s) to the central ion giving the coordination number to 8–9 is expected, but it is not shown for the sake of clarity.

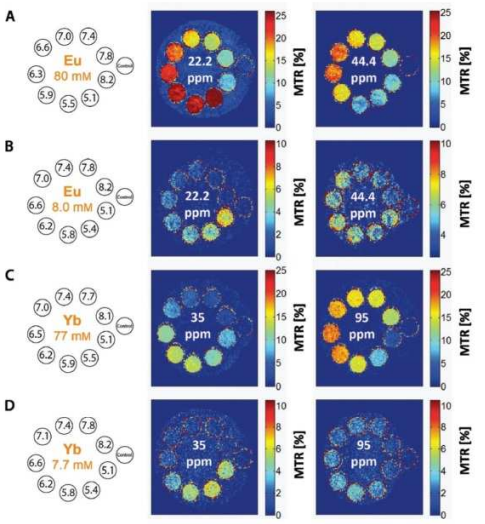

Fig. 7 MRI-CEST images of phantoms consisting of one vial containing an aq. solution of MES and HEPES (1 : 1, 50 mM) as a standard and nine vials containing solutions of (A, B) the [Eu($H_n$do3aNN)] or (C, D) [Yb($H_n$do3aNN)] complexes in the same buffer with different pH values and concentrations. Experimental conditions: RARE pulse sequence, B_0 = 4.7 T, RF presaturation pulse applied for 2 s, T = 298 K, TR = 5 s, TE = 8.9 ms, (B) B_1 = 35 μT (1490 Hz), (A, C, D) B_1 = 25 μT (1060 Hz).

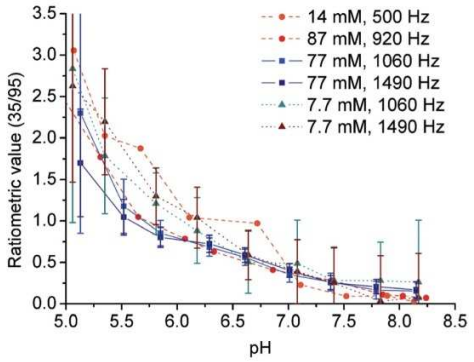

Fig. 8 Ratiometric plots of the 7.7–8.7 mM [Yb($H_n$do3aNN)] complex, 25 °C; RF presaturation pulse applied for 2 s. Circles: aq. solution, B_0 = 7.05 T (NMR), B_1 = 500 Hz (11.8 μT) or 920 Hz (21.7 μT). Squares and triangles: 50 mM HEPES–MES, B_0 = 4.7 T (MRI), B_1 = 1060 Hz (25 μT) or 1490 Hz (35 μT). The ratiometric value (35/95) is the ratio of MTR intensity at 35 ppm to MTR intensity at 95 ppm.

(pH > 11) (*i.e.* their chemical exchange with bulk water is slow) and remain unaffected after water presaturation. A graphical representation of the suggested processes giving rise to the peaks in *Z*-spectra is shown in Scheme 2.

It is evident that the two pools of exchanging amine protons show different dependences of their CEST effects in the pH range relevant to the physiological conditions. The applicability of the [Eu($H_n$do3aNN)] and [Yb($H_n$do3aNN)] complexes as pH-sensitive MRI probes was tested for solutions with different pH values (HEPES/MES buffers) and concentrations of the complex (Fig. 7).

To define the pH-dependent but concentration-independent function, the ratio of MTR intensities was calculated. However, this ratio can be defined reasonably only for the Yb(III) complex (35/95 ppm), as in the case of the Eu(III) complex there is a significant overlap of the low-shift signal of the coordinated secondary amino group (22.2 ppm) with the new signal appearing in the acidic region (attributable to the protonated and uncoordinated primary amine, Fig. 5B).

To prove the suggested concept of ratiometric pH determination, samples of [Yb($H_n$do3aNN)] with different complex concentrations and different pH values were measured by both NMR and MRI techniques. The concentration range used covers about one order of magnitude (7.7–8.7 mM). All calibration curves were very similar (see Fig. 8 and S10†), although standard deviations of the data points from MRI experiments acquired for the low concentration were relatively high due to a high background noise and, thus, a low signal-to-noise ratio was obtained under these conditions. The final curves are compiled in Fig. 8. Although the method has high ESDs with respect to the determination of an exact pH value, the shape of calibration curves enables distinguishing between samples with pH > 7 and those with pH < 6. Such a finding is relevant for the design of contrast agents useful *e.g.* for distinguishing between normal and hypoxic tissues.

Experimental

Materials and methods

All reagents and solvents were commercially available, had synthetic purity and were used as received. Water used for potentiometric titrations was deionized by using a Milli-Q (Millipore).

1,4,7-Tris(*tert*-butylcarboxymethyl)-1,4,7,10-tetraazacyclododecane hydrobromide (tBu$_3$do3a·HBr) was prepared according to the published procedure.[20] THF was dried by the standard method[21] and stored over molecular sieves under an argon atmosphere. Anhydrous MeCN and EtOH were from commercial sources.

NMR characterization data (1D: ^{1}H, ^{13}C{^{1}H}; 2D: HSQC, HMBC, ^{1}H–^{1}H COSY) were recorded on a VNMRS300 or Bruker Avance III 600, using 5-mm sample tubes. Chemical shifts are reported as δ values and are given in ppm. Coupling constants J are reported in Hz. Unless stated otherwise, NMR experiments were performed at 25 °C. For samples dissolved in D_2O, the pD value was calculated by correcting the pH-electrode reading by +0.4, *i.e.* pD = pH reading +0.4. For the ^{1}H and ^{13}C

NMR measurements of diamagnetic compounds in D_2O, *t*BuOH was used as an internal standard (δ_H = 1.25, δ_C = 30.29). For the measurements in $CDCl_3$, TMS was used as an internal standard (δ_H = 0.00, δ_C = 0.00). In the case of paramagnetic complexes, chemical shifts were referenced to the water signal of the sample (δ_H = 0.00) to keep the chemical shift values in ^{1}H NMR spectra consistent with the scale of *Z*-spectra. The abbreviations s (singlet), t (triplet), q (quartet), m (multiplet) and br (broad) are used in order to express the signal multiplicities. Lanthanide(III) concentrations in solutions were determined by measurement of the bulk magnetic susceptibility (BMS) shifts.[22] The ESI-MS spectra were recorded on a Bruker ESQUIRE 3000 spectrometer equipped with an electrospray ion source and ion-trap detection. Measurements were carried out in both the positive and negative modes. UV-Vis solution spectra were recorded using a SPECORD® 50 PLUS (ANALYTIC JENA AG) spectrophotometer at 25 °C in the range of 300–1000 nm with data intervals of 0.2 nm and integration time of 0.04 s. Elemental analysis was performed at the Institute of Macromolecular Chemistry of the Czech Academy of Sciences (Prague, Czech Republic).

Synthesis

Synthesis of 2. Ethyl chloroformate (8.02 g, 73.9 mmol, 2.2 eq.) was added dropwise to a well-stirred solution of **1** (3.5 g, 33.6 mmol) in a mixture of dioxane (30 ml) and H_2O (30 ml), and the reaction mixture was stirred for 2 h at room temperature. In the next step, conc. aq. NH_3 (≈10 ml) was added and the reaction mixture was stirred for 15 min. The mixture was concentrated *in vacuo*, poured into H_2O (50 ml) and extracted with CH_2Cl_2 (3 × 30 ml). The organic layer was dried over anhydrous Na_2SO_4 and concentrated *in vacuo* to yield 4.50 g (54%) of **2** as a colourless oil.

^{1}H NMR (600 MHz, $CDCl_3$): δ 1.15–1.19 (6H, m, CH_2CH_3); 3.28 (2H, br, $NHCH_2$); 3.36 (4H, br, CH_2NCH_2); 3.63–3.69 (2H, br, CH_2OH); 4.02–4.08 (4H, m, OCH_2).

$^{13}C\{^1H\}$ NMR (150.9 MHz, $CDCl_3$): δ 14.61, 14.65 (2C, CH_2CH_3); 40.03, 40.18 (1C, $NHCH_2$); 48.45, 48.74 (1C, CH_2); 51.11, 51.51 (1C, CH_2); 60.91 (1C, OCH_2); 61.15, 61.40 (1C, CH_2OH); 61.66 (1C, OCH_2); 157.30 (2C, *C*O). All four backbone carbon atoms show two ^{13}C NMR signals due to rigid conformations of the molecule locked by different orientations of the amide groups.

MS-ESI: (+) 270.8 ($[M + Na]^+$, calcd 271.1).

Synthesis of 3. CBr_4 (4.11 g, 12.4 mmol, 1.5 eq.) and PPh_3 (3.25 g, 12.4 mmol, 1.5 eq.) were added to a well-stirred solution of **2** (2.05 g, 8.25 mmol) in dry THF (70 ml) in a flask equipped with a drying tube. The reaction mixture was stirred for 1 h at room temperature, filtered and then evaporated in a rotary evaporator. The oily residue was dissolved in a small amount of CH_2Cl_2 and purified by chromatography (silica, 25 × 3.5 cm). Impurities were removed by elution with CH_2Cl_2, and the pure product was eluted using acetone : CH_2Cl_2 (1 : 9). Fractions containing the pure product **3** (as checked by NMR) were combined and evaporated to give compound **3** (2.24 g, 87%) as a colourless oil.

^{1}H NMR (600 MHz, $CDCl_3$): δ 1.16–1.18 (3H, br, CH_2CH_3); δ 1.22 (3H, t, $^3J_{HH}$ = 7.2, CH_2CH_3); 3.28 (2H, br, CH_2); 3.39–3.45 (4H, br, CH_2); 3.58 (2H, br, CH_2Br); 4.04–4.08 (2H, m, CH_2CH_3); 4.10 (2H, q, $^3J_{HH}$ = 7.2, CH_2CH_3).

$^{13}C\{^1H\}$ NMR (150.9 MHz, $CDCl_3$): δ 14.78, 14.84 (2C, CH_2CH_3); 29.28, 29.53 (1C, CH_2Br); 40.04 (1C, $NHCH_2$); 48.11 (1C, CH_2); 49.74, 50.41 (1C, CH_2); 61.05, 62.02 (2C, OCH_2); 156.41, 157.09 (2C, *C*O). Two of the backbone carbon atoms show two ^{13}C NMR signals due to rigid conformations of the molecule locked by different orientations of the amide groups.

Synthesis of 4. A solution of the alkylating reagent **3** (1.79 g, 5.75 mmol, 1.35 eq.) in dry MeCN (10 ml) was added dropwise to a well-stirred suspension of K_2CO_3 (2.94 g, 21.3 mmol, 5 eq.) and *t*Bu$_3$do3a·HBr (2.54 g, 4.26 mmol) in dry MeCN (40 ml) at room temperature. The reaction mixture was stirred at 60 °C for 24 h, filtered, and the filtrate was evaporated in a rotary evaporator. The oily residue was dissolved in $CHCl_3$ (25 ml) and extracted with distilled water (4 × 10 ml). The organic layer was dried over anhydrous Na_2SO_4 and concentrated *in vacuo* to yield a yellow oil (3.76 g) containing a crude compound **4** contaminated with an excess of the alkylating reagent **3**. The excess alkylating reagent was not removed, and the crude product **4** was used in the next step without purification.

MS-ESI: (+) 745.3 ($[M + H]^+$, calcd 745.5); 767.2 ($[M + Na]^+$; calcd 767.5).

Synthesis of 5. A portion (3.70 g) of the crude compound **4** obtained above was dissolved in a mixture of CF_3CO_2H and $CHCl_3$ (1 : 1, 30 ml). The resulting solution was refluxed for 18 h and evaporated in a rotary evaporator. The oily residue was dissolved in a small amount of distilled water and evaporated (this procedure was then repeated three more times) to produce a yellow oil (3.10 g) containing compound **5**, which was used in the next step without purification.

MS-ESI: (+) 577.0 ($[M + H]^+$, calcd 577.3). (−) 574.9 ($[M - H]^-$; calcd 575.3).

Synthesis of 6. The crude product **5** (3.00 g) was dissolved in 10% aq. NaOH (50 ml) and stirred for 24 h at 90 °C. Then, the solution was loaded onto a strong anion exchange column (Dowex 1, OH^--form, 1.5 × 20 cm). Impurities were removed by elution with water and the product **6** was eluted with 5% aq. AcOH. Fractions containing the product (as checked by ^{1}H NMR) were combined, filtered and evaporated to give compound **6** (2.21 g) as a brownish oil. The crude product was dissolved in a water : MeOH mixture (1 : 5, v : v, ≈5 ml) and overlaid with EtOH (≈5 ml) and the mixture was left to stand for 2 d. After this period, the solid product was filtered off and dried under vacuum to yield **6**·2.5H_2O (900 mg, 42% based on *t*Bu$_3$do3a) as a white powder.

^{1}H NMR (600 MHz, D_2O, pD = 5.88): δ 3.05 (2H, br, CH_2CH_2NCO); 3.16 (4H, br, $(CH_2)_2NCH_2CH_2NCO$); 3.20–3.29 (4H, m, $(CH_2)_2NCH_2CO$); 3.33–3.44 (12H, br, CH_2CH_2NCO, CH_2CH_2NH, $(CH_2)_2NCH_2CO$); 3.52 (2H, br s, CH_2CO); 3.57 (2H, t, $^3J_{HH}$ = 8.1, CH_2NH); 3.70 (4H, br s, CH_2CO).

$^{13}C\{^1H\}$ NMR (150.9 MHz, D_2O, pD = 5.88): δ 38.69 (1C, NCH_2CH_2NH); 39.45 (1C, CH_2CH_2NCO); 46.05 (1C, CH_2NH);

49.05 (2C, $(CH_2)_2NCH_2CH_2NCO$); 49.95 (2C, $(CH_2)_2NCH_2CO$); 50.17 (1C, CH_2CH_2NCO); 51.14 (2C, $(CH_2)_2NCH_2CO$); 51.79 (2C, $(CH_2)_2NCH_2CO$); 56.21 (1C, CH_2CO); 57.43 (2C, CH_2CO); 165.09 (1C, NCONH); 173.25 (2C, CH_2CO); 175.78 (1C, CH_2CO).

MS-ESI: (+) 480.9 ($[M + Na]^+$, calcd 481.2). (−) 456.8 ($[M - H]^-$, calcd 457.3).

Elemental analysis: found (calcd for **6**·2.5H_2O, $C_{19}H_{39}N_6O_{9.5}$, M_r = 503.6) C: 45.30 (45.32), H: 7.85 (7.81), N: 16.12 (16.69).

Synthesis of H_3do3aNN. Compound **6**·2.5H_2O (415 mg, 0.824 mmol) was dissolved in aq. HCl (10 ml, 1 : 1) and the resulting solution was stirred for 7 d at 95 °C and evaporated in a rotary evaporator. The oily residue was dissolved in a small amount of distilled water and evaporated to dryness, leaving a glassy solid, which was triturated in dry THF overnight. Next, the product was collected by filtration, and stored in a desiccator (P_2O_5) to give H_3do3aNN in the form of a hydrochloride hydrate (500 mg, 95%) as a white powder.

Mother liquors after crystallization of the intermediate **6** can be also used for the preparation of the title ligand. After acid hydrolysis of impure **6**, the crude H_3do3aNN was converted to its ammonium salt by chromatography on a strong cation exchanger (Dowex 50, 50–100 mesh, H^+-form). Acids were eluted by water and the crude product was collected by 5% aq. ammonia. After evaporation of volatiles, the oily residue was dissolved in water and poured onto a column of a weak cation exchanger (Amberlite CG50, 200–400 mesh, H^+-form). Impurities were eluted with water and the H_3do3aNN compound was collected by 3% aq. HCl. Fractions containing the product were combined and evaporated to dryness leaving a glassy solid, which was triturated as described above.

^{1}H NMR (600 MHz, D_2O, pD = 6.07, 55 °C, Fig. S11†): δ 2.85–2.87 (4H, m, macrocyclic CH_2); 3.01–3.09 (6H, br m, NCH_2CH_2NH, macrocyclic CH_2); 3.11 (2H, s, CH_2CO_2); 3.19 (2H, t, $^3J_{HH}$ = 5.1, NCH_2CH_2NH); 3.30–3.36 (2H, br m, macrocyclic CH_2); 3.42–3.45 (2H, br m, macrocyclic CH_2); 3.47–3.49 (2H, br t, $NHCH_2CH_2NH_2$); 3.54–3.56 (2H, br t, $NHCH_2CH_2NH_2$); 3.57–3.61 (2H, m, macrocyclic CH_2); 3.74–3.80 (2H, br, macrocyclic CH_2); 3.92 (2H, AB-multiplet, CH_2CO_2).

$^{13}C\{^1H\}$ NMR (150.9 MHz, D_2O, pD = 6.07, 55 °C, Fig. S12†): δ 37.07 (1C, $NHCH_2CH_2NH_2$); 46.04 (1C, NCH_2CH_2NH); 46.99 (1C, $NHCH_2CH_2NH_2$); 48.84 (4C, macrocyclic CH_2); 50.45 (1C, NCH_2CH_2NH); 51.23 (2C, macrocyclic CH_2); 53.30 (2C, macrocyclic CH_2); 55.55 (1C, CH_2CO_2); 58.34 (2C, CH_2CO_2); 171.24 (2C, CH_2CO_2); 179.41 (1C, CH_2CO_2).

MS-ESI: (+) 432.9 ($[M + H]^+$, calcd 433.3). (−) 430.8 ($[M - H]^-$, calcd 431.3).

Elemental analysis: found (calcd for H_3do3aNN·5HCl·1.5H_2O, $C_{18}H_{44}Cl_5N_6O_{7.5}$, M_r = 641.8) C: 34.18 (33.68), H: 7.13 (6.91), N: 12.75 (13.09), Cl: 27.57 (27.62).

Synthesis of [Ln($H_n$do3aNN)] complexes. The Ln(III) complexes of H_3do3aNN for NMR, NMR CEST and MRI CEST experiments were prepared by mixing the lanthanide(III) chloride hydrate (Eu^{3+}, Yb^{3+}) with 1.1 equiv. of the ligand in a small amount of distilled water, adjusting the pH to ≈7 with 1 M aq. LiOH, and stirring overnight at 60 °C. Then, the pH was re-adjusted to ≈7 with 1 M aq. LiOH and the solution was again stirred overnight at 60 °C.

All the prepared samples were checked using a xylenol orange test (acetate buffer, pH = 5.7) to exclude the presence of free Ln(III) ions. The exact concentration of the Ln(III) complexes in the solution was determined using Evans's method.[22]

[Eu($H_n$do3aNN)]

MS-ESI: (+) 588.9 ($[M + Li]^+$, calcd 589.2). (−) 616.7 ($[M + Cl]^-$, calcd 617.2).

[Yb($H_n$do3aNN)]

MS-ESI: (+) 609.9 ($[M + Li]^+$, calcd 610.2). (−) 637.7 ($[M + Cl]^-$, calcd 638.2).

PARACEST experiments

All *Z*-spectra were recorded using a VNMRS300 spectrometer operating at 299.9 MHz (B_0 = 7.05 T); 5 mm sample tubes and a coaxial capillary with D_2O and *t*BuOH as an external standard were used. Solutions of the complexes for PARACEST NMR experiments were prepared in pure water with the pH adjusted using aq. HCl/LiOH solutions and had concentrations in the range of 14–87 mM. Standard pulse sequences for presaturation experiments were used. Saturation offsets were set using the array function (increment 200–250 Hz). Data from the PARACEST experiments were plotted as the dependence of normalized water signal intensity (M_z/M_0%) on saturation offset. Here, M_0 represents the magnetization (*i.e.* intensity) of the water signal without RF saturation and M_z corresponds to the water signal when a presaturation pulse is applied. Other experimental parameters are specified in the figure captions.

The magnetization transfer ratio (MTR) was calculated using $MTR = M_{\Delta\omega}/M_0 - M_{-\Delta\omega}/M_0$ in which $M_{\pm\Delta\omega}$ is the magnetization (*i.e.* intensity) of the water signal with the use of a presaturation frequency $\pm\Delta\omega$ away from the bulk water signal.

MRI PARACEST images were measured with a phantom consisting of one vial containing an aqueous solution of buffers [a mixture of 0.025 M 2-(*N*-morpholino)ethanesulfonic acid (MES) and 0.025 M 4-(2-hydroxyethyl)-1-piperazineethanesulfonic acid (HEPES)] as a standard and nine vials containing solutions of the Eu^{3+} or Yb^{3+}-complexes dissolved in buffers (0.025 M MES and 0.025 M HEPES) with different pH values and concentrations. The innocence of the chosen buffers was confirmed by silence of pure buffer solutions in the CEST experiment (*i.e.*, no signal in the *Z*-spectra of the pure buffers was found). All MRI PARACEST images were acquired on a 4.7 T scanner (Bruker BioSpec, Germany) using a modified spin-echo sequence (Rapid Acquisition with Refocused Echoes – RARE). Experimental conditions: repetition time (TR) = 5000 ms, echo time (TE) = 8.9 ms, resolution 0.35 × 0.35 × 2 mm^3, turbo factor = 4. Other experimental parameters are specified in the figure captions. For all MR experiments, a resonator coil with an inner diameter of 70 mm was used. MTR maps were normalized to the signal acquired at a frequency offset $-\Delta\omega$ and reconstructed from a manually outlined region of interest on a pixelwise basis using a custom script

written in Matlab (Mathworks, Natick, MA, USA). MTR maps were visualized on a false-colour scale in percentage units.

Potentiometry

Potentiometric titrations[23] were carried out in a thermostatted vessel at 25.0 ± 0.1 °C at a constant ionic strength $I(NMe_4Cl)$ = 0.1 M. The measurements were taken with an HCl excess added to the initial mixture and the mixtures were titrated with a stock NMe_4OH solution. An inert atmosphere was maintained by constant passage of argon saturated with water vapour. The ligand concentration in the titration vessel was ≈0.004 M.

Ligand protonation constants were determined by standard potentiometric titrations performed in the pH range of 1.6–12.2 (80 points per titration, titrations were carried out four times).

In the cases of the Ln(III)–H_3do3aNN systems, the equilibria were established slowly and, therefore, the out-of-cell technique was used in the pH range of 1.6–7.2 (two titrations per system, 25 points per titration). The metal : ligand ratio was 1 : 1 in all cases. The waiting time was 7 weeks. Then, the potential at each titration point (tube) was determined with a freshly calibrated electrode.

Pre-formed complexes for the determination of their protonation constants were prepared in the following way: in an ampoule, equimolar molar amounts of the ligand and metal stock solutions were mixed and a calculated amount (based on the out-of-cell titration data) of a stock solution of NMe_4OH was gradually added to reach pH ≈ 7, which corresponds to full complexation according to the out-of-cell titration. Ampoules were flame-sealed and left at 55 °C for 3 d. Aliquots were taken from the final solution, a defined amount of an HCl stock solution was added into these samples and the mixtures were immediately titrated by an NMe_4OH stock solution in a way analogous to the procedure described above for the determination of ligand protonation constants in the pH range of 2.3–12.1. The initial volumes were ≈5 cm^3 for the conventional titrations and ≈1 cm^3 for the out-of-cell ones, respectively.

The constants with their standard deviations were calculated by using the OPIUM program package.[24] Overall protonation constants are defined as $\beta_h = [H_hL]/\{[H]^h \cdot [L]\}$, and they can be transferred to the consecutive protonation constants $\log K_P$ by $\log K_P(H_hL) = \log\beta_h - \log\beta_{(h-1)}$; it should be noted that $\log K_P = pK_A$ of the corresponding protonated species H_hL. The overall stability constants β_{hlm} are concentration constants defined as $\beta_{hlm} = [H_hL_lM_m]/\{[H]^h \cdot [L]^l \cdot [M]^m\}$. The water ion product used in the calculations was pK_w = 13.81. Stability constants of metal hydroxido complexes were taken from the literature.[14] In the text, pH means $-\log[H^+]$. The best fits of experimental data are shown in Fig. S13–S15† and the results are compiled in Tables S1–S3.†

Conclusions

The present study revealed significant pH dependence of the Chemical Exchange Saturation Transfer (CEST) effect of selected Ln(III) complexes with the novel macrocyclic ligand H_3do3aNN containing a linear diamine pendant arm. The pH dependence is substantial in the pH range relevant for biological systems (pH ≈ 5.5–8.5). Based on these findings, we have shown that the magnetization transfer ratio of CEST signals of the complexes can be used for pH determination by MRI, and it is independent of the concentration of the probes.

Unfortunately, the studied complexes are not fully kinetically inert in acidic solutions and slowly release the free metal ions, which excludes their direct use in medical applications. However, the study brings proof-of-principle of possibility to use a linear diaminic fragment for pH determination using MRI ratiometry.

Acknowledgements

This work was supported by the Czech Science Foundation (P207-11-1437), by the Grant Agency of the Charles University (no. 110213) and by the project of the Ministry of Health, Czech Republic, for the development of a research organization IN00023001 (Institutional support, Institute for Clinical and Experimental Medicine). We thank Z. Böhmová for potentiometric measurements, I. Císařová for collection of X-ray diffraction data and nH. Blahut for his help with some NMR experiments and for Fig. S9.†

References

1 *The Chemistry of Contrast Agents in Medical Magnetic Resonance Imaging*, ed. A. Merbach, L. Helm and É. Tóth, 2nd edn, Wiley, Chichester, United Kingdom, 2013.
2 (*a*) P. Caravan, J. J. Ellison, T. J. McMurry and R. B. Lauffer, *Chem. Rev.*, 1999, **99**, 2293–2352; (*b*) P. Hermann, J. Kotek, V. Kubíček and I. Lukeš, *Dalton Trans.*, 2008, 3027–3047; (*c*) C. F. G. C. Geraldes and S. Laurent, *Contrast Media Mol. Imaging*, 2009, **4**, 1–23.
3 K. M. Ward, A. H. Aletras and R. S. Balaban, *J. Magn. Reson.*, 2000, **143**, 7987.
4 (*a*) J. Zhou and P. C. M. van Zijl, *Prog. Nucl. Magn. Reson. Spectrosc.*, 2006, **48**, 109–136; (*b*) Y. Wu, M. Evbuomwan, M. Melendez, A. Opina and A. D. Sherry, *Future Med. Chem.*, 2010, **2**, 351–366; (*c*) E. Terreno, D. D. Castelli and S. Aime, *Contrast Media Mol. Imaging*, 2010, **5**, 78–98; (*d*) P. C. M. van Zijl and N. N. Yadav, *Magn. Reson. Med.*, 2011, **65**, 927–948; (*e*) G. Liu, X. Song, K. W. Y. Chan and M. T. McMahon, *NMR Biomed.*, 2013, **26**, 810–828.
5 S. Zhang, M. Merritt, D. E. Woessner, R. E. Lenkinski and A. D. Sherry, *Acc. Chem. Res.*, 2003, **36**, 783–790.
6 (*a*) M. Woods, D. E. Woessner and A. D. Sherry, *Chem. Soc. Rev.*, 2006, **35**, 500–511; (*b*) S. Viswanathan, Z. Kovács, K. N. Green, S. J. Ratnakar and A. D. Sherry, *Chem. Rev.*, 2010, **110**, 2960–3018; (*c*) T. C. Soesbe, Y. Wu and A. D. Sherry, *NMR Biomed.*, 2013, **26**, 829–838.
7 (*a*) M. Woods, D. E. Woessner, R. Zhao, A. Pasha, M.-Y. Yang, C.-H. Huang, O. Vasalitiy, J. R. Morrow and

A. D. Sherry, *J. Am. Chem. Soc.*, 2006, **128**, 10155–10162; (*b*) C.-H. Huang and J. R. Morrow, *Inorg. Chem.*, 2009, **48**, 7237–7243.

8 (*a*) S. J. Dorazio, P. B. Tsitovich, K. E. Sisters, J. A. Spernyak and J. R. Morrow, *J. Am. Chem. Soc.*, 2011, **133**, 14154–14156; (*b*) A. O. Olatunde, S. J. Dorazio, J. A. Spernyak and J. R. Morrow, *J. Am. Chem. Soc.*, 2012, **134**, 18503–18505; (*c*) S. J. Dorazio, A. O. Olatunde, P. B. Tsitovich and J. R. Morrow, *J. Biol. Inorg. Chem.*, 2014, **19**, 191–205; (*d*) A. O. Olatunde, J. M. Cox, D. Daddarion, J. A. Spernyak, J. B. Benedict and J. R. Morrow, *Inorg. Chem.*, 2014, **53**, 8311–8321; (*e*) S. J. Dorazio, A. O. Olatunde, J. A. Spernyak and J. R. Morrow, *Chem. Commun.*, 2013, **49**, 10025–10027; (*f*) P. B. Tsitovich and J. R. Morrow, *Inorg. Chim. Acta*, 2012, **393**, 3–11; (*g*) S. J. Dorazio, P. B. Tsitovich, S. A. Gardina and J. R. Morrow, *J. Inorg. Biochem.*, 2012, **117**, 212–219.

9 (*a*) S. Aime, C. Carrera, D. D. Castelli, S. G. Crich and E. Terreno, *Angew. Chem., Int. Ed.*, 2005, **44**, 1813–1815; (*b*) G. Ferrauto, D. D. Castelli, E. Terreno and S. Aime, *Magn. Reson. Med.*, 2013, **69**, 1703–1711; (*c*) E. Gianolio, R. Stefania, E. D. Gregorio and S. Aime, *Eur. J. Inorg. Chem.*, 2012, 1934–1944.

10 D. V. Hingorani, A. S. Bernstein and M. D. Pagel, *Contrast Media Mol. Imaging*, 2015, **10**, 245–265.

11 (*a*) D. D. Castelli, E. Terreno and S. Aime, *Angew. Chem.*, 2011, **123**, 1838–1840; (*b*) D. D. Castelli, G. Ferrauto, J. C. Cutrin, E. Terreno and S. Aime, *Magn. Reson. Med.*, 2014, **71**, 326–332; (*c*) S. Aime, A. Barge, D. D. Castelli, F. Fedeli, A. Mortillaro, F. U. Nielsen and E. Terreno, *Magn. Reson. Med.*, 2002, **47**, 639–648; (*d*) Y. Wu, T. C. Soesbe, G. E. Kiefer, P. Zhao and A. D. Sherry, *J. Am. Chem. Soc.*, 2010, **132**, 14002–14003; (*e*) D. L. Longo, P. Z. Sun, L. Concolino, F. C. Michelotti, F. Uggeri and S. Aime, *J. Am. Chem. Soc.*, 2014, **136**, 14333–14336; (*f*) D. L. Longo, W. Dastrú, G. Diglio, J. Keupp, S. Langereis, S. Lanzardo, S. Prestigio, O. Steinbach, E. Terreno, F. Uggeri and S. Aime, *Magn. Reson. Med.*, 2011, **65**, 202–211; (*g*) V. R. Sheth, Y. Li, L. Q. Chen, C. M. Howison, C. A. Flask and M. D. Pagel, *Magn. Reson. Med.*, 2012, **67**, 760–768; (*h*) G. Liu, Y. Li, V. R. Sheth and M. D. Pagel, *Mol. Imaging*, 2012, **11**, 47–57; (*i*) N. McVicar, A. X. Li, M. Suchý, R. H. E. Hudson, R. S. Menon and R. Bartha, *Magn. Reson. Med.*, 2013, **70**, 1016–1025.

12 T. Krchová, J. Kotek, D. Jirák, J. Havlíčková, I. Císařová and P. Hermann, *Dalton Trans.*, 2013, **42**, 15735–15747.

13 A. Bianchi, L. Calabi, C. Giorgi, P. Losi, P. Mariani, P. Paoli, P. Rossi, B. Valtancoli and M. Virtuani, *J. Chem. Soc., Dalton Trans.*, 2000, 697–705.

14 A. E. Martell, R. M. Smith and R. J. Motekaitis, *NIST Critically Selected Stability Constants of Metal Complexes, Version 7*, Texas A&M University, College Station, TX, 2003.

15 S. Aime, M. Botta and G. Ermondi, *Inorg. Chem.*, 1992, **31**, 4291–4299.

16 S. Aime, M. Botta, M. Fasano, M. P. M. Marques, C. F. G. C. Geraldes, D. Pubanz and A. E. Merbach, *Inorg. Chem.*, 1997, **36**, 2059–2068.

17 (*a*) T. Vitha, V. Kubíček, J. Kotek, P. Hermann, L. V. Elst, R. N. Muller, I. Lukeš and J. A. Peters, *Dalton Trans.*, 2009, 3204–3214; (*b*) M. Polášek, J. Kotek, P. Hermann, I. Císařová, K. Binnemans and I. Lukeš, *Inorg. Chem.*, 2009, **48**, 455–465.

18 (*a*) S. Viswanathan, S. J. Ratnakar, K. N. Green, Z. Kovács, L. M. De Leónrodríguez and A. D. Sherry, *Angew. Chem., Int. Ed.*, 2009, **48**, 9330–9333; (*b*) S. J. Ratnakar, M. Woods, A. J. M. Lubag, Z. Kovács and A. D. Sherry, *J. Am. Chem. Soc.*, 2008, **130**, 6–7.

19 M. Woods, A. Pasha, P. Zhao, G. Tircso, S. Chowdhury, G. Kiefer, D. E. Woessner and A. D. Sherry, *Dalton Trans.*, 2011, **40**, 6759–6764.

20 B. Jagadish, G. L. Brickert-Albrecht, G. S. Nichol, E. A. Mash and N. Raghunand, *Tetrahedron Lett.*, 2011, **52**, 2058–2061.

21 D. D. Perrin and W. L. F. Armarego, *Purification of Laboratory Chemicals*, Pergamon Press, Oxford, 3rd edn, 1988.

22 D. M. Corsi, C. Platas-Iglesias, H. van Bekkum and J. A. Peters, *Magn. Reson. Chem.*, 2001, **39**, 723–726.

23 (*a*) P. Táborský, P. Lubal, J. Havel, J. Kotek, P. Hermann and I. Lukeš, *Collect. Czech. Chem. Commun.*, 2005, **70**, 1909–1942; (*b*) M. Försterová, I. Svobodová, P. Lubal, P. Táborský, J. Kotek, P. Hermann and I. Lukeš, *Dalton Trans.*, 2007, 535–549.

24 (*a*) M. Kývala and I. Lukeš, International Conference Chemometrics 1995 (Pardubice, Czech Republic), July 3–7, 1995, p. 63; (*b*) M. Kývala, P. Lubal and I. Lukeš, *IX. Solution Equilibria Analysis with the OPIUM Computer Program; Spanish-Italian and Mediterranean Congress on Thermodynamics of Metal Complexes (SIMEC 98) (Girona, Spain)*, June 2–5, 1998, The full version of the OPIUM program is available (free of charge) on http://www.natur.cuni.cz/~kyvala/opium.html.

APPENDIX 2

Electronic Supplementary Material (ESI) for Dalton Transactions.

Electronic Supporting Information

for

Ln(III)-complexes of a DOTA analogue with an ethylenediamine pendant arm as pH-responsive PARACEST contrast agents

Tereza Krchová[a], Andrea Gálisová[b], Daniel Jirák[b,c], Petr Hermann[a], Jan Kotek[a]

[a] Department of Inorganic Chemistry, Faculty of Science, Universita Karlova (Charles University), Hlavova 2030, 128 43 Prague 2, Czech Republic. Tel.: +420-221951261. Fax: +420-221951253. E-mail: modrej@natur.cuni.cz.

[b] Department of Radiodiagnostic and Interventional Radiology, Magnetic Resonance Unit, Institute for Clinical and Experimental Medicine, Vídeňská 1958/9, Prague 4, 140 21 Czech Republic.

[c] Institute of Biophysics and Informatics, 1st Faculty of Medicine, Universita Karlova (Charles University), Salmovská 1, 120 00 Prague 2, Czech Republic.

Contents

X-Ray diffraction

The single-crystal of **6**·2H_2O was prepared from concentrated aqueous solution of the compound **6** by a slow diffusion of EtOH vapours. The diffraction data were collected employing ApexII CCD diffractometer using Mo-K_α radiation (λ = 0.71073 Å) at 150(1) K and analysed using the SAINT V8.27B (Bruker AXS Inc., 2012) program package. The structures were solved by direct methods (SHELXS97[1]) and refined by full-matrix least-squares techniques (SHELXL97[2]). All non-hydrogen atoms were refined anisotropically. Carbon atoms of the ethylene group of amine pendant arm were found to be disordered in two positions with relative occupancy 56:44. Hydrogen atoms attached to carbon atoms were fixed in theoretical positions using a riding model with U_{eq}(H) = 1.2 U_{eq}(C), and those belonging to the oxygen or nitrogen atoms were fully refined.

Crystal data

6·2H_2O: $C_{19}H_{38}N_6O_9$, M = 494.55, monoclinic, a = 7.7686(3), b = 15.4411(5), c = 19.4703(7) Å, β = 93.165(2)°, U = 2332.01(14) Å^3, space group $P2_1/c$, Z = 4, 4582 total reflections, 3599 intense reflections, $R_1[I>2\sigma(I)]$ = 0.0596, wR_2(all data) = 0.1757. CCDC-1430249.

The found protonation scheme (Figure S1) is similar to those found previously for related 2-aminoethyl analogues[3] – two protons are bound to the mutually *trans* macrocycle amino groups bearing acetate moieties and the third one belongs to the "odd" acetate moiety. The conformation of the macrocyclic unit is (3,3,3,3)-B, as usually observed for the double-protonated cyclen rings.[4] Such a conformation is stabilized by the intramolecular hydrogen bonds between the protonated and non-protonated macrocycle amino groups. The whole crystal structure is stabilized by the extended hydrogen bonds network between ligand and the water solvate molecules.

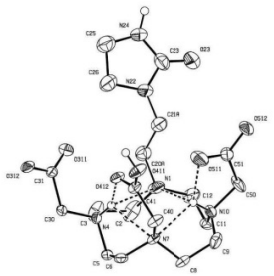

Figure S1 Molecular structure of **6** found in the crystal structure of **6**·2H_2O. Carbon-bound hydrogen atoms are omitted for clarity reasons. Hydrogen bonds are dashed.

Temperature dependence of ^{1}H NMR spectra of [Eu(do3aNN)] in D_2O

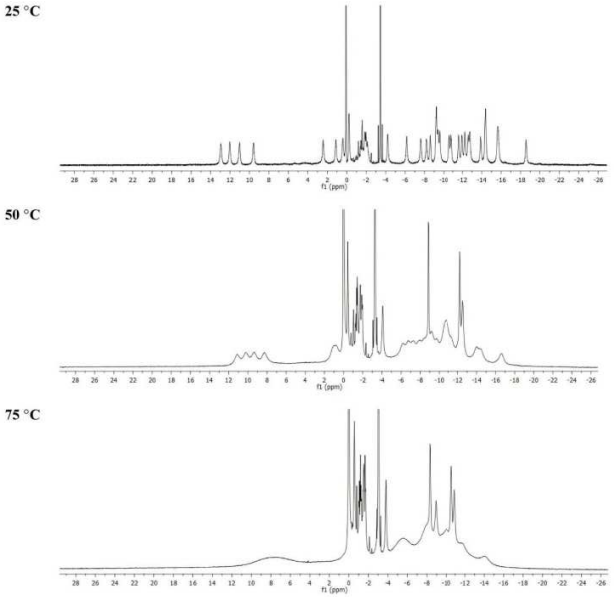

Figure S2 ^{1}H NMR spectra of the [Eu(do3aNN)] complex (~0.08 M solution in D_2O, B_0 = 7.05 T, pD = 10.7) at different temperatures. The chemical shift of HDO in the sample solution was referenced to 0 ppm.

Temperature dependence of ^{1}H NMR spectra of [Yb(do3aNN)] in D_2O

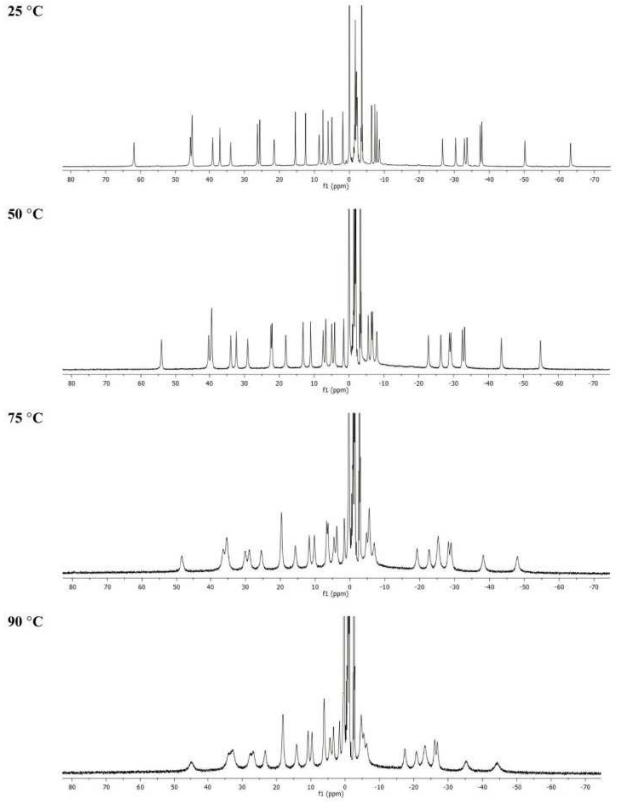

Figure S3 ^{1}H NMR spectra of the [Yb(do3aNN)] complex (~0.08 M solution in D_2O, B_0 = 7.05 T, pD = 11.3) at different temperatures. The chemical shift of HDO in the sample solution was referenced to 0 ppm.

APPENDIX 2

pH dependence of ^{1}H NMR spectra of [Yb(do3aNN)]

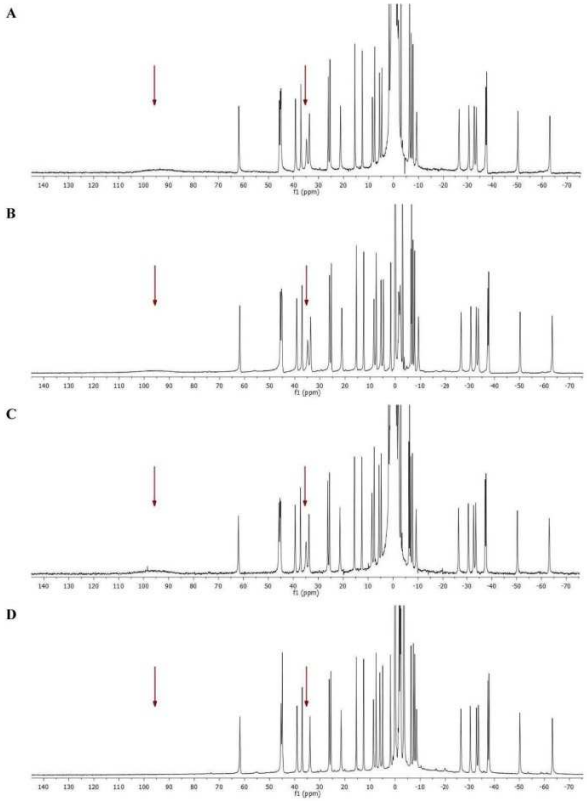

Figure S4 **A**: ^{1}H NMR spectrum of the [Yb(do3aNN)] complex, 0.09 M solution in H_2O, B_0 = 7.05 T, 25 °C, pH = 9.38. **B**: the same sample, water signal was saturated. **C**: the same sample, pH was re-adjusted to 11.3. **D**: 0.04 M solution in D_2O, B_0 = 7.05 T, 25 °C, pD = 11.34. Arrows show the positions of exchangeable (N–H) protons. The chemical shifts of H_2O/HDO in the sample solutions were referenced to 0 ppm.

Low-temperature ^{1}H NMR spectra of [Eu(do3aNN)] and [Yb(do3aNN)] in H_2O

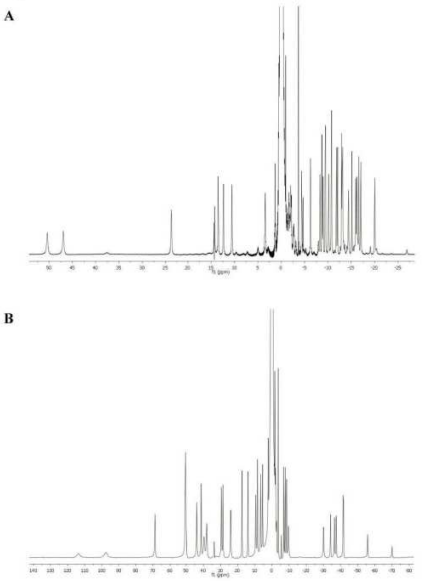

Figure S5 **A**: ^{1}H NMR spectrum of the [Eu(do3aNN)] complex, 47 mM solution in H_2O, B_0 = 14.1 T, 5 °C, pH = 9.5. **B**: ^{1}H NMR spectrum of the [Yb(do3aNN)] complex, 45 mM solution in H_2O, B_0 = 14.1 T, 5 °C, pH = 9.6. The chemical shifts of H_2O in the sample solutions were referenced to 0 ppm.

Temperature dependence of NMR spectra of [Eu($H_n$do3aNN)] in H_2O

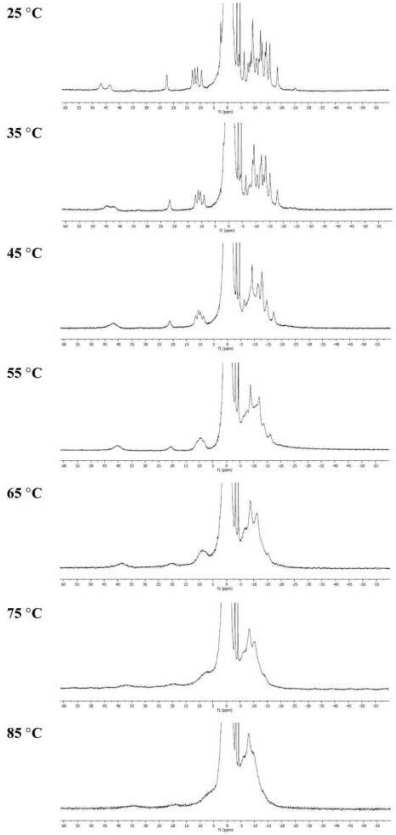

Figure S6 ^{1}H NMR spectra of the [Eu($H_n$do3aNN)] complex (~0.05 M solution in H_2O, B_0 = 7.05 T, pH = 6.75) at different temperatures. The chemical shift of H_2O in the sample solution was referenced to 0 ppm.

Dependence of Z-spectra of [Eu($H_n$do3aNN)] and [Yb($H_n$do3aNN)] on presaturation intensity

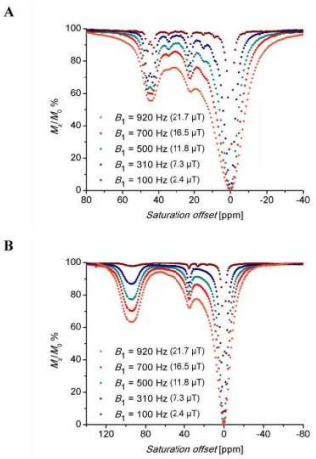

Figure S7 **A**: Z-spectra of an 87 mM aqueous solution of the [Eu($H_n$do3aNN)] complex (B_0 = 7.05 T, RF presaturation pulse applied for 2 s, pH = 6.45, 25 °C). **B**: Z-spectra of an 87 mM aqueous solution of the [Yb($H_n$do3aNN)] complex (B_0 = 7.05 T, RF presaturation pulse applied for 2 s, pH = 6.33, 25 °C).

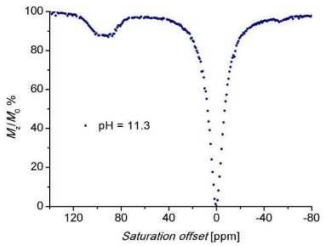

Figure S8 **A**: Z-spectra of an 87 mM aqueous solution of the [Yb(do3aNN)] complex at pH = 11.3 (B_0 = 7.05 T, B_1 = 21.7 μT (920 Hz), RF presaturation pulse applied for 2 s, 25 °C).

Tentative visualization of TSA isomers differing in chirality of coordinated secondary amino group

A **B**

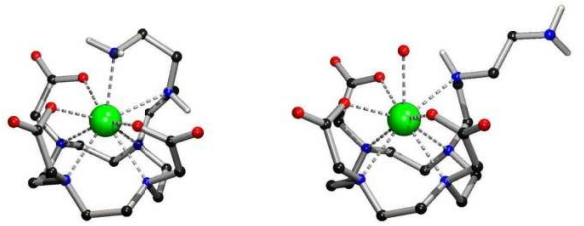

Figure S9 A: TSA Λλλλλ species with *R* chirality of the secondary amino group, enabling coordination of the primary amino group in the apical position. B: TSA Λλλλλ species with *S* chirality of the secondary amino group, disabling coordination of the primary amino group in the apical position. It should be noted that the primary amino group has to be fixed in position close to the central ion, as its protons have resolved the ^{1}H NMR signals and are still somewhat paramagnetically shifted. Such finding points to a some weak coordination of this group to the metal ion or its participation in an intramolecular hydrogen bond system.

Both structures were optimised with Gaussian package (Gaussian 09, Revision D.01)[5] using DFT method with M06 functional[6] and 6-31G(d,p) base set for all atoms but europium, where large core pseudopotencial of Dolg et al. together with appropriate base set were used.[7] Default value for integration grid ("fine") and SCF convergence criteria 10e^{-8} were used. The stationary points found on the potential energy surfaces as a result of the geometry optimizations have been tested to represent energy minima *via* frequency analysis. Solvent effects were evaluated using the polarizable continuum model (PCM) as implemented in Gaussian.

pH dependence of MTR of [Eu(H$_n$do3aNN)] complex

A

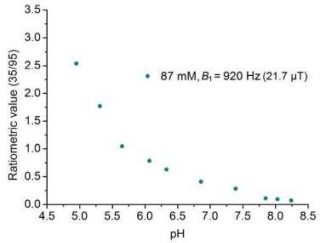

B

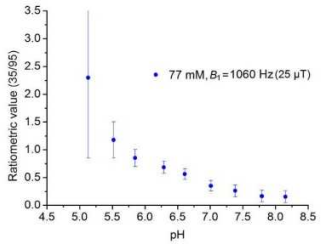

Figure S10 **A**: Ratiometric plot of an 87 mM aq. solution of the [Yb(H$_n$do3aNN)] complex at 25 °C taken by NMR; B_0 = 7.05, B_1 = 21.7 µT (920 Hz), RF presaturation pulse applied for 2 s. **B**: Ratiometric plot of a 77 mM solution of the [Yb(H$_n$do3aNN)] complex in 50 mM HEPES–MES (1:1) at 25 °C taken by MRI; RARE pulse sequence, TR = 5 s, TE = 8.9 ms, B_0 = 4.7 T, B_1 = 25 µT (1060 Hz), RF presaturation pulse applied for 2 s. The ratiometric value (35/95) is the ratio of the MTR intensity at 35 ppm to the MTR intensity at 95 ppm.

^{1}H and ^{13}C{^{1}H} NMR spectra of H$_3$do3aNN

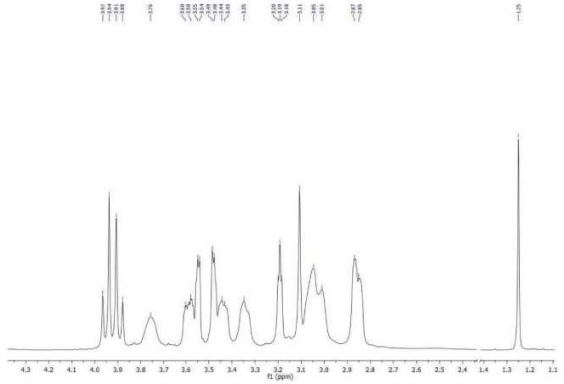

Figure S11 ^{1}H NMR spectrum of H$_3$do3aNN in D$_2$O, pD = 6.07, 55 °C.

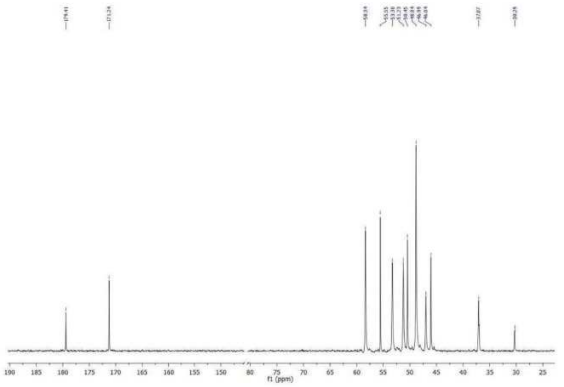

Figure S12 ^{13}C{^{1}H} NMR spectrum of H$_3$do3aNN in D$_2$O, pD = 6.07, 55 °C.

Potentiometric studies – protonation and stability constants of H_3do3aNN and its Eu(III)/Yb(III) complexes

Table S1 Overall protonation constants ($\log\beta_h$)[a] of H_3do3aNN (0.1 M NMe_4Cl, 25 °C).

h	$\log\beta_h$
1	12.62(2)
2	22.90(2)
3	32.57(2)
4	40.87(3)
5	44.17(3)
6	45.75(3)

[a] $\beta_h = [H_hL]/\{[H]^h\cdot[L]\}$

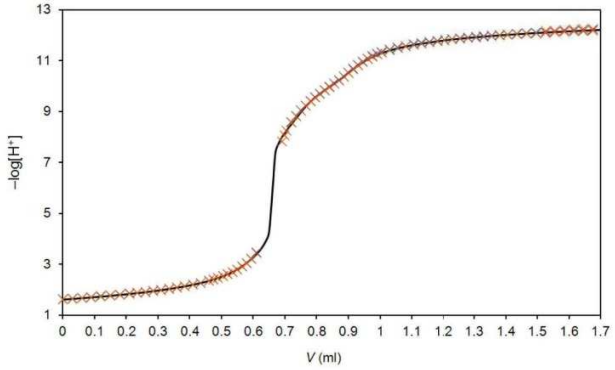

Figure S13 Titration data of the acid-base titration of the free ligand H_3do3aNN showing the best fit calculated using the protonation constants from Table S1 (c_L = 0.004 M, 0.1 M NMe_4Cl, 25 °C).

Table S2 Overall stability constants ($\log\beta_{hlm}$)[a] of [Ln($H_h$do3aNN)] complexes (0.1 M NMe_4Cl, 25 °C).

			$\log\beta_{hlm}$	
h	l	m	Eu	Yb
0	1	1	23.16(5)	22.76(4)
1	1	1	29.19(4)	28.98(3)
2	1	1	34.28(7)	34.05(4)

[a] $\beta_{hlm} = [H_hL_lM_m]/\{[H]^h\cdot[L]^l\cdot[M]^m\}$

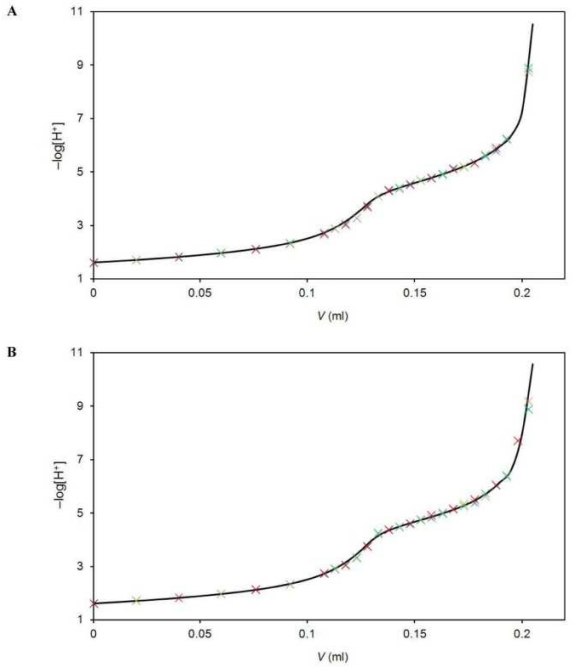

Figure S14 Titration data of the out-of-cell titration of Ln(III)–H_3do3aNN systems showing the best fits calculated using the stability constants from Table S2 (c_M = c_L = 0.004 M, 0.1 M NMe_4Cl, 25 °C, equilibration time = 7 weeks). **A**: Eu(III)–H_3do3aNN system. **B**: Yb(III)–H_3do3aNN system.

Table S3 Overall protonation constants ($\log\beta_{h11}$)[a] of [Ln(do3aNN)] complexes (0.1 M NMe_4Cl, 25 °C).

h	$\log\beta_{h1Eu}$	$\log\beta_{h1Yb}$
1	5.57(3)	5.67(1)
2	10.41(2)	10.52(1)

[a] $\beta_{h11} = [H_hLM]/\{[H]^h[LM]\}$

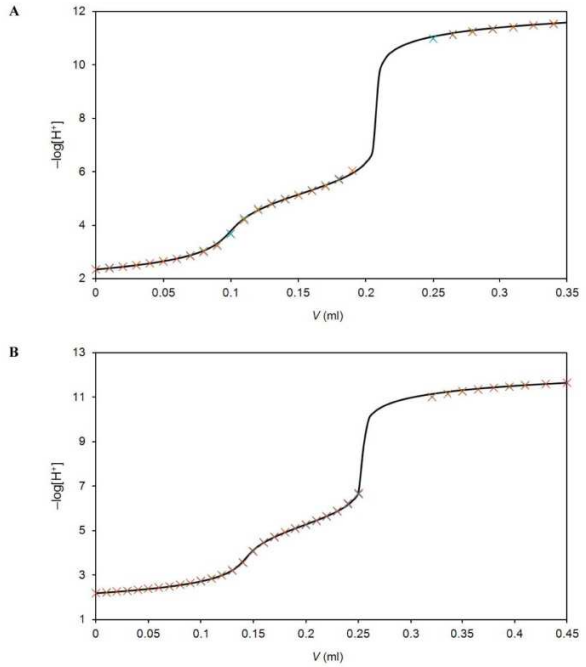

Figure S15 Titration data of the acid-base titration of the pre-formed [Ln(do3aNN)] complexes with the best fits calculated using the protonation constants from Table S3 (c_{ML} = 0.003 M, 0.1 M NMe_4Cl, 25 °C). **A**: H^+–[Eu(do3aNN)] system. **B**: H^+–[Yb(do3aNN)] system.

Schemes – suggested protonation sites of complex species

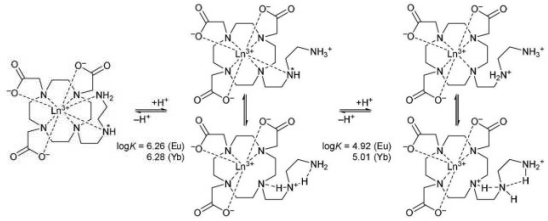

Scheme S1 Suggested species with the tentative protonation sites present in the protonation equilibrium of Ln(III)–H_3do3aNN mixtures during out-of-cell titration. In the protonated species, binding of the water molecule(s) to the central ion filling its coordination sphere to the coordination number 8–9 is expected, but it is not shown for the sake of clarity

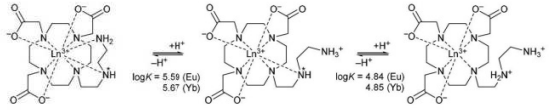

Scheme S2 Suggested species occurring during the non-equilibrium potentiometric acid-base titration of pre-formed [Ln(do3aNN)] complexes. In the hepta/octa-coordinated species, binding of the water molecule(s) to the central ion filling its coordination sphere to the coordination number 8–9 is expected, but it is not shown for the sake of clarity.

UV-Vis spectrophotometry

UV-Vis solution spectra were obtained on a SPECORD® 50 PLUS (ANALYTIC JENA AG) spectrophotometer at 25 °C in the range of 300–1000 nm with the data intervals of 0.2 nm and the integration time of 0.04 s.

The samples for UV-Vis spectra of xylenol orange–Eu^{3+} complex were prepared by the following way: 100 µl of xylenol orange solution (10^{-4} M) in buffer (mixture of 0.025 M aq. HEPES and 0.025 M aq. MES; pH = 5.55) was added to 898 µl of the same buffer (pH = 5.55). Gradually, 2.2 µl portions of aq. solution of $EuCl_3$ in H_2O (4.46 mM) were added, and the UV-Vis spectrum was acquired after each addition (Figure S16).

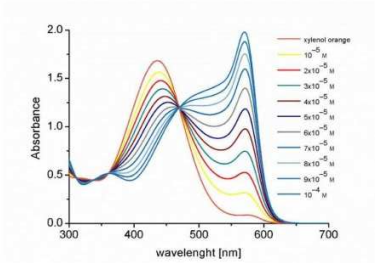

Figure S16 Change of UV-Vis spectra of aq. solution of xylenol orange (10^{-5} M, pH = 5.55, 0.025 M HEPES and 0.025 M MES, 25 °C) with increasing concentration of $EuCl_3$ (10^{-5}–10^{-4} M).

Kinetic stability of [Eu($H_n$do3aNN)] complex was studied by following procedure: 100 µl of aq. solution of [Eu(do3aNN)] complex (8 mM, pH = 7.5) was added to the mixture of 800 µl of buffer solution (mixture of 0.025 M aq. HEPES and 0.025 M aq. MES, pH = 5.55) with 100 µl of xylenol orange solution (10^{-4} M) in the same buffer (pH = 5.55). The evaluation of the absorption spectra with time was measured and is shown in Figure S17.

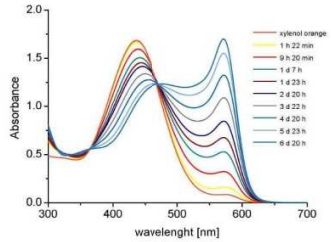

Figure S17 Time dependence of UV-Vis spectra of aq. solution of xylenol orange (10^{-5} M, pH = 5.55, 0.025 M HEPES and 0.025 M MES, 25 °C) in the presence of the [Eu($H_n$do3aNN] complex ($8{\cdot}10^{-4}$ M).

References

[1] G. M. Sheldrick, SHELXS97, Program for Crystal Structure Solution from Diffraction Data, University of Göottingen, Göottingen, 1997.

[2] G. M. Sheldrick, SHELXL97, Program for Crystal Structure Refinement from Diffraction Data, University of Göottingen, Göottingen, 1997.

[3] T. Krchová, J. Kotek, D. Jirák, J. Havlíčková, I. Císařová and P. Hermann, *Dalton Trans*, 2013, **42**, 15735–15747.

[4] M. Meyer, V. Dahaoui-Gindrey, C. Lecomte and R. Guilard, *Coord. Chem. Rev.*, 1998, **178–180**, 1313–1405.

[5] M. J. Frisch, G. W. Trucks, H. B. Schlegel, G. E. Scuseria, M. A. Robb, J. R. Cheeseman, G. Scalmani, V. Barone, B. Mennucci, G. A. Petersson and et al., Gaussian 09, Revision D.01, Gaussian, Inc.: Wallingford.

[6] Y. Zhao and D. G. Truhlar, *Theor. Chem. Acc.*, 2008, **120**, 215–241.

[7] M. Dolg, H. Stoll and H. Preuss, *Theor. Chim. Acta*, 1993, **85**, 441–450.

APPENDIX 3

T. Krchová, V. Herynek, A. Gálisová, J. Blahut, P. Hermann and J. Kotek: "Eu(III) complex with DO3A-amino-phosphonate ligand as a concentration-independent pH-responsive contrast agent for Magnetic Resonance Spectroscopy (MRS)", *Inorg. Chem.*, 2017, DOI: 10.1021/acs.inorgchem.6b02749

Inorganic Chemistry

Article

pubs.acs.org/IC

Eu(III) Complex with DO3A-amino-phosphonate Ligand as a Concentration-Independent pH-Responsive Contrast Agent for Magnetic Resonance Spectroscopy (MRS)

Tereza Krchová,[†] Vít Herynek,[‡] Andrea Gálisová,[‡] Jan Blahut,[†] Petr Hermann,[†] and Jan Kotek*[,†]

[†]Department of Inorganic Chemistry, Faculty of Science, Charles University, Hlavova 2030, Prague 2 128 43, Czech Republic

[‡]Department of Radiodiagnostic and Interventional Radiology, Magnetic Resonance Unit, Institute for Clinical and Experimental Medicine, Vídeňská 1958/9, Prague 4 140 21, Czech Republic

Supporting Information

ABSTRACT: A new DOTA-like ligand H_5do3aNP with a 2-[amino(methylphosphonic acid)]ethyl-coordinating pendant arm was prepared, and its coordinating properties were studied by NMR spectroscopy and potentiometry. The study revealed a rare slow exchange (on the ^{1}H and ^{31}P NMR time scale) between protonated and unprotonated complex species with a corresponding acidity constant $pK_A \sim 8.0$. This unusually slow time scale associated with protonation is caused by a significant geometric change from square-antiprismatic (SA) arrangement observed for protonated complex SA-[Eu(Hdo3aNP)]$^-$ to twisted-square-antiprismatic (TSA) arrangement found for deprotonated complex TSA-[Eu(do3aNP)]$^{2-}$. This behavior results in simultaneous occurrence of the signals of both species in the ^{31}P NMR spectra at approximately −118 and +70 ppm, respectively. Such an unprecedented difference in the chemical shifts between species differing by a proton is caused by a significant movement of the principal magnetic axis and by a change of phosphorus atom position in the coordination sphere of the central Eu(III) ion (i.e., by relative movement of the phosphorus atom with respect to the principal magnetic axis). It changes the sign of the paramagnetic contribution to the ^{31}P NMR chemical shift. The properties discovered can be employed in the measurement of pH by MRS techniques as presented by proof-of-principle experiments on phantoms.

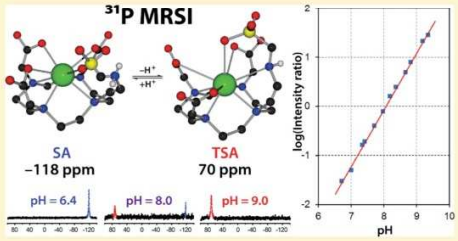

INTRODUCTION

Over the past two decades, the ability to provide essential information about variations in tissue pH has become increasingly important. Therefore, it is not surprising that magnetic resonance imaging (MRI), as one of the most widely used diagnostic methods in clinical medicine,[1] has been proposed as a suitable technique for this purpose. The tumor extracellular microenvironment is often slightly more acidic than healthy tissue due to increased anaerobic glycolysis and a related accumulation of lactic acid, reduced passive buffering capacity, and poor tissue perfusion.[2] For example, the extracellular pH in solid tumors typically ranges between 6.5 and 7.2.[3] Therefore, measurement of extracellular pH using noninvasive techniques is important not only for early detection of disease or metabolic disorder, but also for suggesting the most efficient treatment and for monitoring the effects of pH-altering therapies.[2] Nowadays, several strategies (and appropriate contrast agents, CAs) to measure tissue pH are intensively investigated.[4] Previous studies have suggested relaxation-based MRI CAs with longitudinal relaxivity (r_1) dependent on pH.[5] The Gd(III) complexes investigated were based on a variation in the number of inner-sphere water molecules (q), for example, caused by the presence of β-arylsulfonamide[6] or p-nitrophenol[7] groups on the chelate species. The deprotonation and coordination of these groups is associated with removal of the inner-sphere water molecule, and such a change in q leads to a change in relaxivity r_1. Similarly, in the case of Gd(III) complexes of H_3do3a with 2-aminoethyl pendant arms, such as H_3do3a-ae (Figure 1), a change in the protonation state of the amino group causes a (de)coordination of the pendant arm, and thus, it also leads to changes in relaxivity.[8] Interesting results have been obtained by Hall et al., who studied the Gd(III) complex with terpyridine-containing macrocycle.[9] The authors demonstrated a significant decrease of relaxivity with increasing pH and attributed it to a decrease in q from 3 to 0 due to formation of the hydroxido species and hydroxido-bridged dimer connected with a negligible exchange rate of coordinated OH^- ions.[9] However, for quantification of pH using these relaxation-based CAs, knowledge of the actual agent concentration is needed.[10] This is the reason why new methods employing ratiometric approaches are developed, as they remove dependence of the observed signal on the local concentration of CAs. For example,

Received: November 17, 2016

DOI: 10.1021/acs.inorgchem.6b02749
Inorg. Chem. XXXX, XXX, XXX−XXX

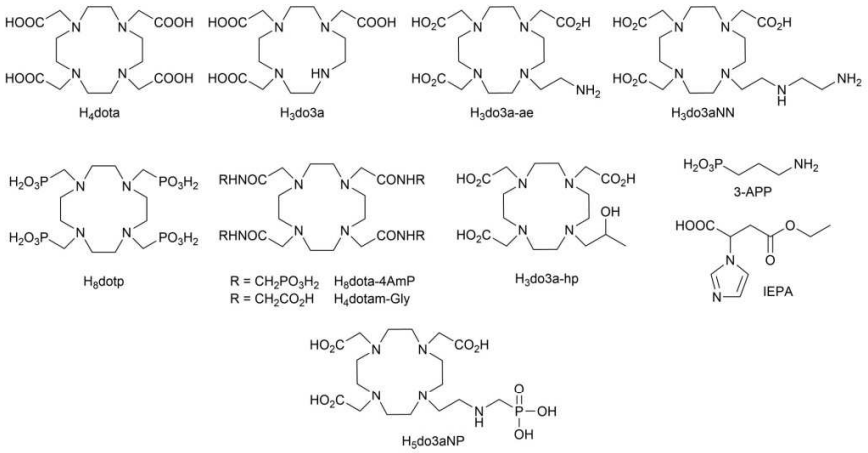

Figure 1. Structural formulas of the ligands discussed in the text.

Gillies and co-workers developed a "dual-injection" relaxivity-based method employing administration of two compounds (pH-sensitive $[Gd(dota\text{-}4AmP)]^{5-}$ and pH-insensitive $[Gd(dotp)]^{5-}$; for structures of both ligands, see Figure 1) with a comparable biodistribution and pharmacokinetics, allowing determination of the concentration of the first agent from the concentration of the second one. It was shown that this approach allowed pH mapping both *in vitro* and *in vivo*.[5b,10,11] An alternative approach was introduced by Aime et al. They investigated the possibility of measuring the ratio of transversal and longitudinal relaxation rates of water protons (R_2/R_1) after injecting a single paramagnetic Gd(III) complex of DOTA-functionalized polypeptide (poly-L-ornithine).[12] Recently, the paramagnetic MRI contrast agents that are detected via the chemical exchange saturation transfer (CEST) effect, so-called PARACEST CAs, have also been used to ratiometrically estimate *in vitro*/*in vivo* pH by utilizating a ratio of two different CEST signals.[3,13] These can originate from the exchangeable protons of the same molecule, as in the case of paramagnetic H_4dotam-Gly (Figure 1) complexes with some Ln(III) ions (Pr, Nd, and Eu) where the protons of a coordinated water molecule and amide protons of the macrocyclic ligand represent two CEST-active exchanging pools.[14] Similarly, the Yb(III) complex of H_3do3aNN (Figure 1) with two proton-exchanging pools of the primary and secondary amino groups has been shown to be suitable for this purpose.[15] Two different CEST signals can also originate from two conformations of the same molecule generating CEST signals at different chemical shifts, as was shown for Yb(III)-analogue of the clinically used $[Gd(do3a\text{-}hp)(H_2O)]$ (ProHance; Figure 1).[13e,16]

An alternative approach to *in vivo* pH measurement is the MRS (magnetic resonance spectroscopy) technique. In general, MRS provides information about abundance and concentration of tissue metabolites, and it can help to characterize many pathologies, including neurological, psychiatric, and metabolic diseases.[17] In addition, spectral information on a metabolite/compound with a particular chemical shift can be encoded into the image, and a map of its spatial distribution can be reconstructed by a method called magnetic resonance spectroscopic imaging (MRSI). Several methods for pH mapping by MRS using different endogenous or exogenous compounds have been used, and these are generally based on a difference in chemical shifts between pH-dependent and pH-independent resonances. Application of MRS to measure pH began early on with the acquisition of the ^{31}P MR spectra of inorganic phosphate (P_i) because its resonance frequency is pH-dependent. The majority of P_i resonance comes from intracellular phosphate,[18] and thus, the chemical shift of the P_i generally reflects the intracellular pH.[2,11,19] To determine the extracellular pH of tumors in animal models, nontoxic exogenous reporter 3-aminopropylphosphonic acid (3-APP; Figure 1) with chemical shift dependence ~1 ppm per pH unit has been used.[2,19] Tissue pH can also be detected *in vivo* using diamagnetic ^{1}H MRS probes with the pH-sensitive signal of ^{1}H nucleus. Exogenously administered 2-imidazol-1-yl-3-ethoxy-carbonyl-propionic acid (IEPA; Figure 1) has been employed for this purpose. The chemical shift of the imidazole ring C-2 hydrogen atom is in the 7−9 ppm range and is pH-sensitive. This compound has been used for imaging extracellular pH in breast or brain tumors.[20] However, the disadvantage of using diamagnetic compounds as pH probes is the fact that their signal can be overlapped with the resonances of other compounds present *in vivo*. Therefore, complexes of paramagnetic metal ions are studied due to the expanded chemical shift scale of NMR-active nuclei. In particular, Ln(III) complexes with macrocyclic ligands have been used because they are stable under *in vivo* conditions. The Yb(III) complex of H_8dotp (Figure 1) has been introduced as a prototype of a new class of pH indicators because stepwise protonation of the complex is accompanied by variations in the protons' chemical shifts (6 resonances in ^{1}H NMR spectrum); this enables creation of a calibration curve for pH determination.[21] Simultaneous determination of pH and temperature by Tm(III) complexes of H_8dotp using three proton chemical shifts was studied by a three-dimensional chemical shift method called biosensor imaging of redundant deviation in shift (BIRDS).[22] The Ln(III) complexes of two metal ions (Tm and Yb) with phosphonate ligand H_8dota-4AmP (Figure 1)

DOI: 10.1021/acs.inorgchem.6b02749
Inorg. Chem. XXXX, XXX, XXX−XXX

also exhibit suitable pH-sensitivities for BIRDS detection using chemical shift difference between two proton resonances. Moreover, these agents are also CEST-active, and thus, the CEST effect observed together with BIRDS opens the way toward high-resolution and quantitative pH imaging.[23]

To contribute to the fields described above, we prepared a new macrocyclic ligand H_5do3aNP (Figure 1). The aminophosphonate-coordinating pendant arm was chosen because, in general, protonation constants of amino and phosphonate groups are close to the physiological pH; thus, the complexes of the new ligand were expected to change their properties in the pH region relevant for living systems. In addition, the presence of a phosphorus atom could be potentially employed in ^{31}P NMR-based applications. In this work, we report on ligand synthesis and the unusual ^{1}H and ^{31}P NMR properties of its europium(III) complex which are employable in ^{31}P MRS/MRSI for determination of pH. In addition, potentiometric and NMR studies found high stability for the studied complex in solution, which is promising for potential *in vivo* use of related compounds.

EXPERIMENTAL SECTION

Materials and Methods. Unless stated otherwise, commercially available chemicals and solvents were used without further purification. Water used for potentiometric titrations was deionized by the Milli-Q device (Millipore).

1,4,7-Tris(*tert*-butylcarboxymethyl)-1,4,7,10-tetraazacyclododecane hydrobromide (*t*Bu$_3$do3a·HBr)[24] and *N*-benzylethanolamine[25] were prepared according to the published procedures. Dichloromethane (DCM) was dried by the standard procedure[26] and stored over molecular sieves under an argon atmosphere.

NMR characterization data (1D: ^{1}H, ^{13}C; 2D: HSQC, HMBC, ^{1}H–^{1}H COSY, ^{1}H–^{1}H EXSY, ^{31}P–^{31}P EXSY) were recorded on VNMRS300, Bruker Avance III 400, or Bruker Avance III 600 spectrometers, using 5 mm sample tubes. The longitudinal relaxation times T_1's of ^{31}P were measured on the VNMRS300 by inversion recovery pulse sequence (15 or 10 increments on d2 exponentially sampled) with the spectrometer offset identical to the compound signal and properly calibrated pulse length. Selectively ^{1}H-decoupled ^{13}C NMR spectra were obtained on the Bruker Avance III 600 spectrometer by standard one-pulse ^{13}C measurement with low-power continuous-wave ^{1}H decoupling at the desired frequency offset. Exchange rates were measured using a selective ^{31}P–^{31}P EXSY pulse sequence with the mixing-time changing from 20 μs to 500 ms exponentially. Exchange rates of isomer interchange were determined by numerical fitting of the mixing-time-dependent ^{31}P NMR integral value with the Bloch–McConnell equation using Matlab.[27] Unless stated otherwise, NMR experiments were performed at 25 °C. The pD value means a reading of the freshly calibrated pH electrode of the sample dissolved in D_2O corrected by +0.4. Chemical shifts δ are given in ppm, and coupling constants J are reported in Hz. For ^{1}H and ^{13}C{^{1}H} measurements of diamagnetic compounds in D_2O, *t*BuOH was used as the internal standard (δ_H = 1.25, δ_C = 30.29). For the measurements in $CDCl_3$, TMS was used as the internal standard (δ_H = 0.00, δ_C = 0.00). For ^{31}P measurements, 85% H_3PO_4 in H_2O was used as the external standard (δ_P = 0.00). In the case of paramagnetic complexes, ^{1}H chemical shifts were referenced to the *t*BuOH signal of the sample (δ_H = 1.25). Abbreviations [s (singlet), d (doublet), t (triplet), m (multiplet), and br (broad)] are used in order to express the signal multiplicities. Lanthanide(III) concentrations in solutions were determined by measuring bulk magnetic susceptibility (BMS) shifts.[28]

The ESI-MS spectra were run on the Bruker ESQUIRE 3000 spectrometer equipped with an electrospray ion source and ion-trap detection. The measurements were carried out in both positive and negative modes.

Luminescence spectra were acquired on a Luminescence Thermo Spectronic spectrometer AMINCO Bowman Series 2. The luminescence spectra were obtained after excitation at the Eu(III) $^5L_6 \leftarrow {}^7F_0$ band (λ = 396 nm).

Syntheses. *Synthesis of 1.* Paraformaldehyde (4.00 g, 133 mmol) was added to a well-stirred solution of *N*-benzylethanolamine (4.00 g, 26.5 mmol) and diethyl-phosphite (17.2 mL, 134 mmol) in dry MeCN (30 mL). The reaction mixture was stirred at 60 °C for 2 days, filtered, and then evaporated on a rotary evaporator. The oily residue was dissolved in a small amount of EtOH, and then the solution was loaded onto a strong cation exchanger column (Dowex 50, H^+-form, 4 cm × 20 cm, in EtOH). Impurities were removed by elution with EtOH, and product **1** was eluted with concentrated aqueous NH_3/EtOH (1/5). The fractions containing product **1** (TLC and ^{1}H NMR check) were combined, evaporated, redissolved in absolute EtOH, and evaporated to give compound **1** (7.62 g, 95.6%) as a brownish oil.

^{1}H NMR (299.9 MHz, CD_3OD): δ 1.34 (6H, t, $^3J_{HH}$ = 7.0, CH_2CH_3); 2.80 (2H, t, $^3J_{HH}$ = 6.0, CH_2CH_2OH); 3.07 (2H, d, $^2J_{HP}$ = 10.0, PCH_2N); 3.67 (2H, t, $^3J_{HH}$ = 6.0, CH_2CH_2OH); 3.85 (2H, s, CH_2Ph); 4.13 (4H, dq, $^3J_{HH}$ = $^3J_{PH}$ = 7.0, CH_2CH_3); 7.25–7.41 (5H, m, arom). ^{13}C{^{1}H} NMR (75.4 MHz, CD_3OD): δ 17.64 (2C, d, $^3J_{CP}$ = 6.0, OCH_2CH_3); 51.09 (1C, d, $^1J_{CP}$ = 162, PCH_2N); 58.89 (1C, d, $^3J_{CP}$ = 8.0, CH_2); 61.9 (1C, CH_2); 62.24 (1C, $^3J_{CP}$ = 7.5, CH_2); 64.39 (2C, $^2J_{CP}$ = 7.0, OCH_2CH_3); 129.16 (1C, arom); 130.18 (2C, arom); 131.02 (2C, arom); 140.83 (1C, arom quaternary). ^{31}P{^{1}H} NMR (121.4 MHz, CD_3OD): δ 27.17 (1P, s). ^{31}P NMR (121.4 MHz, CD_3OD): δ 27.17 (1P, m). MS-ESI: (+) 323.7 ([M + Na]$^+$, calcd 324.1).

Synthesis of 2. A solution of CH_3SO_2Cl (1.14 g, 9.96 mmol, 1.2 equiv) in dry CH_2Cl_2 (10 mL) was dropwise added to a well-stirred solution of **1** (2.50 g, 8.30 mmol) and Et_3N (1.68 g, 16.6 mmol, 2 equiv) in dry CH_2Cl_2 (70 mL) with cooling (ice bath). The reaction mixture was then stirred for 20 min. Next, saturated aqueous $NaHCO_3$ (50 mL) was added, and the mixture was stirred for 10 min. The organic layer was separated, washed with saturated aqueous $NaHCO_3$ (2 × 30 mL) and H_2O (2 × 30 mL), dried over Na_2SO_4, and concentrated *in vacuo* to give 3.05 g (97%) of **2** as a brownish oil. Compound **2** is not stable and must be immediately used for further synthesis.

^{1}H NMR (299.9 MHz, $CDCl_3$): δ 1.31 (6H, t, $^3J_{HH}$ = 7.0, CH_2CH_3); 2.98 (2H, d, $^2J_{HP}$ = 11.0, PCH_2N); 2.99 (3H, s, CH_3); 3.08 (2H, t, $^3J_{HH}$ = 6.0, OCH_2CH_2N); 3.85 (2H, s, CH_2Ph); 4.09 (4H, dq, $^3J_{HH}$ = $^3J_{PH}$ = 7.0, CH_2CH_3); 4.29 (2H, t, $^3J_{HH}$ = 6.0, $S(O)_2CH_2CH_2N$); 7.23–7.35 (5H, m, arom). ^{13}C{^{1}H} NMR (75.4 MHz, $CDCl_3$): δ 16.60 (2C, d, $^3J_{CP}$ = 6.0, OCH_2CH_3); 37.50 (1C, $S(O)_2CH_3$); 49.67 (1C, d, $^1J_{CP}$ = 159, PCH_2N); 53.62 (1C, d, $^3J_{CP}$ = 6.0, CH_2); 60.40 (1C, $^3J_{CP}$ = 9.0, CH_2); 62.03 (2C, $^2J_{CP}$ = 7.0, OCH_2CH_3); 68.19 (1C, CH_2); 127.56 (1C, arom); 128.49 (2C, arom); 129.11 (2C, arom); 138.17 (1C, arom quaternary). ^{31}P{^{1}H} NMR (121.4 MHz, $CDCl_3$): δ 24.80 (1P, s). ^{31}P NMR (121.4 MHz, $CDCl_3$): δ 24.80 (1P, m).

Synthesis of 3. A solution of alkylating reagent **2** (2.71 g, 7.14 mmol, 1.70 equiv) in dry MeCN (30 mL) was dropwise added to a well-stirred suspension of *t*Bu$_3$do3a·HBr (2.50 g, 4.20 mmol) and K_2CO_3 (1.15 g, 8.3 mmol, 2 equiv) in dry MeCN (45 mL). The reaction mixture was stirred at room temperature for 1 day and filtered, and the filtrate was evaporated on a rotary evaporator. The oily residue was dissolved in $CHCl_3$ (30 mL) and extracted with distilled water (4 × 15 mL). The organic layer was dried over Na_2SO_4 and concentrated *in vacuo* to give 4.50 g of a yellow oil containing crude compound **3** contaminated with an excess of the alkylating reagent **2** and the products of its degradation. Crude product **3** was used in the next step without purification.

^{31}P{^{1}H} NMR (121.4 MHz, $CDCl_3$, 25 °C): δ 25.89 (1P, s). ^{31}P NMR (121.4 MHz, $CDCl_3$): δ 25.89 (1P, m). MS-ESI: (+) 797.8 ([M + H]$^+$, calcd 798.5); 819.9 ([M + Na]$^+$, calcd 820.5).

Synthesis of 4. The total amount of crude compound **3** obtained above (4.50 g) was dissolved in a mixture of CF_3CO_2H and $CHCl_3$ (40 mL, 1:1 v:v). The resulting solution was refluxed for 18 h and then evaporated on a rotary evaporator. The oily residue was dissolved in a

DOI: 10.1021/acs.inorgchem.6b02749
Inorg. Chem. XXXX, XXX, XXX–XXX

small amount of distilled water and evaporated, and this procedure was repeated three more times. The oily residue was dissolved in a small amount of distilled water, and the solution was loaded onto a strong cation exchanger column (Dowex 50, H^+-form, 4 cm × 15 cm). The impurities were removed by elution with water, and product **4** was eluted with aq NH_3 (5%). The fractions containing product **4** (^1H NMR check) were combined. After evaporation of volatiles, the oily residue was dissolved in water and poured onto a column of a weak cation exchanger (Amberlite CG50, 200−400 mesh, 4 cm × 15 cm). The impurities were eluted off with water, and product **4** was collected by 20% aq CH_3COOH. The fractions containing product **4** were combined and evaporated to give 2.30 g of brownish oil, which was used in the next step without further purification.

When crude product **4** prepared in another batch was left to stand for several days, it solidified on standing. The sample for elemental analysis was isolated by washing this solid with ethanol, filtering, and then equilibrating the solid in ambient air.

^1H NMR (600 MHz, D_2O, 50 °C, pD = 6.74, Figure S1): δ 1.33 (6H, t, $^3J_{HH}$ = 7.0, CH_2CH_3); 2.94 (2H, t, $^3J_{HH}$ = 6.0, CH_2NCH_2Ph); 3.01−3.85 (6H, br, $CH_2CH_2NCH_2Ph$ + macrocyclic CH_2); 3.11−3.16 (6H, br, NCH_2P + macrocyclic CH_2); 3.18−3.22 (4H, br m, macrocyclic CH_2); 3.29−3.34 (4H, br m, macrocyclic CH_2); 3.45 (4H, br s, CH_2CO); 3.58 (2H, br s, CH_2CO); 3.81 (2H, s, NCH_2Ph); 4.14 (4H, m, CH_2CH_3); 7.38−7.47 (5H, m, arom). $^{13}C\{^1H\}$ NMR (150.9 MHz, D_2O, 50 °C, pD = 6.74, Figure S2): δ 16.30 (2C, OCH_2CH_3); 49.69 (1C, d, $^1J_{CP}$ = 160, PCH_2N); 49.69 (1C, d, $^3J_{CP}$ = 8.0, CH_2NCH_2Ph); 49.91 (2C, macrocyclic CH_2); 50.71 (2C, macrocyclic CH_2); 50.86 (1C, $CH_2CH_2NCH_2Ph$); 51.11 (4C, macrocyclic CH_2); 56.40 (1C, CH_2CO); 57.47 (2C, CH_2CO); 60.66 (1C, d, $^3J_{CP}$ = 8.5, CH_2Ph); 64.22 (1C, d, $^2J_{CP}$ = 6.5, OCH_2CH_3); 128.52 (1C, arom); 129.34 (2C, arom); 13.21 (2C, arom); 138.44 (1C, arom quaternary); 173.73 (1C, CH_2CO); 174.94 (2C, CH_2CO). $^{31}P\{^1H\}$ NMR (121.4 MHz, D_2O, pD = 6.74, Figure S3): δ 28.39 (1P, s). ^{31}P NMR (121.4 MHz, D_2O, pD = 6.74, Figure S4): δ 28.39 (1P, m). MS-ESI: (+) 629.3 ($[M + H]^+$, calcd 630.0); 652.0 ($[M + Na]^+$, calcd 652.3); (−) 627.8 ($[M - H]^-$, calcd 628.3). Elemental analysis found (calcd for **4**·$4H_2O$, $C_{28}H_{56}N_5O_{13}P$, M_r = 701.8): C, 47.90 (47.92); H, 7.54 (8.04); N, 9.76 (9.98); P, 3.94 (4.41).

Synthesis of ***5****.* The total amount of crude product **4** obtained above (2.30 g) was dissolved in concentrated aqueous HCl (20 mL) and stirred at 95 °C for 24 h. Then, the solution was evaporated on a rotary evaporator, dissolved in a small amount of water, and loaded onto a strong cation exchanger column (Dowex 50, H^+-form, 4 cm × 15 cm). The impurities were removed by elution with water, and product **5** was eluted with 5% aq NH_3. The fractions containing the product were combined, filtered, and evaporated to give compound **5** (1.35 g) as a brownish oil which was used in the next step without further purification.

$^{31}P\{^1H\}$ NMR (121.4 MHz, D_2O, pD = 3.9): 7.68 (1P, s). ^{31}P NMR (121.4 MHz, D_2O, pD = 3.9): 7.68 (1P, t, $^2J_{HP}$ = 12.5). MS-ESI: (+) 574.0 ($[M + H]^+$, calcd 574.3); 611.9 ($[M + K]^+$, calcd 612.2); 633.9 ($[M + Na + K - H]^+$, calcd 634.2); (−) 571.8 ($[M - H]^-$, calcd 572.3); 609.8 ($[M + K - 2H]^-$, calcd 610.2).

Synthesis of H_5*do3aNP.* Crude product **5** (1.30 g) was dissolved in 20% aq CH_3CO_2H (50 mL). Next, Pd/C catalyst (10%, 0.26 g) was added, and the flask was evacuated and filled by H_2. The mixture was stirred under a hydrogen atmosphere (using a rubber balloon) for 48 h at room temperature (RT). Then, the catalyst was removed by filtration, and all volatiles were evaporated *in vacuo*. The product H_5do3aNP was purified by chromatography on a strong cation exchanger column (Dowex 50, H^+-form, 3 cm × 15 cm). Impurities were removed by elution with water, and the product H_5do3aNP was eluted with 5% aq pyridine. The fractions containing the product were combined, filtered, and evaporated to dryness leaving a glassy solid which was dissolved in a small amount of water and crystallized by standing for 2 h. The white crystalline solid was isolated by filtration, washed with EtOH, and air-dried to give a white powder of hydrate H_5do3aNP·$4.5H_2O$ (1050 mg, 44% based on $t$$Bu_3$do3a·HBr).

^1H NMR (600 MHz, D_2O, pD = 5.81, Figure S5): δ 2.86−2.94 (4H, br m, macrocyclic CH_2); 3.00−3.05 (4H, br, NCH_2CH_2NH + macrocyclic CH_2); 3.07−3.10 (2H, br m, macrocyclic CH_2); 3.20 (2H, br s, CH_2CO_2); 3.23 (2H, d, $^2J_{HP}$ = 12.0, NCH_2P); 3.30 (2H, br t, $^3J_{HH}$ = 5.0, NCH_2CH_2NH); 3.30−3.37 (2H, br m, macrocyclic CH_2); 3.42−3.45 (2H, br m, macrocyclic CH_2); 3.53−3.56 (2H, br m, macrocyclic CH_2); 3.69−3.72 (2H, br m, macrocyclic CH_2); 3.88 (4H, AB-multiplet, CH_2CO_2). $^{13}C\{^1H\}$ NMR (150.9 MHz, D_2O, pD = 5.81, Figure S6): δ 45.78 (1C, d, $^1J_{CP}$ = 136, NCH_2P); 46.54 (1C, d, $^3J_{CP}$ = 3.5, CH_2NHCH_2P); 48.97 (2C, macrocyclic CH_2); 49.00 (2C, macrocyclic CH_2); 50.36 (1C, $CH_2CH_2NCH_2P$); 51.08 (2C, macrocyclic CH_2); 53.02 (2C, macrocyclic CH_2); 55.71 (1C, CH_2CO); 57.83 (2C, CH_2CO); 170.92 (2C, CH_2CO); 178.98 (1C, CH_2CO). $^{31}P\{^1H\}$ NMR (121.4 MHz, D_2O, pD = 5.81, Figure S7): δ 9.37 (1P, s). ^{31}P NMR (121.4 MHz, D_2O, pD = 5.81, Figure S8): δ 9.37 (1P, t, $^2J_{HP}$ = 12.0). MS-ESI: (+) 483.6 ($[M + H]^+$, calcd 484.2); 505.6 ($[M + Na]^+$, calcd 506.2); (−) 481.3 ($[M-H]^-$, calcd 482.2); 519.1 ($[M + Cl]^-$, calcd 518.2). Elemental analysis found (calcd for H_5do3aNP·$4.5H_2O$, $C_{17}H_{43}N_5O_{13.5}P$, M_r = 564.4): C, 36.22 (36.17); H, 8.09 (7.68); N, 12.17 (12.41); P, 5.61 (5.49).

Synthesis of Eu(III)−H_5*do3aNP Complex.* Three procedures for preparation of the Eu(III) complex of H_5do3aNP for NMR and MRI experiments were used. In the first one, $EuCl_3·6H_2O$ was mixed with 1.05 equiv of the ligand in a small amount of distilled water. The pH was adjusted to 7 with 1 M aq NaOH, and the solution was stirred overnight at 60 °C. Then, the pH was readjusted to 7 with 1 M aq NaOH, and the solution was again stirred overnight at 60 °C.

In the second case, the Eu(III) complex was prepared by mixing the ligand with 1 equiv of Eu(III) acetate stock solution (concentration was determined by measuring BMS shifts)[28] in a small amount of distilled water. The pH was adjusted to ∼8 with concentrated aq NH_3, and the mixture was stirred overnight at 60 °C. Then, the solution was filtered and evaporated to dryness leaving a glassy solid, which was dissolved in distilled water and evaporated on a rotary evaporator at 90 °C to remove ammonium acetate (this procedure was then repeated five more times).

In the third case, the Eu(III) complex was prepared by mixing $EuCl_3·6H_2O$ with 1.05 equiv of the ligand in a small amount of distilled water. The pH was adjusted to ∼8 with 0.8 M aq $(NMe_4)OH$, and the mixture was stirred overnight at 60 °C.

All prepared samples were checked using the xylenol orange test (acetate buffer, pH = 5.7) to exclude the presence of free Eu(III) ions. The exact concentration of Eu(III) complex in solution was determined using Evans' method.[28]

Eu(III)−H_5do3aNP MS-ESI: (−) 631.6 with appropriate isotopic pattern ($[M - H]^-$, calcd 632.1).

X-ray Diffraction Study. Single crystals of H_5do3aNP·$4.75H_2O$ were prepared by slow evaporation of the aqueous solution of H_5do3aNP. Diffraction data were collected by employing an ApexII CCD diffractometer using Mo Kα radiation (λ = 0.71073 Å) at 150(1) K and analyzed using the SAINT V8.27B (Bruker AXS Inc., 2012) program package. The structures were solved by direct methods (SHELXS97)[29] and refined by full-matrix least-squares techniques (SHELXL97).[30] Relevant data for the structures have been deposited at the Cambridge Crystallographic Data Centre. The structure was solved in space group $P\bar{1}$, where the independent unit consists of two ligand molecules which have very similar conformations. However, higher symmetry (c/2) is prevented by disorder of the phosphonate moiety of one of the units. The 10 highest isolated electronic maxima were attributed to the water solvate molecules, one of them half-occupied due to collision with one position of disordered phosphonate oxygen atoms. All non-hydrogen atoms were refined anisotropically, and hydrogen atoms were fixed in theoretical (C−H, N−H) or original (O−H) positions using a riding model $U_H = 1.2U_X$.

Crystal data follow: H_5do3aNP·$4.75H_2O$, $C_{17}H_{43.5}N_5O_{13.75}P$, M = 569.04, triclinic, a = 11.0215(3) Å, b = 12.3502(3) Å, c = 19.0688(6) Å, α = 84.311(1)°, β = 80.106(1)°, γ = 81.467(1)°, U = 2521.46(12) Å^3, space group $P\bar{1}$, z = 4, 11576 total reflections, 8615 intense reflections, R1[$I > 2\sigma(I)$] = 0.0535, wR2(all data) = 0.1543. CCDC-1500120.

Potentiometry. Potentiometric titrations were carried out in a thermostated (25.0 ± 0.1 °C) vessel at a constant ionic strength [I =

DOI: 10.1021/acs.inorgchem.6b02749
Inorg. Chem. XXXX, XXX, XXX−XXX

Scheme 1. Synthesis of H_5do3aNP[a]

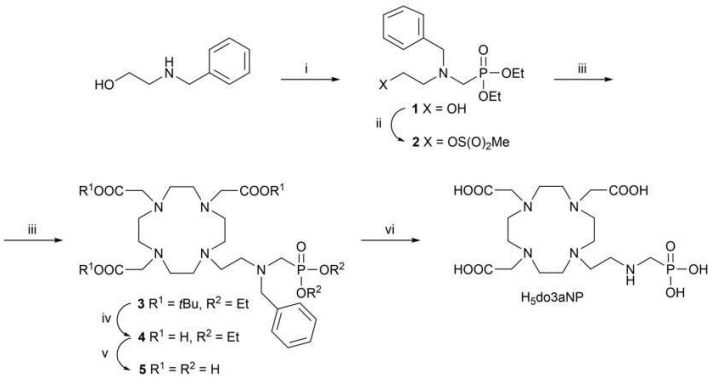

[a](i) $HP(O)(OEt)_2$, $(CH_2O)_n$, dry MeCN, 60 °C, 2 days; (ii) CH_3SO_2Cl, Et_3N, dry CH_2Cl_2, 0 °C−RT, 20 min; (iii) *t*Bu_5do3a·HBr, K_2CO_3, dry MeCN, RT, 24 h; (iv) CF_3COOH:$CHCl_3$ (1:1), reflux 18 h; (v) conc aq HCl, 95 °C, 24 h; (vi) H_2, Pd/C, 20% aq CH_3COOH, RT, 2 days.

0.1 M $(Me_4N)Cl$]. Measurements were taken with an excess of HCl stock solution added to the initial mixture, and the mixtures were titrated with stock solution of $(NMe_4)OH$. The ligand concentration in the titration vessel was ca. 0.004 M. An inert atmosphere was provided by a constant passage of argon saturated with water vapor. Before and after each titration, calibrations [titrations of HCl stock solution with $(NMe_4)OH$ stock solution] were performed for determination of electrode calibration parameters as described previously.[31]

For determination of the ligand protonation constants, a standard technique was used,[31] with the initial volume ca. 5 cm^3 and in the pH range 1.9−12.1. Four titrations were carried out with ∼70 points per titration.

Titrations of the Eu(III)−H_5do3aNP system were performed by an out-of-cell technique[31] as the equilibrium was established slowly. In the experiments, the metal-to-ligand molar ratio was 1.00:1.04, and the starting volume of each titration point [before addition of (NMe_4)-OH] was ca. 1 cm^3. In total, two titration sets in the pH range 1.8−9.0 were prepared with 30 points per titration, and ampules with solutions were flame-sealed. After 4 weeks (waiting time for equilibration), the potential of each solution was determined with a freshly calibrated electrode, with measurement of odd and even data points separately affording four independent data series of 15 data points.

A preformed Eu(III) complex for determination of its protonation constants was prepared in the following way: in the ampule, equimolar amounts of the ligand and metal stock solutions were mixed, and a calculated amount (based on out-of-cell titration data) of $(NMe_4)OH$ stock solution was gradually added to reach pH ca. 6, which corresponds to full complexation according to the out-of-cell titration. Ampules were flame-sealed and left at 55 °C for 3 days. From the final solution, aliquot volumes were pipetted, a defined amount of HCl stock solution was added into these samples, and the mixtures were immediately titrated by $(NMe_4)OH$ stock solution in an analogous way as described above for the determination of the ligand protonation constants; the concentration of the complex in the titration vessel was ca. 0.003 M. The pH range used in these titrations was 1.9−9.5, and the titrations were carried out four times with 30 points per titration.

The OPIUM program package[32] was used for calculation of the ligand protonation constants and stability/protonation constants of the Eu(III) complex. All constants are concentration constants. Calculated protonation constants are defined as $\beta_h = [H_hL]/\{[H]^h[L]\}$, and they can be transferred to consecutive protonation constants log K by log $K(H_hL) = \log \beta_h - \log \beta_{h-1}$. Calculated stability constants β_{hlm} are defined by $\beta_{hlm} = [H_hL_lM_m]/\{[H]^h[L]^l[M]^m\}$. Calculated constants with their standard deviations are compiled in Tables S8−S10, and the fits of titration data are shown in Figures S27, S31, and S32. The water ion product used in all calculations was $pK_w = 13.81$.[33]

^{31}P and ^{1}H NMR Titration of H_5do3aNP and Its Eu(III) Complex. ^{31}P and ^{1}H NMR spectra were performed on a VNMRS300 (B_0 = 7.05 T) using 5 mm sample tubes. A coaxial capillary with 85% H_3PO_4 in H_2O ($\delta_P = 0$) or with *t*BuOH in D_2O ($\delta_H = 1.25$) as the external standard was used. Solution pH was measured with a combined glass electrode (Spintrode Hamilton) employing a pH meter (350S pH Meter, JENWAY) calibrated with standard buffers. Protonation constants were calculated with the OPIUM software package.[32]

^{31}P NMR titration (46 points) for determination of protonation constants and sites of H_5do3aNP was performed at 25 °C (0.05 M ligand concentration; no ionic strength control) in H_2O. The solution pH (0.1−13.6) was adjusted with aq HCl or aq $(NMe_4)OH$ solutions. The fit is shown in Figure S28.

^{1}H NMR titration of H_5do3aNP in the alkaline region (14 points) was performed at 25 °C (0.05 M ligand concentration; no ionic strength control) in H_2O. Solution pH (7.9−12.0) was adjusted with aq HCl or aq KOH solutions. The fit is shown in Figure S29.

^{31}P NMR titration in acidic region (14 points) of preformed Eu(III)−H_5do3aNP complex was performed at 25 °C (0.038 M complex concentration; ∼ 150 mM NaCl) in H_2O. Solution pH (from 7.0 to 2.0) was adjusted with aq HCl solutions. The fit is shown in Figure S20.

MRS Experiments. A phantom consisting of one vial containing an aq solution of H_3PO_4 as a reference and three vials containing ∼50 mM aq solutions of the Eu(III)−H_5do3aNP complex (∼150 mM NaCl) with different pH values (6.4, 8.0, and 9.0) was prepared for MRS experiments. At these pH values, the once protonated complex $[Eu(Hdo3aNP)]^-$ and the fully deprotonated species $[Eu(do3aNP)]^{2-}$ are present, with the former predominant at pH = 6.4 and the latter at pH = 9.0. At pH = 8.0, both species are present in similar abundance (see distribution diagram in Figure 6).

All MRS experiments were performed on a 4.7 T MR scanner BioSpec (Bruker BioSpin, Germany) using a dual ^{1}H/^{31}P surface coil with a diameter of 5 cm (Bruker BioSpin, Germany). Nonlocalized ^{31}P MRS spectra of the phantom were acquired by using a single rectangular pulse with 0.064 ms duration and 20000 Hz bandwidth (BW); the other measurement parameters were the following: acquisition delay 0.05 ms, repetition time (TR) = 1000 ms, number of acquisitions (NA) = 512, and scan time 8.5 min. For ^{1}H reference

DOI: 10.1021/acs.inorgchem.6b02749
Inorg. Chem. XXXX, XXX, XXX−XXX

images, a turbo spin echo sequence was used with the following parameters: TR/TE = 3000 ms/12 ms, turbo factor = 8, matrix size of 256 × 256, field of view (FOV) = 35 mm × 35 mm, slice thickness 1 mm, and scan time 5 min. ^{31}P MRSI spectra localized from 4 × 4 voxels covering the whole phantom volume were acquired by chemical shift imaging sequence using the same rectangular pulse as for the nonlocalized ^{31}P MR spectra. Spectral width 20 kHz (246.44 ppm) was sampled by 8192 points. The spectra were acquired by 16384 accumulations from the volume with field of view = 32 mm × 32 mm and slice thickness 10 mm; the other parameters were TR = 1000 ms, effective echo time (TE_{eff}) = 15 ms, and scan time 4.5 h. Raw data were interpolated to a matrix 32 × 32 × 8192 by zero-filling, and Fourier transform provided a three-dimensional matrix of numbers containing information about signal amplitude spatially encoded in *x*- and *y*-axis; frequency chemical shift was encoded in *z*-axis.

^{31}P MRSI data were processed using ImageJ software (version 1.46r, National Institutes of Health). First, the data were interpolated into a matrix size of 256 × 256 × 256. Then, the images acquired within an interval of 70 ± 4 ppm were summed (to obtain an integral signal) as well as the images in the interval of 0 ± 4 ppm and −118 ± 4 ppm, and were finally false color coded.

■ RESULTS AND DISCUSSION

Synthesis. The target ligand H_5do3aNP was prepared following the multistep synthesis outlined in Scheme 1. The key phosphorus-containing intermediate **1** was obtained by Mannich-type reaction of *N*-benzyl-ethanolamine with diethylphosphite and paraformaldehyde and was isolated after cation-exchange chromatography. It was converted to alkylation agent **2** by reaction with methanesulfonyl chloride, and compound **2** was used in the reaction with *t*Bu$_3$do3a, affording intermediate **3**. After sequential deprotection of *t*Bu-ester and ethyl-ester groups using trifluoroacetic acid and aq hydrochloric acid, respectively, the de-esterified compound **5** was hydrogenated using the Pd/C catalyst to give the target ligand H_5do3aNP that was purified by cation-exchange chromatography and was isolated in the zwitterionic form in the overall 44% yield (based on *t*Bu$_3$do3a·HBr).

The target ligand H_5do3aNP was structurally characterized by single-crystal X-ray diffraction analysis. In the crystal structure of H_5do3aNP·4.75H_2O, two independent ligand molecules are present, but both adopt a very similar conformation. Therefore, only one of them is shown in Figure 2. A zwitterionic molecule is protonated on two nitrogen atoms of the macrocycle (those bearing the "*trans*" acetate groups) and the nitrogen atom of the side arm. The remaining protons are located on the phosphonate and on the "odd" acetate groups. Molecular conformation is stabilized by medium-strength intramolecular hydrogen bonds (Table S1), and the whole structure is stabilized through a wide system of intermolecular hydrogen bonds involving water molecules.

Solution Structure of the Eu(III)−H_5do3aNP Complex. Ln(III) complexes of the DOTA-like ligands are typically present in a solution as a mixture of square-antiprismatic (SA) and twisted-square-antiprismatic (TSA) isomers.[34] These isomers differ in conformation of the five-membered chelate rings of the macrocycle (δ/λ) and course of rotation of the pendant arms (Δ/Λ). Combination of the macrocycle and pendant conformations results in two diastereomeric pairs of the enantiomers (Figure S9). The pair $\Delta\lambda\lambda\lambda\lambda/\Lambda\delta\delta\delta\delta$ forms the SA arrangement while the $\Delta\delta\delta\delta\delta/\Lambda\lambda\lambda\lambda\lambda$ enantiomers correspond to the TSA structure.[35] Typically, two diastereomers are in a slow exchange with respect to the time scale of an NMR experiment, giving rise to two sets of ^{1}H NMR signals. Therefore, both isomers can be distinguished, and their relative

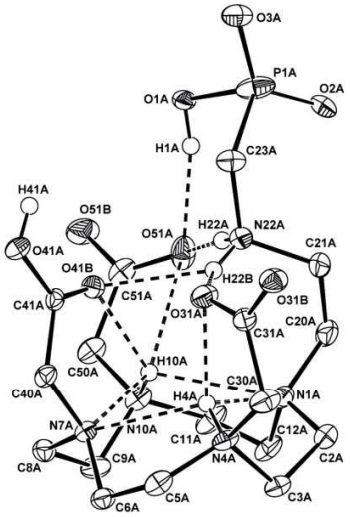

Figure 2. Molecular structure of H_5do3aNP found in the crystal structure of H_5do3aNP·4.75H_2O. Intramolecular hydrogen bonds are dashed (Table S1).

abundance in solution can be easily determined. Isomerism evaluation mostly uses signals of "axial" protons of the macrocyclic ring (Figure S9) because these are the closest ones to the Ln(III) ion and to the principal magnetic axis; thus, they are shifted away from the other signals in the ^{1}H NMR spectra. Typically, "axial" signals of the TSA species of Eu(III) complexes with DOTA-like ligands are found in the ∼7−28 ppm range whereas those of the SA isomers appear in the ∼25−40 ppm region.[36]

Solution structure of the Eu(III) complex species was investigated by ^{1}H NMR spectroscopy in the pD range 6.8−9.9 (Figure 3 and Figure S10). At pD < 7.3, only one set of signals was observed in the ^{1}H NMR spectra, where the signals of the most positively shifted "axial" protons of the complex species appear in the range typical for the SA isomer (20−49 ppm). At higher temperatures, the ^{1}H NMR signals somewhat shift and broaden due to faster conformational changes of the complex molecule (Figure S11). With increasing pD, ^{1}H NMR signals of the SA isomer gradually disappear with a simultaneous appearance of peaks attributable to the TSA isomer with the most shifted signals in the 7−14 ppm range (Figure 3 and Figure S10). Thus, one can suggest that both SA and TSA species are present in the pD range 7.5−9.0 (Figures S10, S12, and S13). At pD > 9.0, only signals of pure TSA species were detected. Heating of the alkaline solution also led to a significant broadening of signals of the TSA isomer, pointing to conformational change of the complex molecule (Figures S12 and S14). On the basis of these observations, one can suggest that two differently protonated species are present in the pD range 7.5−9.0; so, the pK_A of the deprotonation process lies in this range, and thus, the deprotonation obviously occurs on the pendant amino group. The protonated form of the complex exists exclusively in the SA isomer, whereas the pure TSA species is formed upon deprotonation.

DOI: 10.1021/acs.inorgchem.6b02749
Inorg. Chem. XXXX, XXX, XXX−XXX

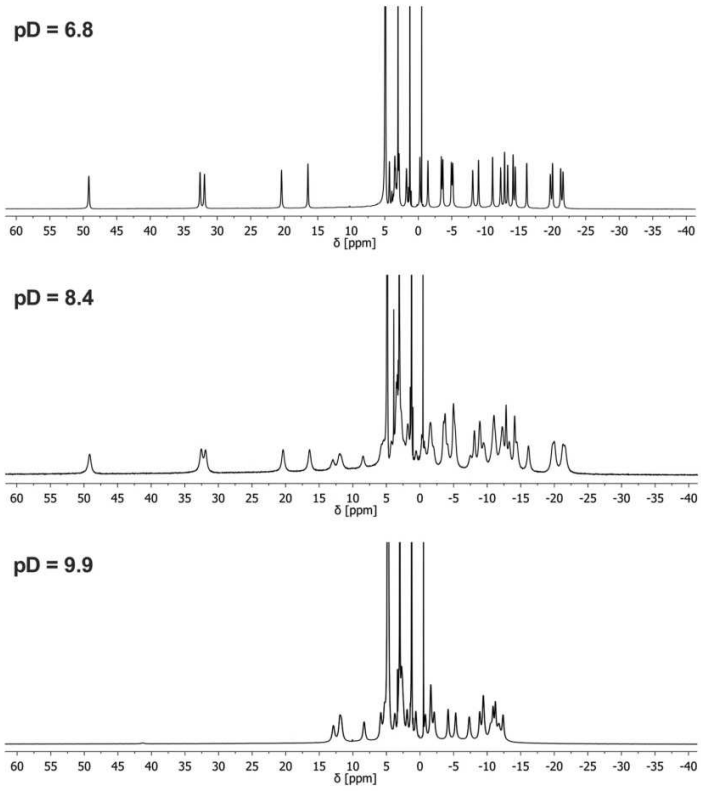

Figure 3. ^{1}H NMR spectra of SA-[Eu(Hdo3aNP)]$^{-}$/TSA-[Eu(do3aNP)]$^{2-}$ (~0.08 M solution in D_2O, B_0 = 7.05 T) at different pD values.

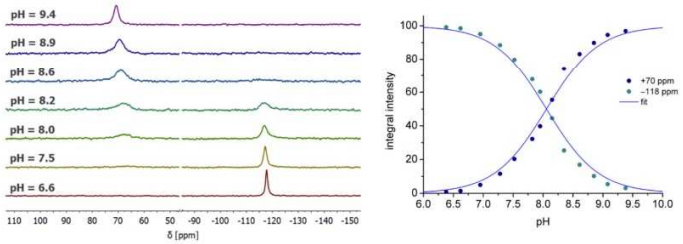

Figure 4. ^{31}P{^{1}H} NMR spectra of SA-[Eu(Hdo3aNP)]$^{-}$/TSA-[Eu(do3aNP)]$^{2-}$ complex species at various pH values and corresponding pH dependence of an integral intensity of ^{31}P NMR signals (50 mM solution in H_2O, ~150 mM NaCl, B_0 = 7.05 T, 25 °C).

^{31}P NMR spectroscopic study also revealed a slow chemical exchange between both complex species with respect to the time scale of the NMR experiment (Figure 4 and Figures S16 and S18) as the signals of both species are present in the ^{31}P NMR spectra acquired in the pH range 7.5−8.9; their chemical shifts remain nearly constant with pH change. ^{31}P NMR 1D-EXSY revealed a rate for isomer interconversions on a millisecond scale (rate constants 191(8) s^{-1} for SA → TSA and 156(7) s^{-1} for TSA → SA rearrangements, respectively, 25 °C, pD = 8.6). In addition, an extreme chemical shift difference (by ~190 ppm) between signals of the SA and TSA species was observed. In both species, the phosphonate group is obviously coordinated, as evidenced by a significantly influenced ^{31}P NMR chemical shift (+70 ppm for the TSA and −118 ppm for

DOI: 10.1021/acs.inorgchem.6b02749
Inorg. Chem. XXXX, XXX, XXX−XXX

the SA species, respectively, Figure 4) compared to that for the diamagnetic La(III) complex (δ = 25.3 ppm at pD = 7.0 and δ = 22.7 ppm at pD = 10.1). The coordination of the phosphonate group was also confirmed by measurement of T_1 relaxation times of ^{31}P NMR signal, which are T_1 = 0.207(4) s for the SA species (measured at pD = 6.8) and T_1 = 0.202(11) s for the TSA species (pD = 9.6), respectively, whereas the La(III) complex relaxes much slower with T_1 = 1.84(8) s (pD = 7.0) and T_1 = 3.09(10) s (pD = 10.1).

The dependence of integral intensities of these signals on pH is sigmoidal and, in accordance with the suggestion stated above, could be successfully modeled by an equilibrium involving just one (de)protonation step (Figure 4 and Figures S16−S18), affording the protonation constant log K(=pK_A) = 7.4−8.5 with dependence on ionic strength, see Table S2. The ^{31}P chemical shifts of both species (Figures S16 and S18) and derived protonation constants (Table S2) are independent of complex concentration; therefore, intermolecular coordination of the phosphonate to the metal ion belonging to a different complex molecule and the formation of polynuclear complexes can be excluded. Furthermore, the protonated complex was found to be fully stable at pD = 5.9 (Figure S19). The value of the protonation constant log K is dependent on the quality and concentration of a background electrolyte: in the presence of NaCl, the value drops with increasing concentration of the salt because the presence of a coordinating metal ion generally facilitates a deprotonation of the donor atoms. In contrast, when ^{31}P NMR titration was performed with the use of $(NMe_4)Cl$ as the background electrolyte, the value of the protonation constant was significantly higher (Table S2). In the presence of $CaCl_2$ and $MgCl_2$, i.e., in the presence of stronger coordinating metal ions (Figure S18), the chemical shifts in ^{31}P NMR spectra remain unaffected, and log K's are lower than those calculated in the case of NaCl-containing solutions (Table S2).

On the basis of the value of log K, the protonation process obviously occurs on the pendant arm amino group, and thus, one can conclude that the equilibrium involves monodeprotonated and fully deprotonated complex species; thus, the complex species are SA-[Eu(Hdo3aNP)]$^-$ and TSA-[Eu(do3aNP)]$^{2-}$. To confirm such an assignment, the ^{1}H NMR spectra were also measured in H_2O solution. In a slightly acid region, no difference between the spectra of SA-[Eu(Hdo3aNP)]$^-$ acquired in D_2O and H_2O was found (Figure S15A,B). At this pH, the side amino group is protonated (and thus uncoordinated), and the hydrogen atoms are exchanged with the solvent (D_2O) or overlaid with others; on the basis of chemical exchange saturation transfer experiments, chemical shift of these hydrogen atoms is −17 ppm if referenced as $\delta(H_2O)$ = 0.[37] In contrast, in a slightly alkaline region, a new signal at 36.4 ppm (if referenced as $\delta(H_2O)$ = 0) appeared in the spectra of TSA-[Eu(do3aNP)]$^{2-}$ acquired in H_2O (Figure S15C,D). This peak can be attributed to a hydrogen atom bound in the coordinated pendant secondary amino group, where this hydrogen atom is not in fast exchange with the solvent. This assignment is also supported by a similarity in the chemical shift of this signal to the values observed for structurally related compounds [Eu(do3a-ae)] and [Eu(do3aNN)] (Figure 1), respectively; one of the ^{1}H NMR signals of the coordinated primary amino group in [Eu(do3a-ae)] lies at 34 ppm,[44] and the signal of one of the isomers of [Eu(do3aNN)] with a coordinated secondary amino group is located at 35 ppm.[15]

With mononuclearity of the complex species taken into account, electrostatic repulsion of the central metal ion and the protonated pendant amino group, as well as general steric hindrances, the phosphonate group should be in the protonated SA-[Eu(Hdo3aNP)]$^-$ species coordinated in the O_4-plane (Scheme 2). In such a case, it opens a space for coordination of

Scheme 2. Suggested Geometry of the SA-[Eu(Hdo3aNP)]$^-$ and TSA-[Eu(do3aNP)]$^{2-}$ Species[a]

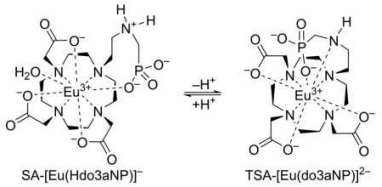

[a]A water molecule in the protonated species is expected to be coordinated in the apical position.

a water molecule in an O_4-capping apical position. Luminescence lifetimes of Eu(III) ion were measured, giving τ = 697 μs for SA-[Eu(Hdo3aNP)]$^-$ species in H_2O (pH = 6.4) and τ = 2.21 ms when this sample was evaporated and dissolved in D_2O, consistent with the assumption of water coordination.[38] After deprotonation, coordination of the secondary amino group occurs and forms an O_3N-coordination plane in the TSA-[Eu(do3aNP)]$^{2-}$ species. The phosphonate group very probably moves to the position capping this O_3N-plane (Scheme 2). However, although the geometry discussed above is the sole possibility making chemical sense, it is a bit contradictory in a comparison of the ^{31}P NMR shift of SA-[Eu(Hdo3aNP)]$^-$ species with that of Eu(III) complexes of DOTA-like ligands having methylenephosphonate/phosphinate pendant moieties, which have a phosphorus atom in a similar spatial position as that expected for SA-[Eu(Hdo3aNP)]$^-$. To the best of our knowledge, in all Eu(III) complexes of phosphinate/phosphonate ligands reported previously, the paramagnetic contribution to the ^{31}P NMR shift is positive, giving signals with 15−70 ppm higher chemical shift compared to that of the free ligands or diamagnetic La(III) complexes (Table S3).[36b,c,e,f,39,40] Contrary to these values, when comparing ^{31}P NMR shift differences between Eu(III) and La(III) complexes of H_5do3aNP in acid media, the paramagnetic contribution to chemical shift of SA-[Eu(Hdo3aNP)]$^-$ is $\Delta\delta$ = −143 ppm.

The origin of this contradiction probably lies in the low symmetry of the ligand field of the SA-[Eu(Hdo3aNP)]$^-$ complex, which can lead to a discrepancy between principal magnetic and pseudo-C_4 axes and to significant anisotropy of magnetically induced shifts.[41] Typically, the complexes of DOTA-like ligands have (pseudo)-C_4 symmetry, and it is usually suggested that the principal magnetic axis is identical with (or very close to) the (pseudo)symmetry C_4 axis. In such axially symmetric systems, the phosphorus atoms lie outside the McConnell cone, which defines a sign of paramagnetic contribution to the chemical shift [in relevant crystal structures, angle between (pseudo)-C_4 axis and Ln−P vector is 73−89° (Figure S22 and Table S4),[36e,b,40,42] whereas the McConnell critical angle is 54.7°]. It should be noted that, for historical reasons, the direction of upfield−downfield shifts differs for ^{1}H

DOI: 10.1021/acs.inorgchem.6b02749
Inorg. Chem. XXXX, XXX, XXX−XXX

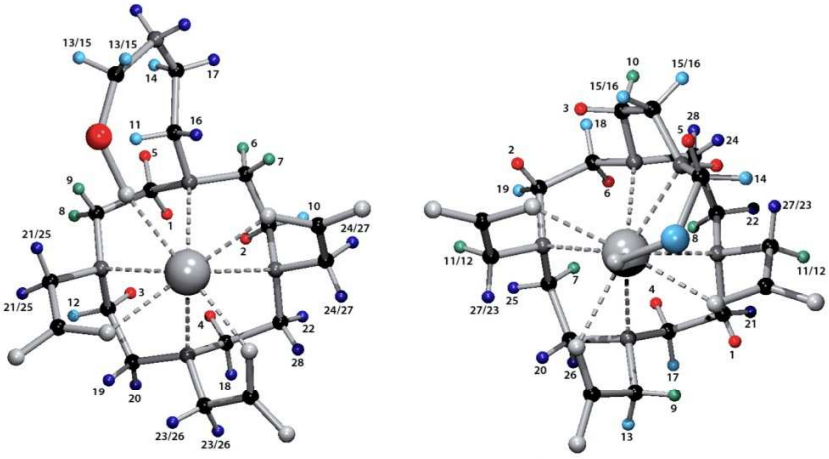

Figure 5. Assignment of the ^{1}H NMR spectra of SA-[Eu(Hdo3aNP)]$^{-}$/TSA-[Eu(do3aNP)]$^{2-}$ complex species. Geometry of the complex species is tentative and was not optimized. Atoms are labeled by order numbers from the spectra going from left to right according to Figure S24. For better visualization, protons with positive paramagnetic contribution are red, those with small negative contribution are pale blue, those with large negative contribution dark blue, and those which are not influenced are green. For phosphorus atom, the red color indicates a negative ^{31}P NMR shift contribution (i.e., position in space with positive ^{1}H NMR shift contribution), and blue indicates a positive ^{31}P NMR shift contribution (i.e., space with negative ^{1}H NMR shift contribution).

Table 1. Equilibrium Constants (log K and log K_{ML})[a] of H_5do3aNP (0.1 M NMe_4Cl, 25 °C) and Its Eu(III) Complexes and Comparison with Corresponding Constants Reported for Related Ligands

equilibrium	H_5do3aNP potentiometry	H_5do3aNP ^{31}P NMR	H_3do3aNN[b]	H_3do3a-ae[c]	H_4dota
$H^+ + L^{n-} \leftrightarrow HL^{1-n}$	12.56(1)	12.52(17)	12.62	13.19	12.9[e]
$H^+ + HL^{1-n} \leftrightarrow H_2L^{2-n}$	10.37(1)	10.59(3)	10.28	10.51	9.72[e]
$H^+ + H_2L^{2-n} \leftrightarrow H_3L^{3-n}$	9.23(1)	9.37(8)	9.67	8.90	4.60[e]
$H^+ + H_3L^{3-n} \leftrightarrow H_4L^{4-n}$	6.17(1)	5.96(8)	8.30	3.87	4.15[e]
$H^+ + H_4L^{4-n} \leftrightarrow H_5L^{5-n}$	4.19(1)		3.30	1.27	2.29[e]
$H^+ + H_5L^{5-n} \leftrightarrow H_6L^{6-n}$	1.90(1)	2.05(9)	1.58		1.34[e]
$Eu^{3+} + L^{n-} \leftrightarrow [Eu(L)]^{3-n}$	23.49(3)		23.16	22.23[d]	24.2[f]
$H^+ + [Eu(L)]^{3-n} \leftrightarrow [Eu(HL)]^{4-n}$	8.00(3)		6.03	5.83[d]	
$H^+ + [Eu(HL)]^{4-n} \leftrightarrow [Eu(H_2L)]^{5-n}$	3.75(4)		5.09		
$H^+ + [Eu(H_2L)]^{5-n} \leftrightarrow [Eu(H_3L)]^{6-n}$	4.35(4)				
$H^+ + [Eu(H_3L)]^{6-n} \leftrightarrow [Eu(H_4L)]^{7-n}$	3.31(4)				

[a] $K = [H_hL]/\{[H][H_{h-1}L]\}$ or $[H_hLM]/\{[H][H_{h-1}LM]\}$; $K_{ML} = [ML]/\{[L]\cdot[M]\}$. [b] Ref 15. [c] Ref 44. [d] Data reported for Gd(III) complex. [e] Ref 45. [f] Ref 33.

and ^{31}P NMR scales; therefore, in the same space, the ^{31}P NMR paramagnetic induced shift contribution is positive whereas that of ^{1}H NMR is negative (and *vice versa*). However, in the case of the SA-[Eu(Hdo3aNP)]$^{-}$ complex, there is a large difference in chemical shifts of "axial" macrocycle protons [these protons have a similar position with respect to pseudo-C_4 symmetry defined by the central ion and the barycenter of the N_4-plane, and thus, they should have a similar chemical shift when the magnetic axis is identical to the (pseudo)symmetry axis]; this points to some difference between positions of pseudosymmetric-C_4 and principal magnetic axes. Therefore, the phosphorus atom could fall into a space close to the principal magnetic axis direction with induced positive ^{1}H/negative ^{31}P NMR shifts. To confirm this assumption, the signals found in ^{1}H NMR spectra of both SA-[Eu(Hdo3aNP)]$^{-}$ and TSA-[Eu(do3aNP)]$^{2-}$ complexes were assigned on the basis of ^{1}H COSY and ^{1}H EXSY experiments and ^{13}C NMR spectra with selectively tuned ^{1}H decoupling (Figure S23−S26 and Tables S5−S7). The assignment is shown in Figure 5 (for detailed description see SI). This assignment confirmed that the position of the phosphorus atom moves from a space with induced positive ^{1}H/negative ^{31}P NMR shifts in SA-[Eu(Hdo3aNP)]$^{-}$ to an area with negative ^{1}H/positive ^{31}P NMR shifts in TSA-[Eu(do3aNP)]$^{2-}$ complexes, respectively. Another surprising finding is the fact that the most shifted signals in ^{1}H NMR spectra of TSA-[Eu(do3aNP)]$^{2-}$ species are not the "axial" ones. In this case, the direction of the most positive ^{1}H induced shift probably lies almost parallel in respect to the N_4-plane, so the principal magnetic axis should be almost perpendicular to the pseudo-C_4 axis. The phosphorus atom falls outside this direction, and so, its induced ^{31}P paramagnetic shift is positive in the ^{31}P NMR scale.

DOI: 10.1021/acs.inorgchem.6b02749
Inorg. Chem. XXXX, XXX, XXX−XXX

Further acidification of the solution of the SA-[Eu(Hdo3aNP)]$^-$ species leads to a gradual change of the ^{31}P chemical shift from −118 ppm at pH = 7 to −156 ppm at pH = 2 (Figure S20). Obviously, as the chemical shift is very affected in the whole of this pH region, the phosphonate group is still coordinated, and the gradual change of the chemical shift corresponds to formation of the SA-[Eu(H_2do3aNP)] species. From the ^{31}P NMR data, log K = 3.40(1) was calculated which confirms this assignment because the protonation constant of the free phosphonate group (log K ∼ 5−7) drops to the log K ∼ 3−4 range upon coordination to the metal ion.[43] Formation of the SA-[Eu(H_2do3aNP)] species was also supported by the ^{1}H NMR spectra of the complex in acidic solution (Figure S21).

Thermodynamic Behavior of H_5do3aNP and Its Eu(III) Complex. To obtain information on thermodynamic stability of the studied Eu(III) complex and confirm the conclusions stated above, potentiometric studies of the H_5do3aNP, equilibrated Eu(III)−H_5do3aNP system and preformed Eu(III)−H_5do3aNP complex were performed.

The potentiometric titrations of H_5do3aNP performed in the pH range 1.9−12.1 revealed six consecutive protonation processes (Table 1 and Table S8; fit shown in Figure S27); the ligand distribution diagram is shown in Figure S30. Five of these constants could also be calculated from the pH dependence of the ^{31}P NMR spectra (Table 1 and Table S8, fit shown in Figure S28). On the basis of comparison with the literature data,[43] the first protonation step (log K(HL) = 12.56) can be attributed to a proton shared by the macrocycle amino groups. This assignment of the protonation site is consistent with a relatively small change (+0.5 ppm) of the ^{31}P NMR shift and a large change of the ^{1}H chemical shift of the α-acetate protons (+0.21 and +0.28 ppm for "double" and "odd" acetates, respectively) compared to that of the NCH_2P group (+0.05 ppm), see Table S8 and Figure S29. According to the highest change (∼6 ppm) in ^{31}P chemical shift during the NMR titration, the second protonation step (log K(H_2L) = 10.37) obviously occurs on the amino group belonging to the pendant moiety. It is also consistent with changes observed in ^{1}H NMR spectra; change of δ(^{1}H) of NCH_2P is 0.25 ppm, much higher than the δ(^{1}H) changes of the acetate groups (0.11 and 0.08 ppm, respectively, see Table S8). The value of the protonation constant is higher than the value reported for the analogous protonation of the 2-aminoethyl arm for H_3do3a-ae (log K = 8.90)[44] due to the positive induction effect of the phosphonate moiety.[43] Analogous protonation of H_3do3aNN occurs in this pH region, although in that case it was not possible to assign an exact value due to a number of protonation steps occurring with similar log K's.[15] The third protonation (log K(H_3L) = 9.23) corresponds to the second protonation of the macrocycle amino groups. The log K(H_3L) is somewhat lower than the second ring-amine protonation of related ligands due to electrostatic repulsion with a protonated pendant amino group. The third protonation locks two protons on the macrocycle nitrogen atoms bearing "*trans*" acetate groups due to mutual electrostatic repulsion, as evidenced by change of δ(^{1}H) (+0.38 and −0.26 ppm for "double" and "odd" acetates, respectively, see Figure S29). The fourth protonation with log K(H_4L) = 6.17 occurs on the phosphonate moiety, as evidenced by a reverse change of the ^{31}P NMR shift (Figure S28). The next one (log K(H_5L) = 4.19) is associated with the protonation of the acetate *trans* to the aminophosphonate arm, and it has no influence on the chemical shift of the ^{31}P NMR signal due to a long distance between these groups, so this constant cannot be calculated from ^{31}P NMR data. The last (sixth) protonation occurs on one of the remaining acetate arms or macrocycle amino groups. The suggested protonation scheme is fully consistent with the molecular structure found in the solid state (see above).

The stability constant of the [Eu(do3aNP)]$^{2-}$ complex (log K_{ML} = 23.49, Table 1) was obtained by an out-of-cell titration technique. The value falls into the expected range, as can be seen from a comparison with the stability constants reported for the related ligands (Table 1). According to the distribution diagrams of the Eu(III)−H_5do3aNP system shown in Figure 6, the metal ion complexation is quantitative at pH ∼ 4.5.

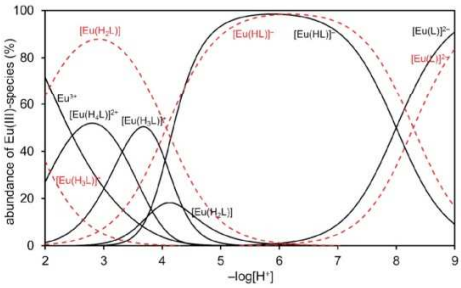

Figure 6. Distribution diagram of metal-containing species in the Eu(III)−H_5do3aNP system (black solid lines, c_M = c_L = 0.004 M) and of species present in acid−base titration of the preformed [Eu(do3aNP)]$^{2-}$ complex (red dashed lines) Conditions: 25 °C, I = 0.1 M NMe_4Cl.

The first protonation of the fully deprotonated species, [Eu(do3aNP)]$^{2-}$, proceeds with log K(HLM) = 8.0. In the analysis of the NMR spectra (see above), this protonation was suggested to occur on the side arm secondary amino group. The protonation constant of this group in the free ligand has the value log K(H_2L) = 10.37, and so a significant metal-induced decrease of this value confirms coordination of the deprotonated amino group to the central Eu(III) ion.

A further three protonation steps in the equilibrated solutions occur with log K's in a narrow range ∼3−4 (Table 1). These processes occur at pH higher than that corresponding to protonation of the coordinated acetate group and, thus, can be attributed to simultaneous protonations of the phosphonate group and the macrocycle nitrogen atoms. Therefore, the equilibrated species H_3LM and H_4LM are expected to be out-of-cage complexes with double-protonated macrocycle amino groups similar to those suggested for other systems with DOTA-like ligands.[40]

To support the conclusions stated above, an acid−base titration of the preformed complex was performed. In this case, only three stepwise protonation constants were found: log K(HLM) = 8.29(2), log K(H_2LM) = 4.07(3), and log K(H_3LM) = 1.75(3) (see Table S10 and distribution diagram in Figure 6). According to the interpretation above, the first constant corresponds to a protonation of the pendant amino group, and this value is consistent with the results of ^{31}P NMR and out-of-cell potentiometric studies. The second constant is assigned to protonation of the coordinated phosphonate group, consistent with the ^{31}P NMR data presented above. The

DOI: 10.1021/acs.inorgchem.6b02749
Inorg. Chem. XXXX, XXX, XXX−XXX

differences between values obtained by the ^{31}P NMR and potentiometric titrations can be attributed to a difference in ionic strength, different methods of pH electrode calibration, and temperature of the pH measurement. The third constant calculated for the preformed complex is significantly lower compared to constants observed in the equilibrated solutions (out-of-cell titration). One can assume that during the short time scale of the potentiometric titration only the in-cage complex is present (i.e., no dissociation of macrocycle−Eu(III) bonds occurs) due to relative kinetic inertness of the complexes with DOTA-like ligands,[1] and therefore, this constant corresponds very probably to the protonation of a coordinated carboxylate group.

Overall, the results of the potentiometric study are fully consistent with the results of ^{31}P NMR studies discussed above and support the interpretation shown in Scheme 2.

pH Mapping Using MRS. To address possible pH determination from ^{31}P NMR data, the logarithm-weighted ratio of integral intensity of the ^{31}P NMR signals of TSA-[Eu(do3aNP)]$^{2-}$ and SA-[Eu(Hdo3aNP)]$^{-}$ was calculated. This function is linear in the pH range 6.5−9.5, as shown in Figure 7, proving the principle of the suggested method (the data were observed at various experimental conditions).

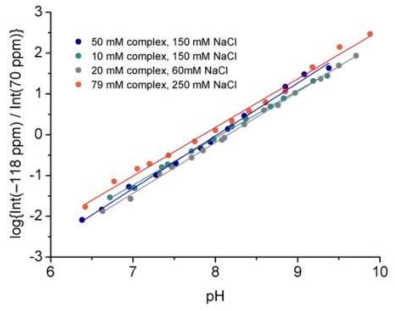

Figure 7. Dependence of y = log{Int(−118 ppm)/Int(70 ppm)} ∼ log{[SA]/[TSA]} on pH in solutions with different concentrations of the complex probe and at different ionic strengths relevant for physiologic conditions.

Finally, we tested the applicability of the [Eu(do3aNP)]$^{2-}$/[Eu(Hdo3aNP)]$^{-}$ system as a pH probe for MRI. However, this experiment had some limitations due to the accessible hardware. The broad spectral width (20 kHz/246 ppm) necessary for the experiment required a short excitation pulse. Due to hardware limitations, a block pulse (instead of modulated one) had to be used for excitation to reach sufficient pulse intensity. As the excitation profile of the block pulse is inhomogeneous, intensities at different frequencies may not exactly correspond to the concentrations. The space-localized ^{31}P MR spectra were measured in the phantom consisting of four vials: a vial containing an aqueous solution of H_3PO_4 as a reference and three vials containing the Eu(III)−H_5do3aNP complex solutions having different pH values (6.4, 8.0, and 9.0). The localized spectra and intensity of individual signals from different parts of the phantom are shown in Figure 8, and the results clearly show a spatial resolution of areas with different pH values, proving the suggested concept.

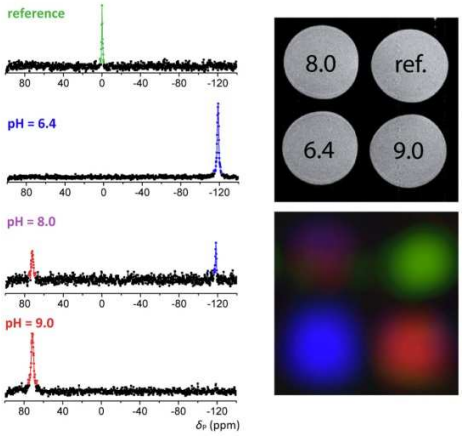

Figure 8. Left: localized ^{31}P MR spectra. Right: pH map and legend (^{1}H MR reference image) of phantom consisting of one vial containing aqueous H_3PO_4 as a reference and three vials containing aqueous solutions of the Eu(III)−H_5do3aNP complex with different pH values. Postprocessing included interpolation to a spatial 256 × 256 matrix, integration over the selected signals, and false color coding. Color scheme: red, signal at +70 ppm; blue, −118 ppm; purple color results from red/blue superposition; green, 0 ppm.

■ CONCLUSIONS

New ligand H_5do3aNP with a 2-[amino(methylphosphonic acid)]ethyl pendant arm was synthesized, and its coordination properties were studied by potentiometry and NMR spectroscopy. Full in-cage complexation of Eu(III) is finished at pH > 4.5, forming the protonated SA-[Eu(Hdo3aNP)]$^{-}$ complex with square-antiprismatic (SA) geometry. Upon deprotonation with pK_A ∼ 8, the twisted-square-antiprismatic TSA-[Eu(do3aNP)]$^{2-}$ complex is formed. Both complexes are in a slow equilibrium on the NMR time scale, and their ^{31}P NMR shifts differ by ∼190 ppm due to significant movement of the principal magnetic axis leading to different paramagnetic contributions to the ^{31}P NMR shift. To the best of our knowledge, such a strict change of the coordination geometry with (de)protonation has not been observed before.

The existence of two separate signals in the ^{31}P NMR spectra allows ratiometric determination of pH by MRS. As both signals belong to the same compound (differing just by its protonation state), this ensures the same biodistribution of both species, and the ratiometric approach brings the advantage of independence of the measured data on the probe concentration. Unfortunately, the pK_A of the studied complex lies somewhat outside the region optimal for *in vivo* use; nevertheless, this parameter can be altered by a suitably designed ligand, and thus, the discovered principle shows promising potential for *in vivo* applications.

■ ASSOCIATED CONTENT

Supporting Information

The Supporting Information is available free of charge on the ACS Publications website at DOI: 10.1021/acs.inorgchem.6b02749.

DOI: 10.1021/acs.inorgchem.6b02749
Inorg. Chem. XXXX, XXX, XXX−XXX

NMR spectra and studies, hydrogen bond lengths, and potentiometric results (PDF)
Crystal data (CIF)

AUTHOR INFORMATION

Corresponding Author

*E-mail: modrej@natur.cuni.cz. Phone: +420-221951261. Fax: +420-221951253.

ORCID

Jan Kotek: 0000-0003-1777-729X

Notes

The authors declare no competing financial interest.

ACKNOWLEDGMENTS

We thank Z. Böhmová for the potentiometric measurements and Dr. I. Císařová for the X-ray diffraction study. Support from the Grant Agency of the Czech Republic (Project 16-03156S) is acknowledged. We really appreciate remarks from the referees regarding the spatial dependence of the paramagnetic contribution to chemical shift.

REFERENCES

(1) *The Chemistry of Contrast Agents in Medical Magnetic Resonance Imaging*, 2nd ed.; Merbach, A., Helm, L., Tóth, É., Eds.; Wiley: Chichester, United Kingdom, 2013.

(2) Gillies, J. R.; Raghunand, N.; Garcia-Martin, M. L.; Gatenby, R. A. pH imaging: A review of pH measurement methods and applications in cancers. *IEEE Eng. Med. Biol.* **2004**, *23*, 57−64.

(3) Hingorani, D. V.; Bernstein, A. S.; Pagel, M. D. A review of responsive MRI contrast agents: 2005−2014. *Contrast Media Mol. Imaging* **2015**, *10*, 245−265.

(4) Zhu, L.; Yang, Y.; Farquhar, K.; Wang, J.; Tian, C.; Ranville, J.; Boyes, S. G. Surface Modification of Gd Nanoparticles with pH-Responsive Block Copolymers for Use As Smart MRI Contrast Agents. *ACS Appl. Mater. Interfaces* **2016**, *8*, 5040−5050.

(5) (a) Zhang, S.; Wu, K.; Sherry, A. D. A Novel pH-Sensitive MRI Contrast Agent. *Angew. Chem., Int. Ed.* **1999**, *38*, 3192−3194. (b) Raghunand, N.; Howison, C.; Sherry, A. D.; Zhang, S.; Gillies, R. J. Renal and systemic pH imaging by contrast-enhanced MRI. *Magn. Reson. Med.* **2003**, *49*, 249−257. (c) Kálmán, F. K.; Woods, M.; Caravan, P.; Jurek, P.; Spiller, M.; Tircso, G.; Kiraly, R.; Brücher, E.; Sherry, A. D. Potentiometric and Relaxometric Properties of Gadolinium-based MRI Contrast Agent for Sensing Tissue pH. *Inorg. Chem.* **2007**, *46*, 5260−5270.

(6) Lowe, M. P.; Parker, D.; Reany, O.; Aime, S.; Botta, M.; Castellano, G.; Gianolio, E.; Pagliarin, R. pH-dependent modulation of relaxivity and luminescence in macrocyclic gadolinium and europium complexes based on reversible intramolecular sulfonamide ligation. *J. Am. Chem. Soc.* **2001**, *123*, 7601−7609.

(7) Woods, M.; Kiefer, G. E.; Bott, S.; Castillo-Muzquiz, A.; Eshelbrenner, C.; Michaudet, L.; McMillan, K.; Mudigunda, S. D. K.; Ogrin, D.; Tircso, G.; Zhang, S.; Zhao, P.; Sherry, A. D. Synthesis, Relaxometric and Photophysical Properties of a New pH-Responsive MRI Contrast Agent: The Effect of Other Ligating Groups on Dissociation of a *p*-Nitrophenolic Pendant Arm. *J. Am. Chem. Soc.* **2004**, *126*, 9248−9256.

(8) (a) Giovenzana, G. B.; Negri, R.; Rolla, G. A.; Tei, L. Gd-Aminoethyl-DO3A Complexes: A Novel Class of pH-Sensitive MRI Contrast Agents. *Eur. J. Inorg. Chem.* **2012**, *2012*, 2035−2039. (b) Baranyai, Z.; Rolla, G. A.; Negri, R.; Forgács, A.; Giovenzana, G. B.; Tei, L. Comprehensive Evaluation of the Physicochemical Properties of Ln^{III} Complexes of Aminoethyl-DO3A as pH-Responsive T_1-MRI Contrast Agents. *Chem. - Eur. J.* **2014**, *20*, 2933−2944.

(9) Hall, J.; Haner, R.; Aime, S.; Botta, M.; Faulkner, S.; Parker, D.; de Sousa, A. S. Relaxometric and luminescence behaviour of triaquahexaazamacrocyclic complexes, the gadolinium complex displaying a high relaxivity with a pronounced pH dependence. *New J. Chem.* **1998**, *22*, 627−631.

(10) de Leon-Rodriguez, L. M.; Lubag, A. J. M.; Malloy, C. R.; Martinez, G. V.; Gillies, R. J.; Sherry, A. D. Responsive MRI agents for sensing metabolism *in vivo*. *Acc. Chem. Res.* **2009**, *42*, 948−957.

(11) Garcia-Martin, M. L.; Martinez, G. V.; Raghunand, N.; Sherry, A. D.; Zhang, S.; Gillies, R. J. High resolution pH(e) imaging of rat glioma using pH-dependent relaxivity. *Magn. Reson. Med.* **2006**, *55*, 309−315.

(12) Aime, S.; Fedeli, F.; Sanino, A.; Terreno, E. R_2/R_1 Ratiometric Procedure for a Concentration-Independent, pH-Responsive, Gd(III)-Based MRI Agent. *J. Am. Chem. Soc.* **2006**, *128*, 11326−11327.

(13) (a) Soesbe, T. C.; Wu, Y.; Sherry, A. D. Advantages of paramagnetic CEST complexes having slow-to-intermediate water exchange properties as responsive MRI agents. *NMR Biomed.* **2013**, *26*, 829−838. (b) Dorazio, S. J.; Olatunde, A. O.; Spernyak, J. A.; Morrow, J. R. CoCEST: cobalt(II) amide-appended paraCEST MRI contrast agents. *Chem. Commun.* **2013**, *49*, 10025−10027. (c) Sheth, V. R.; Li, Y.; Chen, L. Q.; Howison, C. M.; Flask, C. A.; Pagel, M. D. Measuring in vivo tumor pHe with CEST-FISP MRI. *Magn. Reson. Med.* **2012**, *67*, 760−768. (d) Liu, G.; Li, Y.; Sheth, V. R.; Pagel, M. D. Imaging in vivo extracellular pH with a single paramagnetic chemical exchange saturation transfer magnetic resonance imaging contrast agent. *Mol. Imaging* **2012**, *11*, 47−57. (e) Castelli, D. D.; Ferrauto, G.; Cutrin, J. C.; Terreno, E.; Aime, S. In vivo maps of extracellular pH in murine melanoma by CEST-MRI. *Magn. Reson. Med.* **2014**, *71*, 326−332.

(14) Aime, S.; Castelli, D. D.; Terreno, E. Novel pH-reporter MRI contrast agents. *Angew. Chem., Int. Ed.* **2002**, *41*, 4334−4336.

(15) Krchová, T.; Gálisová, A.; Jirák, D.; Hermann, P.; Kotek, J. Ln(III)-complexes of a DOTA analogue with an ethylenediamine pendant arm as pH-responsive PARACEST contrast agents. *Dalton Trans.* **2016**, *45*, 3486−3496.

(16) Castelli, D. D.; Terreno, E.; Aime, S. YbIII-HPDO3A: A Dual pH- and Temperature-Responsive CEST Agent. *Angew. Chem.* **2011**, *123*, 1838−1840.

(17) Posse, S.; Otazo, R.; Dager, S. R.; Alger, J. MR spectroscopic imaging: principles and recent advances. *J. Magn. Reson. Imaging.* **2013**, *37*, 1301−1325.

(18) Griffiths, R. J. Are cancer cells acidic? *Br. J. Cancer* **1991**, *64*, 425−427.

(19) Gillies, R. J.; Morse, D. L. In vivo magnetic resonance spectroscopy in cancer. *Annu. Rev. Biomed. Eng.* **2005**, *7*, 287−326.

(20) (a) van Sluis, R.; Bhujwalla, Z. M.; Raghunand, N.; Ballesteros, P.; Alvarez, J.; Cerdan, S.; Galons, J. P.; Gillies, R. J. In vivo imaging of extracellular pH using ^{1}H MRSI. *Magn. Reson. Med.* **1999**, *41*, 743−750. (b) Garcia-Martin, M. L.; Herigault, G.; Remy, C.; Farion, R.; Ballesteros, P.; Coles, J. A.; Cerdan, S.; Ziegler, A. Mapping Extracellular pH in Rat Brain Gliomas in Vivo by H Magnetic Resonance Spectroscopic Imaging: Comparison with Maps of Metabolites. *Cancer Res.* **2001**, *61*, 6524−6531.

(21) Aime, S.; Botta, M.; Milone, L.; Terreno, E. Paramagnetic complexes as novel NMR pH indicators. *Chem. Commun.* **1996**, 1265−1266.

(22) Coman, D.; Trubel, H. K.; Rycyna, R. E.; Hyder, F. Brain temperature and pH measured by (1)H chemical shift imaging of a thulium agent. *NMR Biomed.* **2009**, *22*, 229−239.

(23) Huang, Y.; Coman, D.; Ali, M. M.; Hyder, F. Lanthanide ion (III) complexes of 1,4,7,10-tetraazacyclododecane-1,4,7,10-tetraaminophosphonate (DOTA-4AmP^{8-}) for dual biosensing of pH with CEST (chemical exchange saturation transfer) and BIRDS (biosensor imaging of redundant deviation in shifts). *Contrast Media Mol. Imaging* **2015**, *10*, 51−58.

(24) Jagadish, B.; Brickert-Albrecht, G. L.; Nichol, G. S.; Mash, E. A.; Raghunand, N. On the Synthesis of 1,4,7-Tris(tert-butoxycarbonylmethyl)-1,4,7,10-tetraazacyclododecane. *Tetrahedron Lett.* **2011**, *52*, 2058−2061.

(25) Jiang, X.-J.; Lo, P.-Ch; Tsang, Y.-M.; Yeung, S.-L.; Fong, W.-P.; Ng, D. K. P. Phthalocyanine−Polyamine Conjugates as pH-Controlled

DOI: 10.1021/acs.inorgchem.6b02749
Inorg. Chem. XXXX, XXX, XXX−XXX

Photosensitizers for Photodynamic Therapy. *Chem. - Eur. J.* **2010**, *16*, 4777−4783.
(26) Perrin, D. D.; Armarego, W. L. F. *Purification of Laboratory Chemicals*, 3rd ed.; Pargamon Press: Oxford, 1988.
(27) *MATLAB R2015b*; The MathWorks Inc.: Natick, MA, 2000.
(28) Corsi, D. M.; Platas-Iglesias, C.; van Bekkum, H.; Peters, J. A. Determination of paramagnetic lanthanide (III) concentrations from bulk magnetic susceptibility shifts in NMR spectra. *Magn. Reson. Chem.* **2001**, *39*, 723−726.
(29) Sheldrick, G. M. *SHELXS97, Program for Crystal Structure Solution from Diffraction Data*; University of Göttingen: Göttingen, Germany, 1997.
(30) Sheldrick, G. M. *SHELXL97, Program for Crystal Structure Refinement from Diffraction Data*; University of Göttingen: Göttingen, Germany, 1997.
(31) (a) Táborský, P.; Lubal, P.; Havel, J.; Kotek, J.; Hermann, P.; Lukeš, I. Thermodynamic and Kinetic Studies of Lanthanide(III) Complexes with H_3do3ap (1,4,7,10-Tetraazacyclododecane-1,4,7-triacetic-10-(methylphosphonic Acid)), a Monophosphonate Analogue of H_4dota. *Collect. Czech. Chem. Commun.* **2005**, *70*, 1909−1942. (b) Försterová, M.; Svobodová, I.; Lubal, P.; Táborský, P.; Kotek, J.; Hermann, P.; Lukeš, I. Thermodynamic study of lanthanide(III) complexes with bifunctional monophosphinic acid analogues of H_4dota and comparative kinetic study of yttrium(III) complexes. *Dalton Trans.* **2007**, 535−549.
(32) Kývala, M.; Lukeš, I. *International Conference Chemometrics 95*; Pardubice, Czech Republic, 1995; p 63. Full version of *OPIUM* available (free of charge) on http://web.natur.cuni.cz/~kyvala/opium.html.
(33) Martell, A. E.; Smith, R. M.; Motekaitis, R. J. *NIST Critically Selected Stability Constants of Metal Complexes (Version 7)*; Texas A&M University: College Station, TX.
(34) Aime, S.; Botta, M.; Ermondi, G. NMR study of solution structures and dynamics of lanthanide(III) complexes of DOTA. *Inorg. Chem.* **1992**, *31*, 4291−4299.
(35) (a) Caravan, P.; Ellison, J. J.; McMurry, T. J.; Lauffer, R. B. Gadolinium(III) Chelates as MRI Contrast Agents: Structure, Dynamics, and Applications. *Chem. Rev.* **1999**, *99*, 2293−2352. (b) Hermann, P.; Kotek, J.; Kubíček, V.; Lukeš, I. Gadolinium(III) complexes as MRI contrast agents: ligand design and properties of the complexes. *Dalton Trans.* **2008**, 3027−3047. (c) Geraldes, C. F. G. C.; Laurent, S. Classification and basic properties of contrast agents for magnetic resonance imaging. *Contrast Media Mol. Imaging* **2009**, *4*, 1−23.
(36) (a) Aime, S.; Botta, M.; Fasano, M.; Marques, M. P. M.; Geraldes, C. F. G. C.; Pubanz, D.; Merbach, A. E. Conformational and Coordination Equilibria on DOTA Complexes of Lanthanide Metal Ions in Aqueous Solution Studied by (1)H-NMR Spectroscopy. *Inorg. Chem.* **1997**, *36*, 2059−2068. (b) Lebdušková, P.; Hermann, P.; Helm, L.; Tóth, É.; Kotek, J.; Binnemans, K.; Rudovský, J.; Lukeš, I.; Merbach, A. E. Gadolinium(III) Complexes of Mono- and Diethyl Esters of Monophosphonic Acid Analogue of DOTA as Potential MRI Contrast Agents: Solution Structures and Relaxometric Studies. *Dalton Trans.* **2007**, 493−501. (c) Vitha, T.; Kubíček, V.; Kotek, J.; Hermann, P.; Vander Elst, L.; Muller, R. N.; Lukeš, I.; Peters, J. A. Gd(III) complex of a monophosphinate-bis(phosphonate) DOTA analogue with a high relaxivity; Lanthanide(III) complexes for imaging and radiotherapy of calcified tissues. *Dalton Trans.* **2009**, 3204−3214. (d) Castelli, D. D.; Caligara, M. C.; Botta, M.; Terreno, E.; Aime, S. Combined high resolution NMR and H-1 and O-17 relaxometric study sheds light on the solution structure and dynamics of the Lanthanide(III) complexes of HPDO3A. *Inorg. Chem.* **2013**, *52*, 7130−7138. (e) Rudovský, J.; Cígler, P.; Kotek, J.; Hermann, P.; Vojtíšek, P.; Lukeš, I.; Peters, J. A.; Vander Elst, L.; Muller, R. N. Lanthanide (III) complexes of a mono (methylphosphonate) analogue of H_4dota: The influence of protonation of the phosphonate moiety on the TSAP/SAP isomer ratio and the water exchange rate. *Chem. - Eur. J.* **2005**, *11*, 2373−2384. (f) Rudovský, J.; Kotek, J.; Hermann, P.; Lukeš, I.; Mainero, V.; Aime, S. Synthesis of a Bifunctional Monophosphinic Acid DOTA Analogue Ligand and Its Lanthanide(III) Complexes. A Gadolinium(III) Complex Endowed with an Optimal Water Exchange Rate for MRI Applications. *Org. Biomol. Chem.* **2005**, *3*, 112−117.
(37) Krchová, T.; Kotek, J. Unpublished results.
(38) Beeby, A.; Clarkson, I. M.; Dickins, R. S.; Faulkner, S.; Parker, D.; Royle, L.; de Sousa, A. S.; Williams, J. A. G.; Woods, M. Non-radiative deactivation of the excited states of europium, terbium and ytterbium complexes by proximate energy-matched OH, NH and CH oscillators: an improved luminescence method for establishing solution hydration states. *J. Chem. Soc., Perkin Trans. 2* **1999**, 493−504.
(39) (a) Rudovský, J.; Botta, M.; Hermann, P.; Koridze, A.; Aime, S. Relaxometric and solution NMR structural studies on ditopic lanthanide(III) complexes of a phosphinate analogue of DOTA with a fast rate of water exchange. *Dalton Trans.* **2006**, 2323−2333. (b) Kotková, Z.; Pereira, G. A.; Djanashvili, K.; Kotek, J.; Rudovský, J.; Hermann, P.; Vander Elst, L.; Muller, R. N.; Geraldes, C. F. G. C.; Lukeš, I.; Peters, J. A. Lanthanide(III) Complexes of Phosphorus Acid Analogues of H_4DOTA as Model Compounds for the Evaluation of the Second-Sphere Hydration. *Eur. J. Inorg. Chem.* **2009**, *2009*, 119−136. (c) Pereira, G. A.; Ball, L.; Sherry, A. D.; Peters, J. A.; Geraldes, C. F. G. C. NMR Characterization of Lanthanide(3+) Complexes of Tetraazatetrakisphosphinato and Tetraazatetrakisphosphonato Ligands. *Helv. Chim. Acta* **2009**, *92*, 2532−2551. (d) Rohovec, J.; Lukeš, I.; Hermann, P. Lanthanide complexes of a cyclen derivative with phenylphosphinic pendant arms for possible ^{1}H and ^{31}P MRI temperature sensitive probes. *New J. Chem.* **1999**, *23*, 1129−1132. (e) Rohovec, J.; Kývala, M.; Vojtíšek, P.; Hermann, P.; Lukeš, I. Synthesis, Crystal Structures, and Solution Properties of *N*-Methylene(phenyl)phosphinic Acid Derivatives of Cyclen and Cyclam. *Eur. J. Inorg. Chem.* **2000**, *2000*, 195−203. (f) Aime, S.; Batsanov, A. S.; Botta, M.; Howard, J. A. K.; Parker, D.; Senanayake, K.; Williams, J. A. G. Solution and Solid-state Characterization of Highly Rigid, Eight-Coordinate Lanthanide(III) Complexes of a Macrocyclic Tetrabenzylphosphinate. *Inorg. Chem.* **1994**, *33*, 4696−4706. (g) Aime, S.; Batsanov, A. S.; Botta, M.; Dickins, R. S.; Faulkner, S.; Foster, C. E.; Harrison, A.; Howard, J. A. K.; Moloney, J. M.; Norman, T. J.; Parker, D.; Royle, L.; Williams, J. A. G. Nuclear magnetic resonance, luminescence and structural studies of lanthanide complexes with octadentate macrocyclic ligands bearing benzylphosphinate groups. *J. Chem. Soc., Dalton Trans.* **1997**, 3623−3636.
(40) Campello, M. P. C.; Lacerda, S.; Santos, I. C.; Pereira, G. A.; Geraldes, C. F. G. C.; Kotek, J.; Hermann, P.; Vaněk, J.; Lubal, P.; Kubíček, V.; Tóth, E.; Santos, I. Lanthanide(III) complexes of 4,10-bis(phosphonomethyl)-1,4,7,10-tetraazacyclododecane-1,7-diacetic acid (trans-H_6do2a2p) in solution and in the solid state: structural studies along the series. *Chem. - Eur. J.* **2010**, *16*, 8446−8465.
(41) (a) Blackburn, O. A.; Edkins, R. M.; Faulkner, S.; Kenwright, A. M.; Parker, D.; Rogers, N. J.; Shuvaev, S. Electromagnetic susceptibility anisotropy and its importance for paramagnetic NMR and optical spectroscopy in lanthanide coordination chemistry. *Dalton Trans.* **2016**, *45*, 6782−6800. (b) Cucinotta, G.; Perfetti, M.; Luzon, J.; Etienne, M.; Car, P.-E.; Caneschi, A.; Calvez, G.; Bernot, K.; Sessoli, R. Magnetic Anisotropy in a Dysprosium/DOTA Single-Molecule Magnet: Beyond Simple Magneto-Structural Correlations. *Angew. Chem., Int. Ed.* **2012**, *51*, 1606−1610.
(42) (a) Rohovec, J.; Vojtíšek, P.; Hermann, P.; Mosinger, J.; Žák, Z.; Lukeš, I. Synthesis, crystal structures and NMR and luminescence spectra of lanthanide complexes of 1,4,7,10-tetraazacyclododecane with *N*-methylene(phenyl)phosphinic acid pendant arms. *J. Chem. Soc., Dalton Trans.* **1999**, 3585−3592. (b) Avecilla, F.; Peters, J. A.; Geraldes, C. F. G. C. X-ray Crystal Structure of a Sodium Salt of $[Gd(DOTP)]^{5-}$: Implications for Its Second-Sphere Relaxivity and the ^{23}Na NMR Hyperfine Shift Effects of $[Tm(DOTP)]^{5-}$. *Eur. J. Inorg. Chem.* **2003**, *2003*, 4179−4186. (c) Vojtíšek, P.; Cígler, P.; Kotek, J.; Rudovský, J.; Hermann, P.; Lukeš, I. Crystal Structures of Lanthanide(III) Complexes with Cyclen Derivative Bearing Three Acetate and One Methylphosphonate Pendants. *Inorg. Chem.* **2005**, *44*, 5591−5599. (d) Luck, R. L.; Maupin, C. L.; Parker, D.; Riehl, J. P.; Williams,

DOI: 10.1021/acs.inorgchem.6b02749
Inorg. Chem. XXXX, XXX, XXX−XXX

J. A. G. Circularly polarized luminescence and structural studies of a dysprosium(III) complex with an octadentate macrocyclic ligand bearing benzylphosphinate groups. *Inorg. Chim. Acta* **2001**, *317*, 331–337.

(43) Lukeš, I.; Kotek, J.; Vojtíšek, P.; Hermann, P. Tetraazacycles with Methylphosphinic/phosphonic Acid Pendant Arms. A Comparison with their Acetic Acid Analogues. *Coord. Chem. Rev.* **2001**, *216–217*, 287–312.

(44) Krchová, T.; Kotek, J.; Jirák, D.; Havlíčková, J.; Císařová, I.; Hermann, P. Lanthanide(III) complexes of aminoethyl-DO3A as PARACEST contrast agents based on decoordination of the weakly bound amino group. *Dalton Trans.* **2013**, *42*, 15735–15747.

(45) Pniok, M.; Kubíček, V.; Havlíčková, J.; Kotek, J.; Sabatie-Gogova, A.; Plutnar, J.; Huclier-Markai, S.; Hermann, P. Thermodynamic and kinetic study of scandium(III) complexes of DTPA and DOTA: a step toward scandium radiopharmaceuticals. *Chem. - Eur. J.* **2014**, *20*, 7944–7955.

DOI: 10.1021/acs.inorgchem.6b02749
Inorg. Chem. XXXX, XXX, XXX–XXX

APPENDIX 3

Electronic supplementary information for:

Eu(III) Complex with DO3A-amino-phosphonate Ligand as a Concentration-Independent pH-Responsive Contrast Agent for Magnetic Resonance Spectroscopy (MRS)

Tereza Krchová,[a] Vít Herynek,[b] Andrea Gálisová,[b] Jan Blahut,[a] Petr Hermann,[a] Jan Kotek[a]

[a] Department of Inorganic Chemistry, Faculty of Science, Charles University, Hlavova 2030, 128 43 Prague 2, Czech Republic. Tel.: +420-221951261. Fax: +420-221951253. E-mail: modrej@natur.cuni.cz.
[b] Department of Radiodiagnostic and Interventional Radiology, Magnetic Resonance Unit, Institute for Clinical and Experimental Medicine, Vídeňská 1958/9, Prague 4, 140 21 Czech Republic.

Contents

^{1}H and ^{13}C{^{1}H} NMR spectra of compound 4

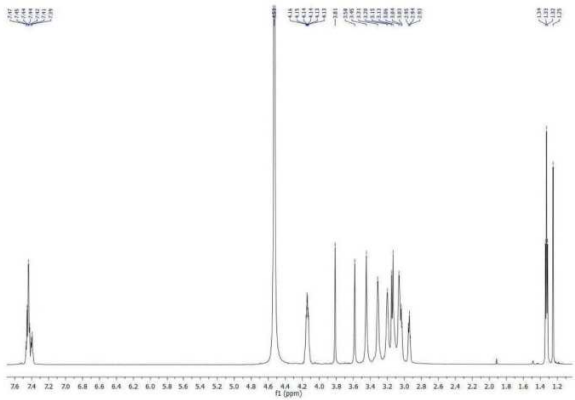

Figure S1: ^{1}H NMR spectrum of compound **4** in D_2O, pD = 6.74, 50 °C.

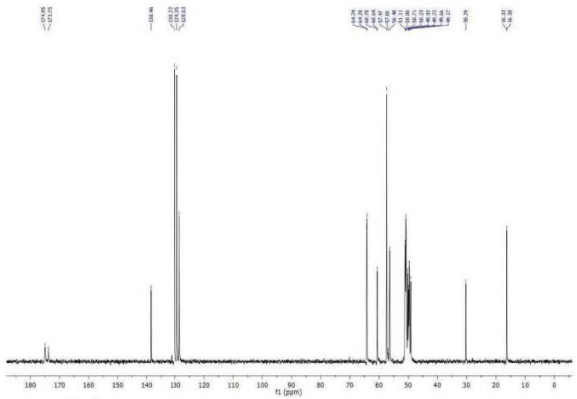

Figure S2: ^{13}C{^{1}H} NMR spectrum of compound **4** in D_2O, pD = 6.74, 50 °C.

^{31}P and ^{31}P{^{1}H} NMR spectra of compound 4

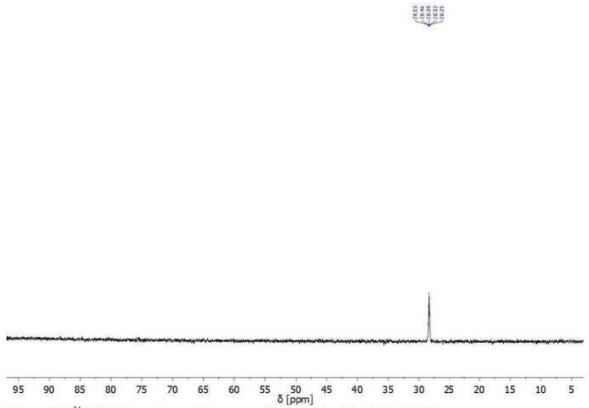

Figure S3: ^{31}P NMR spectrum of compound **4** in D_2O, pD = 6.74, 25 °C.

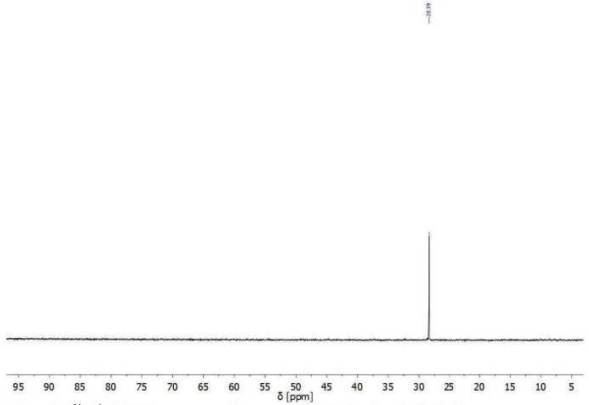

Figure S4: ^{31}P{^{1}H} NMR spectrum of compound **4** in D_2O, pD = 6.74, 25 °C.

^{1}H and ^{13}C{^{1}H} NMR spectra of H_5do3aNP

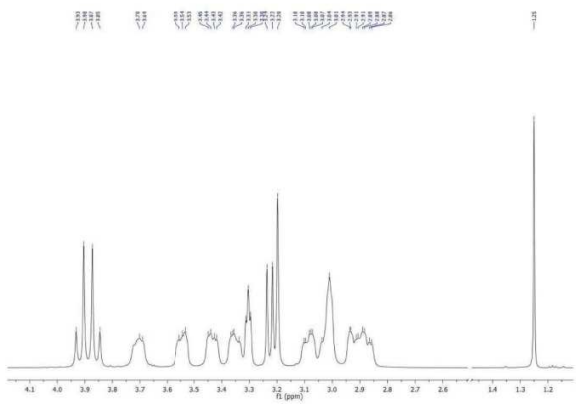

Figure S5: ^{1}H NMR spectrum of H_5do3aNP in D_2O, pD = 5.81, 25 °C.

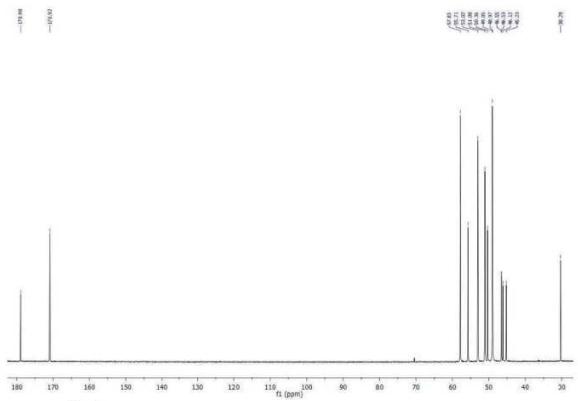

Figure S6: ^{13}C{^{1}H} NMR spectrum of H_5do3aNP in D_2O, pD = 5.81, 25 °C.

^{31}P and $^{31}P\{^1H\}$ NMR spectra of $H_5do3aNP$

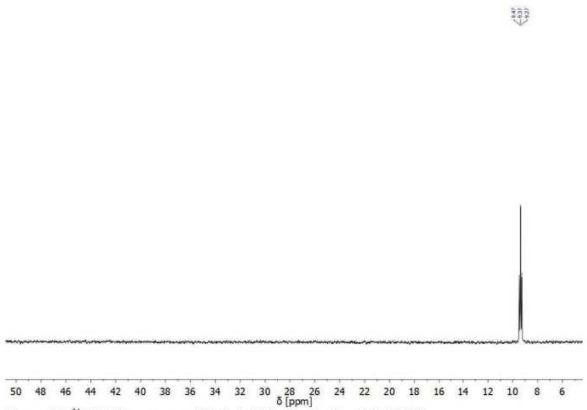

Figure S7: ^{31}P NMR spectrum of $H_5do3aNP$ in D_2O, pD = 5.81, 25 °C.

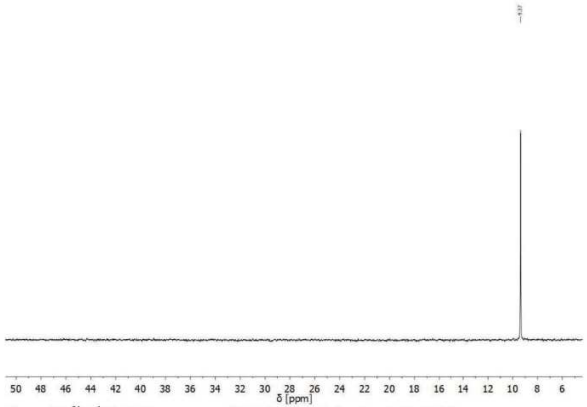

Figure S8: $^{31}P\{^1H\}$ NMR spectrum of $H_5do3aNP$ in D_2O, pD = 5.81, 25 °C.

Selected hydrogen bonds found in the crystal structure of $H_5do3aNP{\cdot}4.75H_2O$

Table S1: Selected hydrogen bonds found in the crystal structure of $H_5do3aNP{\cdot}4.75H_2O$.

D–H	*d*(D–H)	*d*(H···A)	<DHA	*d*(D···A)	A
molecule A					
N4A–H4A	0.930	2.068	117	2.627(2)	O31A
N4A–H4A	0.930	2.580	111	3.034(2)	N1A
N4A–H4A	0.930	2.376	113	2.867(2)	N7A
N10A–H10A	0.930	2.184	136	2.924(2)	O41B
N10A–H10A	0.930	2.614	92	2.809(2)	O51A
N10A–H10A	0.930	2.524	109	2.964(2)	N1A
N10A–H10A	0.930	2.558	110	3.005(2)	N7A
N22A–H22A	0.920	1.808	175	2.726(2)	O51A
N22A–H22B	0.920	2.021	138	2.772(2)	O31A
N22A–H22B	0.920	2.225	119	2.789(2)	O41B
O1A–H1A	0.873	1.971	167	2.829(6)	O51A
O41A–H41A	0.840	1.719	165	2.539(2)	O31Y
molecule X					
N4X–H4X	0.930	2.042	117	2.605(2)	O31X
N4X–H4X	0.930	2.584	111	3.043(2)	N1X
N4X–H4X	0.930	2.390	112	2.876(2)	N7X
N10X–H10X	0.930	2.220	134	2.941(2)	O41Y
N10X–H10X	0.930	2.563	92	2.752(2)	O51X
N10X–H10X	0.930	2.490	111	2.956(2)	N1X
N10X–H10X	0.930	2.547	110	2.998(2)	N7X
N22X–H22X	0.920	2.578	112	3.040(2)	O1X
N22X–H22X	0.920	1.865	154	2.722(2)	O51X
N22X–H22Y	0.920	2.157	129	2.829(2)	O31X
N22X–H22Y	0.920	2.212	125	2.845(2)	O41Y
O1X–H1X	0.893	1.812	171	2.698(2)	O5W
O41X–H41X	0.840	1.765	165	2.586(2)	O31B

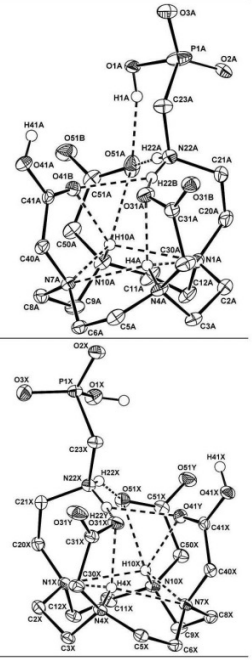

^{1}H NMR studies of Eu(III) complex of H_5do3aNP

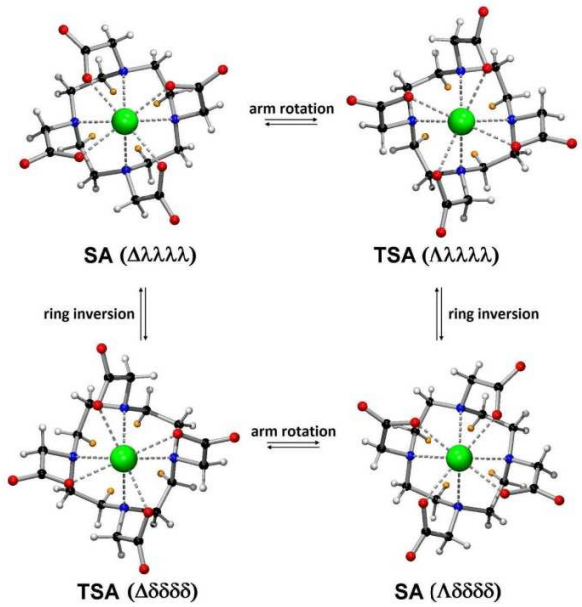

Figure S9: Schematic structure of SA/TSA-[Ln(dota)]$^-$ complex species highlighting the "axial" protons (orange).

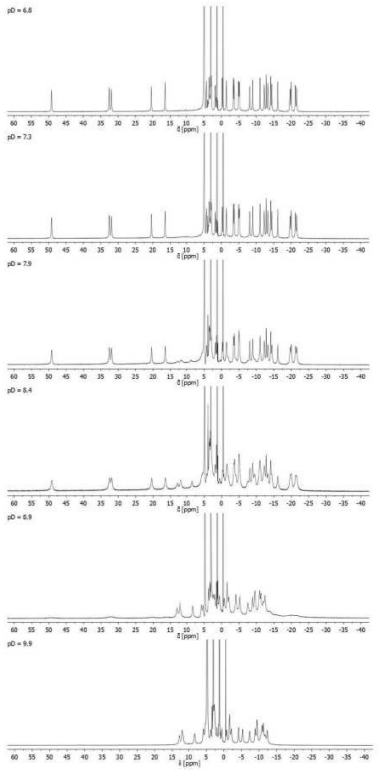

Figure S10: ^{1}H NMR spectra of SA-[Eu(Hdo3aNP)]$^-$/TSA-[Eu(do3aNP)]$^{2-}$ (~80 mM solution in D_2O, ~250 mM NaCl, B_0 = 7.05 T, 25 °C) at different pH values (referenced to δ(*t*BuOH) = 1.25 ppm).

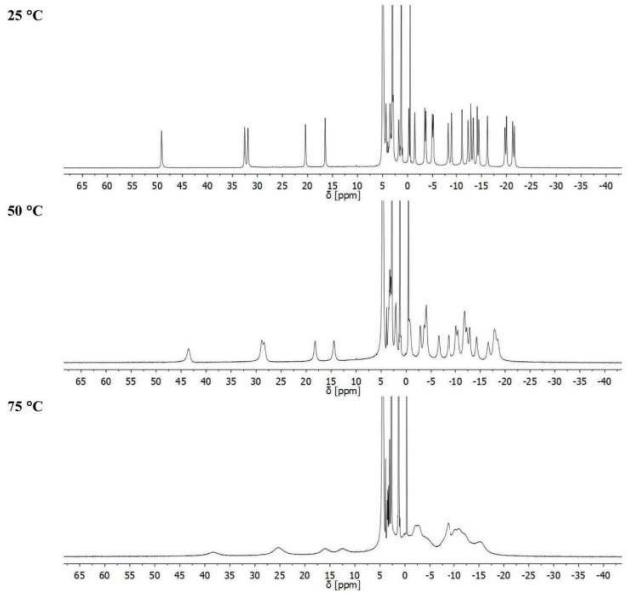

Figure S11: ^{1}H NMR spectra of SA-[Eu(Hdo3aNP)]$^{-}$ (~80 mM solution in D_2O, ~250 mM NaCl, B_0 = 7.05 T, pD = 6.8) at different temperatures (referenced to δ(*t*BuOH) = 1.25 ppm).

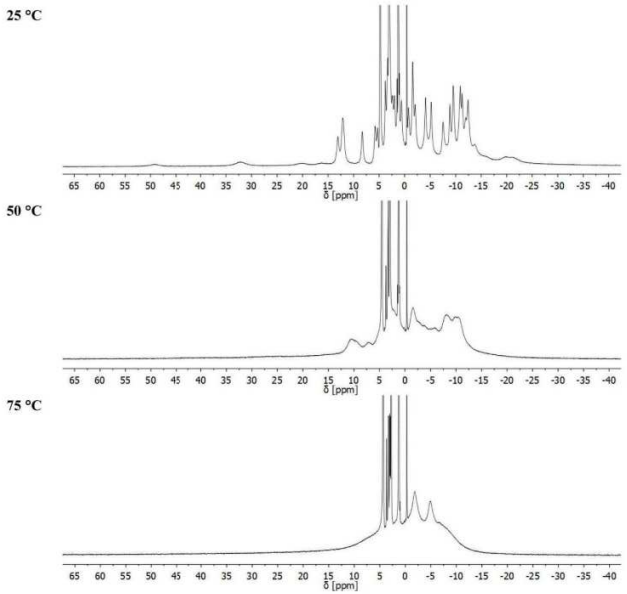

Figure S12: ^{1}H NMR spectra of SA-[Eu(Hdo3aNP)]$^{-}$/TSA-[Eu(do3aNP)]$^{2-}$ (~80 mM solution in D_2O, ~250 mM NaCl, B_0 = 7.05 T, pD = 8.9) at different temperatures (referenced to δ(*t*BuOH) = 1.25 ppm).

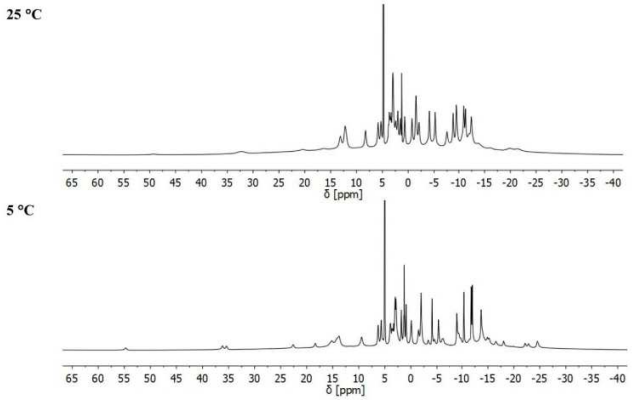

Figure S13: ^{1}H NMR spectra of SA-[Eu(Hdo3aNP)]$^{-}$/TSA-[Eu(do3aNP)]$^{2-}$ (~80 mM solution in D_2O, ~250 mM NaCl, B_0 = 14.1 T, pD = 9.05) at 25 and 5 °C (referenced to δ(*t*BuOH) = 1.25 ppm).

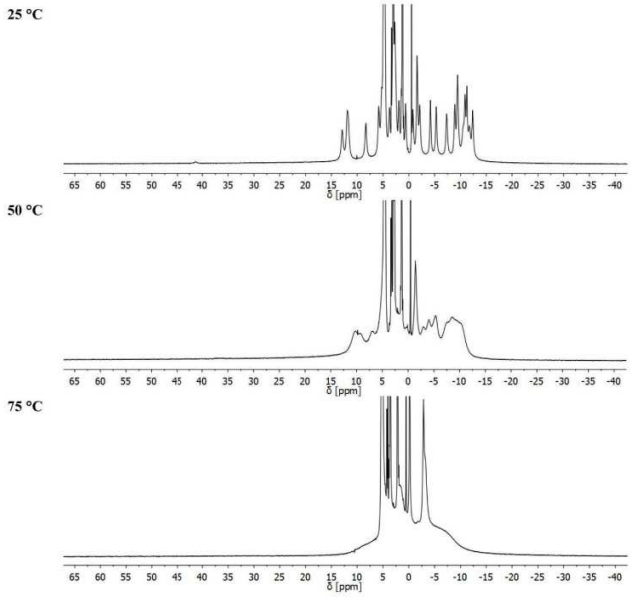

Figure S14: ^{1}H NMR spectra of TSA-[Eu(do3aNP)]$^{2-}$ (~80 mM solution in D_2O, ~250 mM NaCl, B_0 = 7.05 T, pD = 9.9) at different temperatures (referenced to δ(*t*BuOH) = 1.25 ppm).

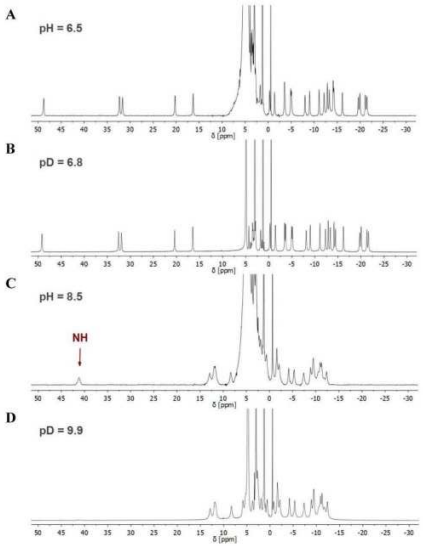

Figure S15: ^{1}H NMR spectra of SA-[Eu(Hdo3aNP)]$^{-}$/TSA-[Eu(do3aNP)]$^{2-}$ complex species (~80 mM solution in **A**, **C**: H_2O; **B**, **D**: D_2O; ~250 mM NaCl, B_0 = 7.05 T, 25 °C) at different pH/pD values (referenced to δ(*t*BuOH) = 1.25 ppm).

^{31}P NMR studies of Eu(III) complex of H_5do3aNP

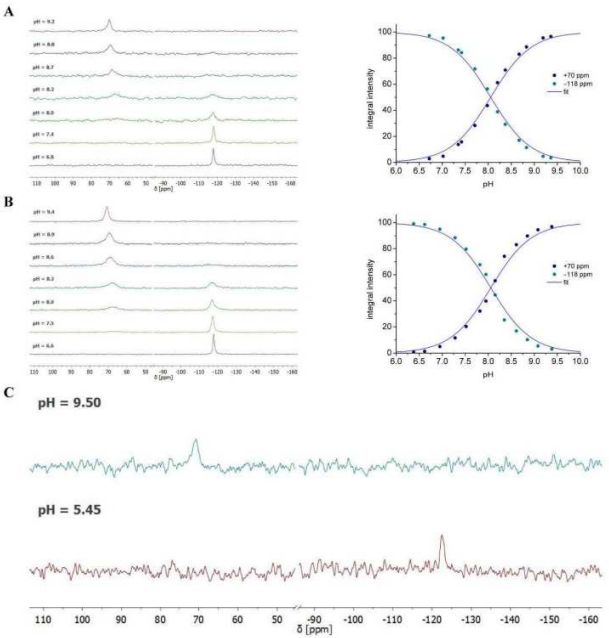

Figure S16: The pH dependence of ^{31}P{^{1}H} NMR spectra of SA-[Eu(Hdo3aNP)]$^{-}$/TSA-[Eu(do3aNP)]$^{2-}$ species. **A**: 10 mM solution, **B**: 50 mM solution, **C**: 2 mM solution. Conditions: H_2O, ~150 mM NaCl, B_0 = 7.05 T, 25 °C. For **A** and **B**, right charts show the pH dependence of an integral intensity of the corresponding ^{31}P NMR signals.

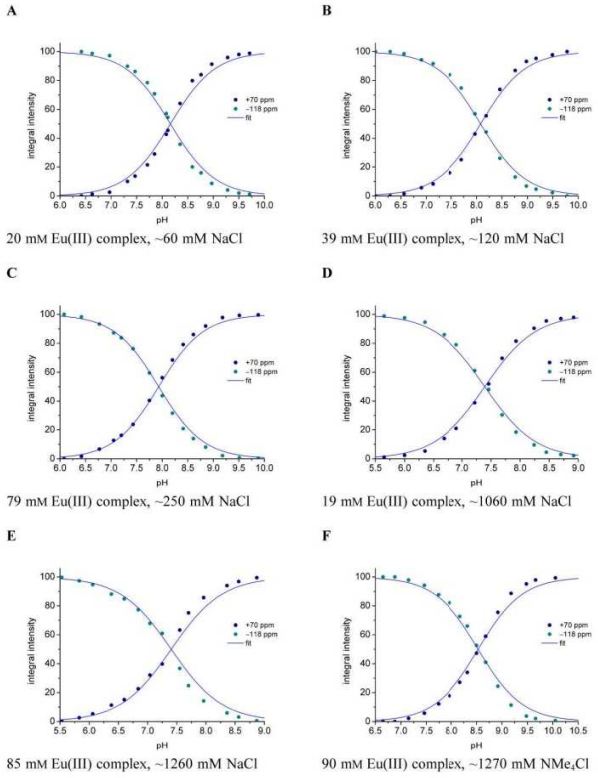

Figure S17: The pH dependence of an integral intensity of the ^{31}P NMR signals of SA-[Eu(Hdo3aNP)]$^-$/TSA-[Eu(do3aNP)]$^{2-}$ species at various concentrations and ionic strengths. B_0 = 7.05 T, 25 °C.

Table S2: Calculated protonation constants log$K$(HLM) characterizing SA-[Eu(Hdo3aNP)]$^-$/TSA-[Eu(do3aNP)]$^{2-}$ equilibrium (25 °C). Fits of the experimental data are shown in Figure S16, Figure S17 and Figure S18.

background electrolyte	electrolyte concentration (mM)	complex concentration (mM)	log$K$(HLM)	data
NaCl	60	20	8.16(3)	Figure S17-A
NaCl	120	39	8.08(2)	Figure S17-B
NaCl	154	10	8.05(2)	Figure S16-A
NaCl	154	50	8.06(3)	Figure S16-B
NaCl	250	79	7.93(3)	Figure S17-C
NaCl	1060	19	7.39(2)	Figure S17-D
NaCl	1260	85	7.40(5)	Figure S17-E
$(NMe_4)Cl$	1270	90	8.53(3)	Figure S17-F
NaCl + $CaCl_2$	190 + 65	65	7.48(3)	Figure S18-A
NaCl + $MgCl_2$	190 + 65	65	7.58(3)	Figure S18-B

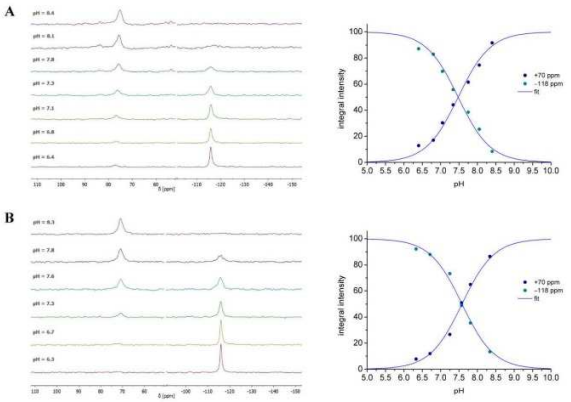

Figure S18: Left: the pH dependence of $^{31}P\{^1H\}$ NMR spectra of SA-[Eu(Hdo3aNP)]$^-$/TSA-[Eu(do3aNP)]$^{2-}$ species, and right: the pH dependence of an integral intensity of the corresponding ^{31}P NMR signals. Conditions: 65 mM solution, H_2O, ~190 mM NaCl, B_0 = 7.05 T, 25 °C; **A**: ~65 mM $CaCl_2$, **B**: ~65 mM $MgCl_2$.

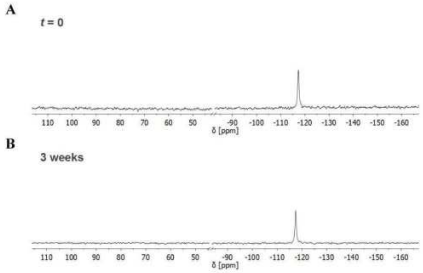

Figure S19: $^{31}P\{^{1}H\}$ NMR spectra of SA-[Eu(Hdo3aNP)]$^{2-}$ (~80 mM solution in D_2O; ~250 mM NaCl, B_0 = 7.05 T, 25 °C) at pD = 5.9 measured **A**: immediately after the pD of the solution was changed from ~8 to 5.9, and **B**: after heating at 60 °C for 3 weeks. In both cases, the xylenol orange test was negative.

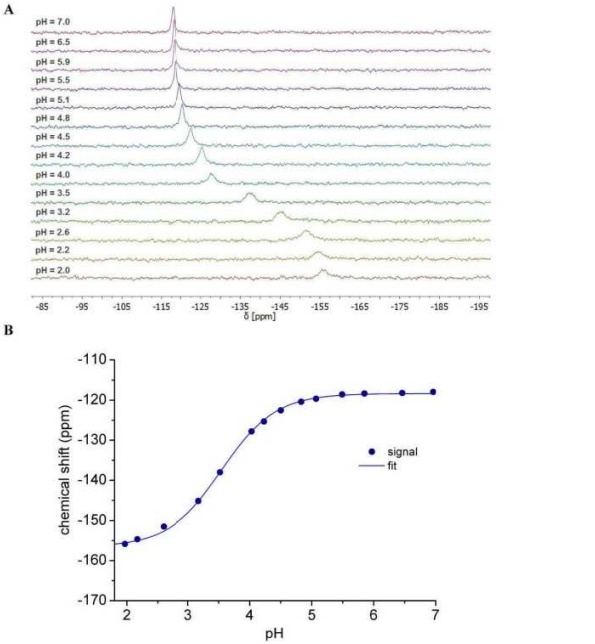

Figure S20: **A**: ^{31}P NMR signals for the SA-[Eu(H_2do3aNP)]/SA-[Eu(Hdo3aNP)]$^-$ equilibrium in acidic region and **B**: the related titration data showing the best fit affording log$K$ = 3.55(1) (38 mm complex concentration; ~150 mm NaCl, no ionic strength control).

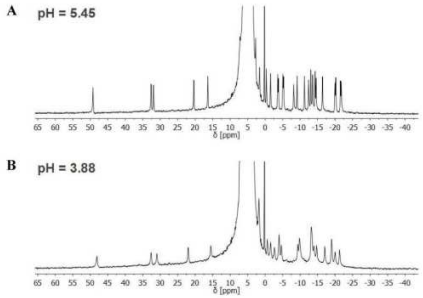

Figure S21: ^{1}H NMR spectra of the Eu(III) complex of H_5do3aNP (~50 mM solution in H_2O, ~150 mM NaCl, B_0 = 7.05 T, 25 °C) at **A**: pH = 5.45, **B**: pH = 3.88 (referenced to δ(*t*BuOH) = 1.25 ppm).

Overview of ^{31}P NMR shifts of the ligands having methylenephosphonate or methylenephosphinate pendant moieties and their Eu(III)/La(III) complexes

Table S3: ^{31}P NMR shifts (given in ppm) of the ligands and their La(III) and Eu(III) complexes and differences between chemical shifts of the Eu(III) complex and free ligand and/or La(III) complex (Lanthanide-Induced Shift, LIS).

Ligand formula	δ_P L/[La(L)]	δ_P [Eu(L)] TSA	$\Delta\delta_P$ ΔTSA	δ_P [Eu(L)] SA	$\Delta\delta_P$ ΔSA
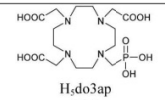 H_5do3ap ref. 1	L: 20	35	15	46–49	26–29
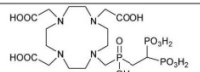 H_8do3ap^{BP} ref. 2	L: 42 La: 48	82	40 LIS: 34	95	53 LIS: 47
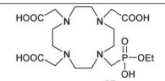 H_4do3ap^{OEt} ref. 3	L: 15	33, 35	18, 20	45, 49	30, 34
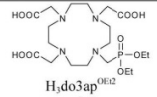 H_3do3ap^{OEt2} ref. 3	L: 33	49	16	55	22
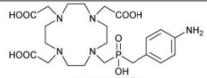 H_4do3ap^{ABn} ref. 4	L: 33	80, 92	47, 59	87	54
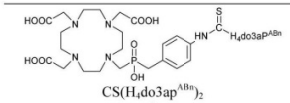 $CS(H_4do3ap^{ABn})_2$ ref. 5	L: 33	75–82, 90	42–49, 55	82–89, 94	49–56, 61

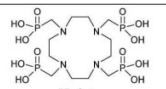 H_4dotp ref. 6	–	–	LIS: 29	–	–
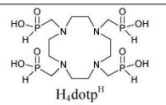 H_4dotp^{H} ref. 7	L: 23	55–95	32–72	–	–
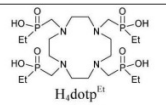 H_4dotp^{Et} ref. 7,8	La: 47	101, 96, 99	LIS: 54, 49, 52	–	–
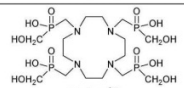 H_4dotp^{hm} ref. 7	L: 38	83, 80, 86, 105	45, 42, 48, 67	–	–
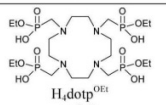 H_4dotp^{OEt} ref. 7	L: 19	35–63	16–44	–	–
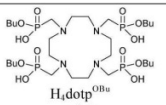 H_4dotp^{OBu} ref. 7	–	40–55	–	–	–
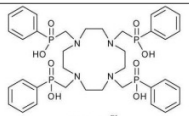 H_4dotp^{Ph} ref. 9,10	L: 29	*Δδδδδ-RRRR* 67	38	–	–

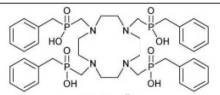 H_4dotp^{Bn} ref. 11,12	La: 38, 39	86	LIS: 47,48	–	–
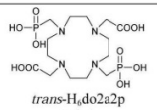 *trans*-H_6do2a2p ref. 6	L: 6 La: 15	44	38 LIS: 29	–	–
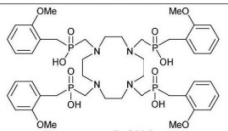 H_4dotp$^{Bn\text{-}2\text{-}MeO}$ ref. 12	L: 37	90	53	–	–
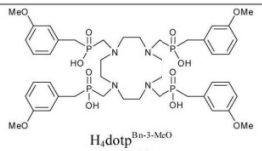 H_4dotp$^{Bn\text{-}3\text{-}MeO}$ ref. 12	L: 32 La: 38, 39	87	55 LIS: 48,49	–	–
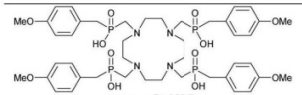 H_4dotp$^{Bn\text{-}4\text{-}MeO}$ ref. 12	L: 22, 36	85	63, 49	–	–

Overview of complex geometries found in the solid state

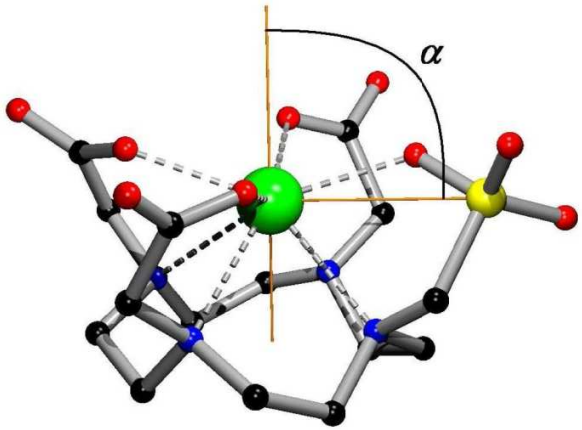

Figure S22: Graphical definition of angle between Ln–P vector and arbitrary magnetic axis (= pseudo-C_4 axis).

Table S4: Angles between Ln–P vector and pseudo-C_4 axis observed in crystal structures of Ln(III) complexes with DOTA-like ligands.

Ligand formula	Ln	α(°)	Coord. no.
 *trans*-H_6do2a2p ref. 6	Ce	79.2, 81.3	9
trans-H_6do2a2p ref. 6	Dy	73.6	8
trans-H_6do2a2p ref. 6	Er	73.2	8
trans-H_6do2a2p ref. 6	Eu	74.6	8
trans-H_6do2a2p ref. 6	Nd	78.7, 80.4	9

trans-H_6do2a2p ref. 6	Sm	74.6	8
trans-H_6do2a2p ref. 6	Sm	78.7, 79.2 78.6, 79.3	9
trans-H_6do2a2p ref. 6	Tb	73.8	8
trans-H_6do2a2p ref. 6	Yb	72.8	8
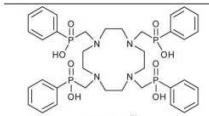 H_4dotp^{Ph} ref. 13	La	81.6, 81.9, 84.5, 88.9 82.0, 83.3, 84.1, 86.1	9 9
H_4dotp^{Ph} ref. 13	Ce	81.4, 82.3, 83.5, 87.8 81.8, 83.5, 84.0, 85.6	9 9
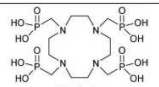 H_8dotp ref. 14	Gd	78.0	8
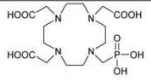 H_5do3ap ref. 1	Nd	84.7 85.6	9 9
H_5do3ap ref. 15	Dy	80.8	8
H_5do3ap ref. 15	Er	77.4	8
H_5do3ap ref. 15	Lu	79.4	8
H_5do3ap ref. 15	Lu	77.3	8
H_5do3ap ref. 15	Tb	81.7	9

APPENDIX 3

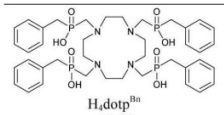 H_4dotp^{Bn} ref. 12	Eu	76.5, 77.5, 77.8, 79.0	8
H_4dotp^{Bn} ref. 12	La	81.6, 82.2, 82.3, 82.7	9
H_4dotp^{Bn} ref. 12	Yb	75.4, 75.9, 76.6, 76.8 75.1, 75.9, 76.3, 78.0	8
H_4dotp^{Bn} ref. 16	Dy	76.6, 76.8, 77.8, 78.8	8
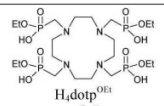 H_4dotp^{OEt} ref. 7	Gd	76.6, 77.6, 77.9, 78.4 76.7, 76.9, 77.1, 79.4	8
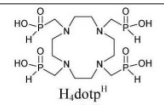 H_4dotp^{H} ref. 7	Gd	76.5, 77.1	8

Assignment of hydrogen atom signals in ^{1}H NMR spectra of Eu(III)–H_5do3aNP complexes

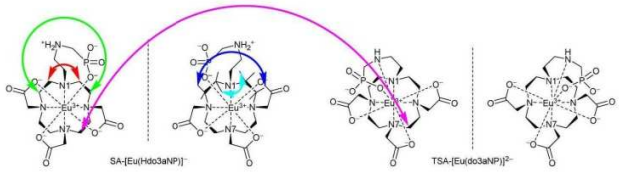

Figure S23: Enantiomeric pairs of SA-[Eu(Hdo3aNP)]$^-$ and TSA-[Eu(do3aNP)]$^{2-}$ complexes showing EXSY interactions between hydrogen atoms.

^{1}H-^{1}H COSY spectra distinguished groups of four protons belonging to ethylene groups (typically, each proton has cross-peaks with two of remaining three protons of given ethylene) and pairs belonging to methylene groups of acetate and N–C–P fragment.

^{1}H-^{1}H EXSY spectra distinguished pairs of hydrogen atoms of the same isomer (SA or TSA, respectively) related through C_s-symmetry (plane defined by aminophosphonate and "odd" acetate pendants), N1, N7 and Eu atoms.

^{1}H-^{1}H EXSY spectra distinguished between "odd" and "double" methylene groups of acetate pendant arms.

Selectively ^{1}H-presaturated ^{13}C NMR spectra assigned hydrogen atoms bound to given carbon atom (geminal hydrogen atoms).

Few very weak ^{1}H-^{1}H COSY cross-peaks of "odd" and "double" methylene protons of SA isomer to some macrocycle hydrogen atoms were assigned as interactions to closest macrocycle hydrogen atom, fixing position of macrocycle ethylene bridge.

With assumption that most shifted signals of the SA isomer (signals 1A, 2A, 3A and 4A) are the "axial" ones, remaining hydrogen signals were assigned.

From ^{1}H-^{1}H EXSY spectra showing weak cross peaks between SA and TSA isomers, assignment of TSA skeleton was done, showing that "axial" protons are not the most shifted ones, but they are 4B, 6B, 7B and 8B (the second option with 19B, 21B, 26B and 28B as "axial" protons did not give a sense as induced chemical shift of other signals was random with no spatial rules).

Hydrogen atoms belonging to ethylene of aminophosphonate pendant groups were randomly assigned on the basis of sign and magnitude of induced shift to give a "optical" sense in Figure 5.

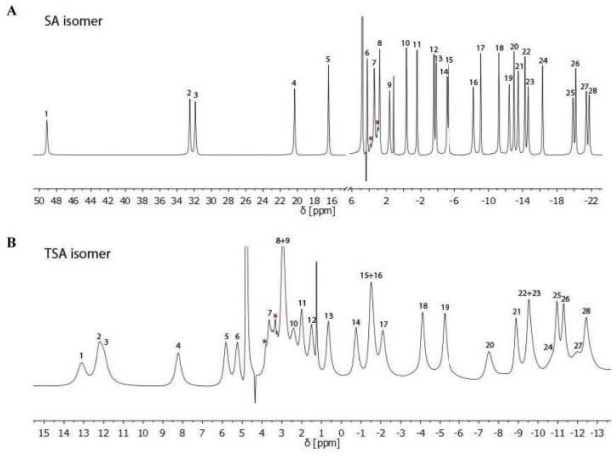

Figure S24: ^{1}H NMR spectra with numbering of the signals of **A**: SA-[Eu(Hdo3aNP)]$^{-}$ at pD = 6.78 and **B**: TSA-[Eu(do3aNP)]$^{2-}$ at pD = 9.05 (~80 mM solution in D_2O, ~250 mM NaCl, B_0 = 14.1 T, 25 °C; referenced to δ(*t*BuOH) = 1.25 ppm). ^{1}H NMR resonances of the free ligand are labelled with *.

Table S5: Table of cross-peaks in 2D ^{1}H-^{1}H COSY NMR spectra of SA-[Eu(Hdo3aNP)]$^{-}$ at pD = 6.78 (left) and TSA-[Eu(do3aNP)]$^{2-}$ at pD = 9.05 or 9.30 (right); ~80 mM solution in D_2O, ~250 mM NaCl, B_0 = 14.1 T, 5 or 25 °C). Less intensive cross-peaks are in brackets.

Signal of the proton of SA-isomer	COSY cross-peak with:	Signal of the proton of TSA-isomer	COSY cross-peak with:
1A	5A, 9A	1B	21B
2A	10A, 7A, (6A)	2B	19B
3A	12A, 19A, (20A, 22A)	3B	–
4A	18A, 28A, (22A)	4B	17B
5A	1A, 8A, (9A)	5B	14B
6A	7A, (2A, 10A)	6B	18B
7A	6A, 2A	7B	25B
8A	9A, 5A	8B	22B
9A	8A, 1A	9B	13B
10A	2A, 6A, 7A, (24A)	10B	–
11A	16A, (17A)	11B	–
12A	3A, 20A, 19A, (28A)	12B	–
13A	15A	13B	9B
14A	17A, (16A)	14B	5B
15A	13A	15B	–
16A	11A, (14A)	16B	–
17A	14A, (11A)	17B	4B
18A	4A, 22A, 28A, (26A)	18B	6B
19A	20A, 3A, 12A	19B	2B
20A	19A, 3A, 12A	20B	26B
21A	25A, (27A)	21B	–
22A	28A, 18A, 4A, (3A)	22B	8B
23A	26A	23B	–
24A	27A, (25A)	24B	–
25A	21A, (24A)	25B	7B
26A	23A	26B	20B
27A	24A, (21A)	27B	–
28A	22A, 4A, (12A)	28B	–

Table S6: Table of cross-peaks in 2D ^{1}H-^{1}H EXSY NMR spectra of SA-[Eu(Hdo3aNP)]$^{-}$ at pD = 6.78 (left) or 8.66 and TSA-[Eu(do3aNP)]$^{2-}$ at pD = 9.05 or 8.66 (right); ~80 mM solution in D_2O, ~250 mM NaCl, B_0 = 14.1 T, 5 or 25 °C).

Signal of the proton of SA-isomer	EXSY with:	Signal of the proton of TSA-isomer	EXSY with:
1A	6A (6B, 28B)	1B	25B (28A, 12A)
2A	8A (8B, 19B)	2B	22B (10A, 9A)
3A	22A (7B, 21B)	3B	10B (16A, 11A)
4A	20A (4B, 26B)	4B	26B (20A, 4A)
5A	7A (18B, 24B)	5B	14B (13A, 15A)
6A	1A (6B, 28B)	6B	28B (1A, 6A)
7A	5A (18B, 24B)	7B	21B (22A, 3A)
8A	2A (8B, 19B)	8B	19B (2A, 8A)
9A	10A (2B, 22B)	9B	13B (26A, 23A)
10A	9A (2B, 22B)	10B	3B (11A, 16A)
11A	16A (3B, 10B)	11B	23B (21A, 27A)
12A	28A (1B, 25B)	12B	27B (25A, 24A)
13A	15A (5B, 14B)	13B	9B (26A, 23A)
14A	17A (15B, 16B)	14B	5B (13A, 15A)
15A	13A (5B, 14B)	15B	16B (14A, 17A)
16A	11A (3B, 10B)	16B	15B (14A, 17A)
17A	14A (15B, 16B)	17B	20B (18A, 19A)
18A	19A (17B, 20B)	18B	24B (7A, 5A)
19A	18A (17B, 20B)	19B	8B (2A, 8A)
20A	4A (4B, 26B)	20B	17B (18A, 19A)
21A	27A (11B, 23B)	21B	7B (22A, 3A)
22A	3A (7B, 21B)	22B	2B (10A, 9A)
23A	26A (9B, 13B)	23B	11B (27A, 21A)
24A	25A (12B, 27B)	24B	18B (5A, 7A)
25A	24A (12B, 27B)	25B	1B (28A, 12A)
26A	23A (9B, 13B)	26B	4B (20A. 4A)
27A	21A (11B, 23B)	27B	12B (24A, 25A)
28A	12A (1B, 25B)	28B	6B (1A, 6A)

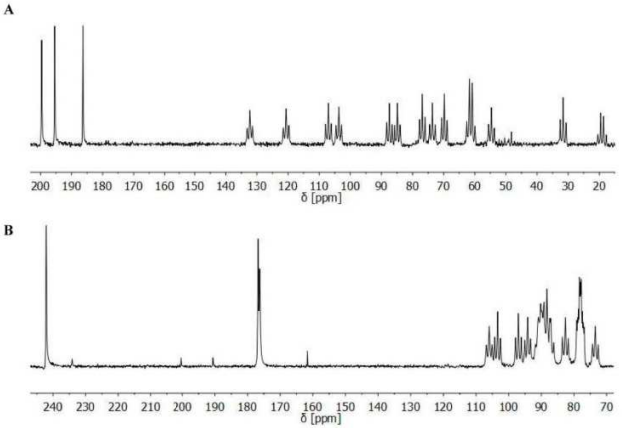

Figure S25: ^{13}C NMR spectra of **A**: SA-[Eu(Hdo3aNP)]$^{-}$ at pD = 6.78 and 25 °C and **B**: TSA-[Eu(do3aNP)]$^{2-}$ at pD = 9.70 and 5 °C without ^{1}H decoupling.

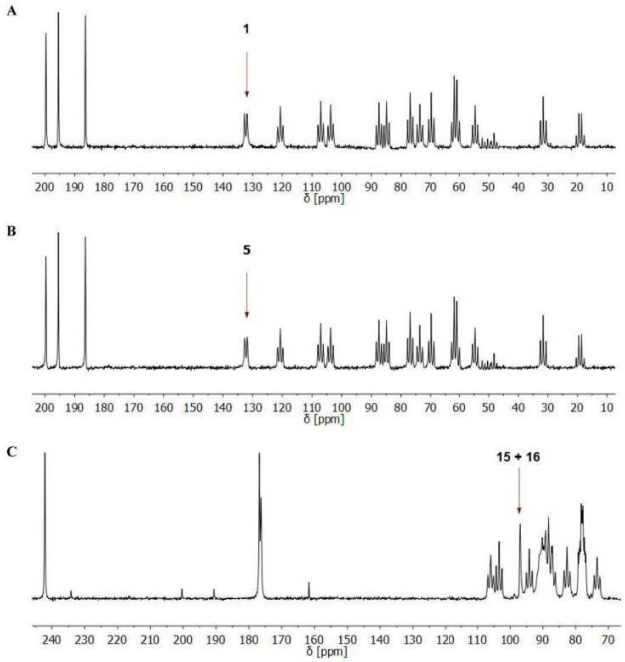

Figure S26: Examples of ^{13}C NMR spectra of **A**, **B**: SA-[Eu(Hdo3aNP)]$^{-}$ at pD = 6.78 and 25 °C and **C**: TSA-[Eu(do3aNP)]$^{2-}$ at pD = 9.70 and 5 °C with ^{1}H decoupling at the ^{1}H frequency of **A**: 1A, **B**: 5A, **C**: 15B + 16B.

Table S7: The couples of geminal proton signals in the NMR spectra of SA-[Eu(Hdo3aNP)]$^{-}$ at pD = 6.78 and 25 °C (left) and TSA-[Eu(do3aNP)]$^{2-}$ at pD = 9.70 and 5 °C (right); ~80 mM solution in D_2O, ~250 mM NaCl, B_0 = 14.1 T). Assignment comes from selective ^{1}H decoupled ^{13}C NMR spectra.

Signal of the proton of SA-isomer	Signal of the geminal proton	Signal of the proton of TSA-isomer	Signal of the geminal proton
1A	5A	1B	21B
2A	10A	2B	19B
3A	12A	3B	10 B
4A	18A	4B	17B
5A	1A	5B	14B
6A	7A	6B	18B
7A	6A	7B	25B
8A	9A	8B	22B
9A	8A	9B	13B
10A	2A	10B	3B
11A	16A	11B	27B
12A	3A	12B	23B
13A	15A	13B	9B
14A	17A	14B	5B
15A	13A	15B	16B
16A	11A	16B	15B
17A	14A	17B	4B
18A	4A	18B	6B
19A	20A	19B	2B
20A	19A	20B	26B
21A	25A	21B	1B
22A	28A	22B	8B
23A	26A	23B	12B
24A	27A	24B	28B
25A	21A	25B	7B
26A	23A	26B	20B
27A	24A	27B	11B
28A	22A	28B	24B

Potentiometric, ^{1}H and ^{31}P NMR studies – protonation and stability constants of H_5do3aNP and its Eu(III) complex

Table S8: Overall protonation constants ($\log\beta_h$)[a] and derived consecutive protonation constants ($\log K(H_hL)$)[b] of H_5do3aNP. Potentiometric conditions: 0.1 M (NMe_4)Cl, 25 °C. Conditions of ^{31}P NMR and ^{1}H NMR titration: HCl/(NMe_4)OH and HCl/KOH, respectively; no ionic strength control, 25 °C.

h	$\log\beta_h$ (potent.)	$\log K(H_hL)$ (potent.)	$\log\beta_h$ (^{31}P NMR)	$\log K(H_hL)$ (^{31}P NMR)	$\delta(^{31}P)$ ppm	$\delta(^{1}H)$ NCH_2P ppm	$\delta(^{1}H)$ odd acetate ppm	$\delta(^{1}H)$ trans acetates ppm
0	–	–	–	–	16.86(4)	2.55(4)	3.11(9)	3.15(9)
1	12.561(6)	12.56	12.52(17)	12.52	16.32(8)	2.61(2)	3.39(3)	3.36(2)
2	22.935(6)	10.37	23.11(3)	10.59	10.43(18)	2.86(2)	3.47(2)	3.47(3)
3	32.164(7)	9.23	32.48(8)	9.37	8.16(2)	2.98(1)	3.21(1)	3.85(1)
4	38.336(8)	6.17	38.44(8)	5.96	9.30(2)	–	–	–
5	42.522(8)	4.19	40.49(32)[c]	–	9.19(2)	–	–	–
6	44.426(9)	1.90	–	2.05[c]	–	–	–	–

[a] $\beta_h = [H_hL]/\{[H]^h\cdot[L]\}$ [b] $K(H_hL) = [H_hL]]/\{[H]\cdot[H_{h-1}L]\}$. Charges of species are omitted for clarity reasons. [c] In fact, this step corresponds to a sixth protonation (corresponding $\log K = 40.49 - 38.44 = 2.05$), although it was formally calculated as the fifth one. It is due to the fact, that the fifth protonation occurs far away from the phosphonate group (on the pendant acetate group located *trans* to the aminophosphonate moiety) and thus, it does not influence the ^{31}P NMR chemical shift.

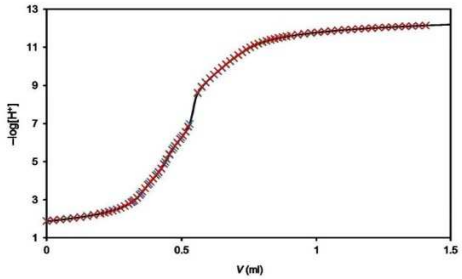

Figure S27: Titration data of the acid-base titration of the free ligand H_5dc3aNP showing the best fit calculated using the protonation constants from Table S8.

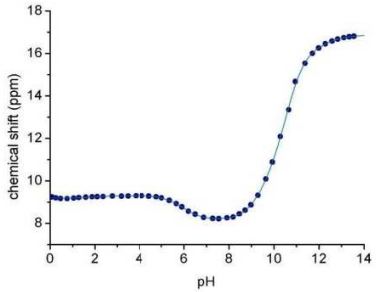

Figure S28: Titration data of the ^{31}P NMR titration of the free ligand H_5do3aNP showing the best fit calculated using the protonation constants and chemical shifts from Table S8.

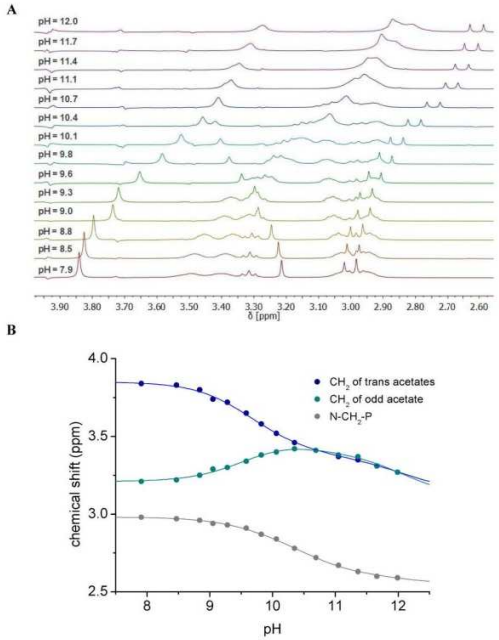

Figure S29: **A**: ^{1}H NMR signals of ^{1}H NMR titration of the free ligand H_5do3aNP and **B**: titration data of the ^{1}H NMR titration of the showing the best fit.

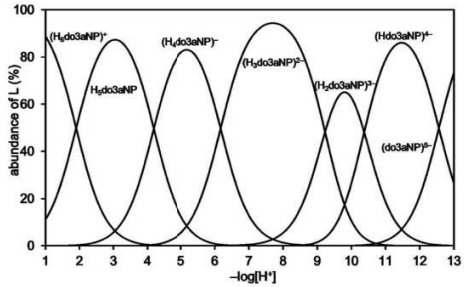

Figure S30: Distribution diagram of variously protonated species of the free ligand H_5do3aNP (c_L = 0.004 M, 0.1 M (NMe_4)Cl, 25 °C).

Table S9: Overall stability constants ($\log\beta_{h11}$)[a] of [Eu($H_h$do3aNP)] complexes and derived consecutive protonation constants ($\log K(H_hLM)$)[b] (0.1 M (NMe_4)Cl, 25 °C).

h	*l*	Eu	$\log\beta_{h11}$	$\log K(H_hLM)$
0	1	1	23.49(3)	–
1	1	1	31.49(3)	8.00
2	1	1	35.23(5)	3.75
3	1	1	39.59(4)	4.35
4	1	1	42.90(3)	3.31

[a] $\beta_{h11} = [H_hLEu]/\{[H]^h\cdot[L]\cdot[Eu]\}$. [b] $K(H_hLM) = [H_hLM]]/\{[H]\cdot[H_{h-1}LM]\}$. Charges of species are omitted for clarity reasons.

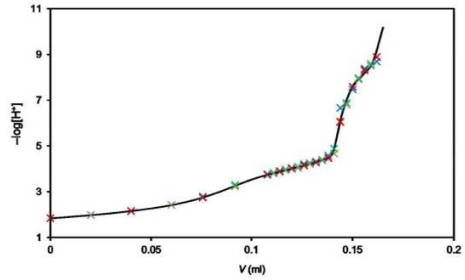

Figure S31: Titration data of the out-of-cell titration of Eu(III)–H_5do3aNP systems showing the best fits calculated using the stability constants from Table S9 ($c_M = c_L$ = 0.004 M, 0.1 M (NMe_4)Cl, 25 °C, equilibration time = 4 weeks).

Table S10: Overall protonation constants ($\log\beta_{h11}$)[a] of pre-formed $[Eu(do3aNP)]^{2-}$ complex and derived consecutive protonation constants ($\log K(H_hLM)$)[b] (0.1 M $(NMe_4)Cl$, 25 °C).

h	$\log\beta_{h11Eu}$	$\log K(H_hLM)$
1	8.29(2)	8.29
2	12.36(3)	4.07
3	14.11(3)	1.75

[a] $\beta_{h11} = [H_hLM]/\{[H]^h\cdot[LM]\}$. [b] $K(H_hL) = [H_hLM]]/\{[H]\cdot[H_{h-1}LM]\}$. Charges of species are omitted for clarity reasons.

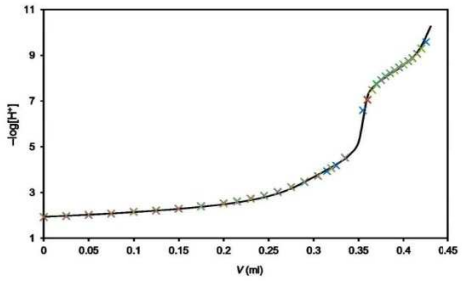

Figure S32: Titration data of the acid-base titration of the pre-formed $[Eu(do3aNP)]^{2-}$ complex with the best fits calculated using the protonation constants from Table S10 ($c_{M,L}$ = 0.003 M, 0.1 M $(NMe_4)Cl$, 25 °C).

[1] Rudovský, J.; Cígler, P.; Kotek, J.; Hermann, P.; Vojtíšek, P.; Lukeš, I.; Peters, J. A.; Vander Elst, L.; Muller, R. N. Lanthanide (III) complexes of a mono (methylphosphonate) analogue of H_4dota: The influence of protonation of the phosphonate moiety on the TSAP/SAP isomer ratio and the water exchange rate. *Chem. - Eur. J.* **2005**, *11*, 2373–2384.

[2] Vitha, T.; Kubíček, V.; Kotek, J.; Hermann, P.; Vander Elst, L.; Muller, R. N.; Lukeš, I., Peters, J. A. Gd(III) complex of a monophosphinate-bis(phosphonate) DOTA analogue with a high relaxivity; Lanthanide(III) complexes for imaging and radiotherapy of calcified tissues. *Dalton Trans.* **2009**, 3204–3214.

[3] Lebdušková, P.; Hermann, P.; Helm, L.; Tóth, É.; Kotek, J.; Binnemans, K.; Rudovský, J.; Lukeš, I.; Merbach, A. E. Gadolinium(III) Complexes of Mono- and Diethyl Esters of Monophosphonic Acid Analogue of DOTA as Potential MRI Contrast Agents: Solution Structures and Relaxometric Studies. *Dalton Trans.* **2007**, 493–501.

[4] Rudovský, J.; Kotek, J.; Hermann, P.; Lukeš, I.; Mainero, V.; Aime, S. Synthesis of a Bifunctional Monophosphinic Acid DOTA Analogue Ligand and Its Lanthanide(III) Complexes. A Gadolinium(III) Complex Endowed with an Optimal Water Exchange Rate for MRI Applications. *Org. Biomol. Chem.* **2005**, *3*, 112–117.

[5] Rudovský, J.; Botta, M.; Hermann, P., Koridze, A.; Aime, S. Relaxometric and solution NMR structural studies on ditopic lanthanide(III) complexes of a phosphinate analogue of DOTA with a fast rate of water exchange. *Dalton Trans.* **2006**, 2323–2333.

[6] Campello, M. P. C.; Lacerda, S.; Santos, I. C.; Pereira, G. A.; Geraldes, C. F. G. C.; Kotek, J.; Hermann, P.; Vaněk, J.; Lubal, P.; Kubíček, V.; Tóth, E.; Santos, I. Lanthanide(III) complexes of 4,10-bis(phosphonomethyl)-1,4,7,10-tetraazacyclododecane-1,7-diacetic acid (trans-H_6do2a2p) in solution and in the solid state: structural studies along the series. *Chem. - Eur. J.* **2010**, *16*, 8446–8465.

[7] Kotková, Z.; Pereira, G. A.; Djanashvili, K.; Kotek, J.; Rudovský, J., Hermann, P.; Vander Elst, L.; Muller, R. N.; Geraldes, C. F. G. C.; Lukeš, I.; Peters, J. A. Lanthanide(III) Complexes of Phosphorus Acid Analogues of H_4DOTA as Model Compounds for the Evaluation of the Second-Sphere Hydration. *Eur. J. Inorg. Chem.* **2009**, 119–136.

[8] Pereira, G. A.; Ball, L.; Sherry, A. D.; Peters, J. A.; Geraldes, C. F. G. C. NMR Characterization of Lanthanide(3+) Complexes of Tetraazatetrakisphosphinato and Tetraazatetrakisphosphonato Ligands. *Helv. Chim. Acta.* **2009**, *92*, 2532–2551.

[9] Rohovec, J.; Lukeš, I; Hermann, P. Lanthanide complexes of a cyclen derivative with phenylphosphinic pendant arms for possible ^{1}H and ^{31}P MRI temperature sensitive probes. *New J. Chem.* **1999**, *23*, 1129–1132.

[10] Rohovec, J.; Kývala, M.; Vojtíšek, P.; Hermann, P.; Lukeš, I. Synthesis, Crystal Structures, and Solution Properties of *N*-Methylene(phenyl)phosphinic Acid Derivatives of Cyclen and Cyclam. *Eur. J. Inorg. Chem.* **2000**, 195–203.

[11] Aime. S.; Batsanov, A. S.; Botta, M.; Howard, J. A. K.; Parker, D.; Senanayake, K.; Williams, J. A. G. Solution and Solid-state Characterization of Highly Rigid, Eight-Coordinate Lanthanide(III) Complexes of a Macrocyclic Tetrabenzylphosphinate. *Inorg. Chem.* **1994**, *33*, 4696–4706.

[12] Aime, S.; Batsanov, A. S.; Botta, M.; Dickins, R. S.; Faulkner, S.; Foster, C. E.; Harrison, A.; Howard, J. A. K.; Moloney, J. M.; Norman, T. J.; Parker, D.; Royle, L.; Williams, J. A. G. Nuclear magnetic resonance, luminescence and structural studies of lanthanide complexes with octadentate macrocyclic ligands bearing benzylphosphinate groups. *J. Chem. Soc., Dalton Trans.* **1997**, 3623–3636.

[13] Rohovec, J.; Vojtíšek, P.; Hermann, P.; Mosinger, J.; Žák, Z.; Lukeš, I. Synthesis, crystal structures and NMR and luminescence spectra of lanthanide complexes of 1,4,7,10-tetraazacyclododecane with *N*-methylene(phenyl)phosphinic acid pendant arms. *J. Chem. Soc., Dalton Trans.* **1999**, 3585–3592.

[14] Avecilla, F.; Peters, J. A.; Geraldes, C. F. G. C. X-ray Crystal Structure of a Sodium Salt of $[Gd(DOTP)]^{5-}$: Implications for Its Second-Sphere Relaxivity and the ^{23}Na NMR Hyperfine Shift Effects of $[Tm(DOTP)]^{5-}$. *Eur. J. Inorg. Chem.* **2003**, 4179–4186.

[15] Vojtíšek, P.; Cígler, P.; Kotek, J.; Rudovský, J.; Hermann, P.; Lukeš, I. Crystal Structures of Lanthanide(III) Complexes with Cyclen Derivative Bearing Three Acetate and One Methylphosphonate Pendants. *Inorg. Chem.* **2005**, *44*, 5591–5599.

[16] Luck, R. L.; Maupin, C. L.; Parker, D.; Riehl, J. P.; Williams, J. A. G. Circularly polarized luminescence and structural studies of a dysprosium(III) complex with an octadentate macrocyclic ligand bearing benzylphosphinate groups. *Inorg. Chim. Acta.* **2001**, *317*, 331–337.